2019

Innovations in integral abutment connection details for accelerated bridge construction

Austin James DeJong
Iowa State University

Innovations in integral abutment connection details for accelerated bridge construction

by

Austin DeJong

A thesis submitted to the graduate faculty

in partial fulfillment of the requirements for the degree of

MASTER OF SCIENCE

Major: Civil Engineering

Program of Study Committee:
Behrouz Shafei, Major Professor
Brent Phares
Jennifer Shane

The student author, whose presentation of the scholarship herein was approved by the program of study committee, is solely responsible for the content of this thesis. The Graduate College will ensure this thesis is globally accessible and will not permit alterations after a degree is conferred.

Iowa State University

Ames, Iowa

2019

DEDICATION

This thesis is dedicated to the people who provided me with unending support throughout the process of conducting the research for this thesis, my parents Scott and Cheryl DeJong. Also, the hard work involved with compiling this thesis is dedicated to my girlfriend, Jalissa Irmiter, since without her I would not have been able to push through to get to the finish.

TABLE OF CONTENTS

Page

LIST OF FIGURES

Page

ACKNOWLEDGMENTS

I would like to thank my committee chair, Dr. Behrouz Shafei, the Principal Investigator for the laboratory research done for this thesis, Travis Hosteng, and my committee members, Dr. Brent Phares, and Dr. Jennifer Shane, for their guidance and support throughout the course of this research. I would also like to extend acknowledgement to the Iowa Department of Transportation and the Accelerated Bridge Construction University Transportation Center for the financial support.

In addition, I would also like to thank my family, friends, colleagues, the department faculty and staff for the unending support during my time at Iowa State University. I want to also offer my appreciation to Doug Wood, Owen Steffens, and the undergraduate hourly workers of the Iowa State University Structural Laboratory for their input and construction aid, as well as Shahin Hajilar for his help with the finite element simulations, without whom, this thesis would not have been possible.

ABSTRACT

During bridge construction, closures have significant impacts on traffic flow for the public. To alleviate this impact, the presence of precast elements is being introduced in the design and construction of bridges, which would increase the efficiency of construction and convert month-, or even year-, long closures into a matter of weeks, or perhaps even days. This strategy, known as accelerated bridge construction (ABC), is growing in popularity within the bridge community and is gaining traction for research projects to investigate how the construction of bridge elements can be expedited.

One such element being investigated is the integral abutment. This structural connection for bridges was introduced to eliminate the need for expansion joints between the substructure and superstructure, where the presence of water and other deteriorating chemicals caused long-term and frequent maintenance issues. The integral abutment alleviates the need for the expansion joint by having the superstructure rigidly connected to the foundation to cause the two elements to act together in response to traffic loads, as well as thermal expansions and contractions. Due to this area needing to be heavily reinforced, congestion issues arise when attempting to apply ABC methods.

Moreover, the construction tolerances and weight of the integral abutments cause some problems for ABC projects. Addressing these issues was the main motivation for the research performed in this thesis in which the use of couplers and ultra-high-performance concrete, while applying ABC techniques, is investigated. The foundation element of focus was the pile cap, while the superstructure element investigated was the integral diaphragm, which consists of the deck and cast-in-place girder. Three different connection details were investigated such as grouted reinforcing bar coupler, pile coupler,

and UHPC-Joint. The strength and durability of the connection details were evaluated through full-scale laboratory testing that applied simulated thermal loads and live loads. Strain gauges were used to capture the development and strength of the specimen and connecting materials, and displacement transducers monitored the propagation and magnitude of precast joint openings between the integral diaphragm and pile cap to evaluate the durability of the connection details. The results of these tests were compared to the control specimen tested in the previous phase of the project. (Hosteng, Phares, & Redd, 2016) A separate set of three-dimensional finite element (FE) simulations were also conducted to complement the findings obtained from the laboratory experiments. The effect of the number of bar couplers on enhancing the performance of the abutment connections was evaluated in detail. The outcome of this study resulted in high quality results for integral abutment connections for ABC applications, not only through laboratory test results, but also by finite element simulations that could aid the bridge engineering community in the progression towards implementation of this connection area for future use.

CHAPTER 1. INTRODUCTION

1.1 Background

Accelerated Bridge Construction (ABC) has started to become the construction procedure of use by many bridge engineering agencies around the world and in the United States. ABC is being analyzed and formulated to replace conventional bridge construction due to the significant decrease in construction time and traffic impact, as well as the increase in bridge element quality and worker/public safety. ABC can replace an existing bridge in a matter of weeks, or even days, due to the presence of Prefabricated Bridge Element and Systems (PBES) that can be quickly assembled. This introduces several advantages compared to conventional bridge construction, which can have construction times of months and cause detours that greatly affect the flow of traffic, as well as the safety of the public and construction workers.

ABC differs from conventional bridge construction by utilizing PBES and other technologies to lift, slide, and rotate parts of a bridge into the connection. These connections have been, and still are being, researched and tested for many locations within a bridge. One connection still under research and testing is the integral abutment. An integral abutment is a connection composed of combined shear and moment connections between the bridge superstructure and substructure. This connection is appealing to bridge designers since it results in the elimination of the expansion joint, which typically is the common location of structural deterioration.

The superstructure and substructure, in conventional bridge construction, is connected by an expansion joint. These components allow the infiltration of water, debris, and deicing chemicals when not designed properly. These infiltrations can cause structural deterioration

and corrode elements of the abutment connection, which may compromise the integrity of the bridge. These issues cause the need for the integral abutment connection, which can reduce the cost of maintaining the bridge since there are no joints to allow infiltration.

Since the integral abutment reinforcement can be highly congested to resist the different forces acting on both the substructure and superstructure, the issue of transporting and installing these elements govern the design in ABC applications. The issue of transporting comes from the weight of the specimen, and the installation issues are the result of the splices that will need to be connected after the lift and slide have been completed.

To alleviate these issues, the method of cast-in-place integral abutments has been the common procedure for this ABC connection. This procedure facilitates the tolerances of the connection during construction by creating a simpler integral connection, which is done by placing the prefabricated pile cap on the driven piles, setting the prefabricated girder, and then placing a closure pour over the connection to create the integral connectivity. A major shortcoming of this connection detail is the closure pour typically consists of High-Performance Concrete (HPC) or regular concrete. These materials need up to a week of curing time to be structurally safe for traffic and causes delays in opening the bridge.

1.2 Research Scope, Objectives, and Tasks

The scope of this research is to revise the connection detail designs from (Hosteng, Phares, & Redd, 2016), provide information for the construction of each connection detail, specifically any issues encountered, and laboratory test results to aid in the planning, design, and construction of the integral abutment to be used in ABC projects. Bridge Engineering Center (BEC) at Iowa State University (ISU) discussed other possible connection details, as well as revisions to the connection detail designs from (Hosteng, Phares, & Redd, 2016), for integral abutments for ABC, of which, three designs were selected for full-scale laboratory

investigation. The laboratory specimens were evaluated on three criteria: constructability, strength, and durability. The following five tasks were completed to meet the objectives of this thesis:

1. Conduct a detailed review of ABC procedures with respect to integral abutments, which focused on previous research into integral abutments both for conventional construction as well as ABC and research into integral abutment connections for both conventional construction and ABC.
2. Develop and design connection details for an integral abutment using ABC methods, as well as results of (Hosteng, Phares, & Redd, 2016).
3. Investigate and evaluate the constructability aspects of the connection details and adjust designs accordingly. Also, test the flowability of UHPC through the designed cross-section of the UHPC-Joint connection detail.
4. Construct and test full-scale specimens of the connection details in the laboratory, measuring the performance of the detail in terms of durability and strength.
5. Create a Finite Element model in ABAQUS to simulate structural response recorded during laboratory testing and expand the investigations to the configurations beyond those tested in the laboratory.
6. Summarize the results of this study for the future use of integral abutments in ABC applications.

CHAPTER 2. LITERATURE REVIEW

Accelerated Bridge Construction (ABC) is the practice of speeding up the construction time for a bridge, either new or restoration. ABC is intended to cause less traffic delays and on-site construction time. The use of Prefabricated Bridge Element Systems (PBES) is one way of implementing ABC into a bridge project. PBES require that elements of a bridge be prefabricated off site of the final location. These elements can either be shipped to site, or fabricated just adjacent to the bridge, and then installed using ABC techniques. By doing this, detours or even closures for traffic can be minimized compared to conventional construction. Through years of research, design, and construction, there have been many advances in the design of bridge elements to be used for PBES in ABC.

For designing, constructing, and evaluating a bridge, it is important to know the verbiage for different parts of the bridge. Overall, there are two parts to every bridge, the superstructure and substructure. The superstructure consists of elements directly loaded with traffic, which are the deck and beams. The elements supporting the superstructure are known as the substructure which consist of abutments, piers, pile caps, and a foundation system. Focusing on the substructure, specially the abutment and piers, there are even further subcategories for classification.

The abutment has three main classifications, which are cantilever, semi-integral, and integral. The cantilever abutment utilizes walls and footings to provide support for the beams. The footing is placed directly onto the soil, or onto piles, the wall stem rests on the footing and is primarily reinforced to resist bending moment induced from retaining soil along the height of the stem. If desired to lessen the complexity of construction, the wall element for the abutment may use a wall cap. The wall cap, which varies in thickness along

its height to provide grade change over the width of the bridge, is placed onto the wall stem. The wall cap is the top of the cantilever abutment and is where the beam seat is placed, which can be adjusted for the final elevation of the beam. Also, the wall cap may or may not incorporate the backwall, and the backwall may also be a separate element for the abutment system. An example design for the PBES cantilever abutment is shown in Figure 2.1 (Culmo, et al., 2013). An abutment like the design shown in Figure 2.1 was constructed in New Hampshire in less than three days once the excavations were complete (Culmo M. P., 2011).

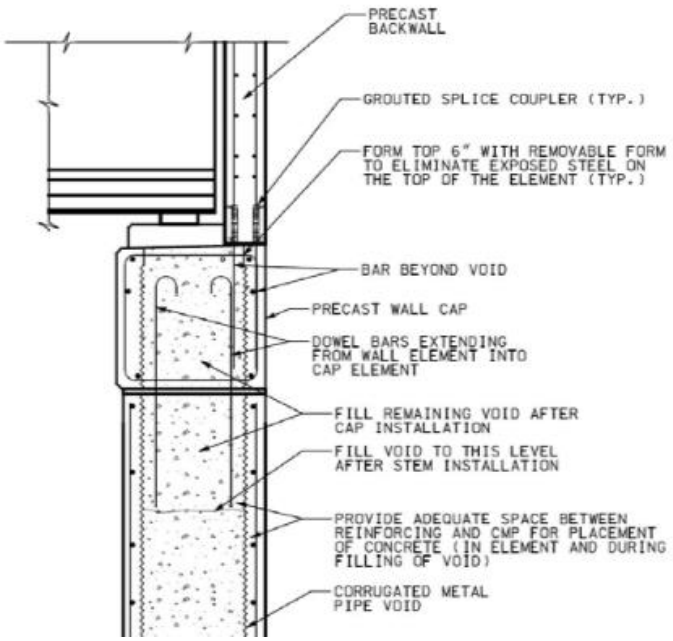

Figure 2.1 *Example of cantilever abutment design using PBES.* (Culmo, et al., 2013)

The semi-integral abutment connects the superstructure to the substructure but does not contain a moment connection like the integral abutment does (i.e. a pinned connection). The foundation system for semi-integral abutments uses driven piles being connected to a pile cap, or abutment stem. The beam is connected to the abutment stem either through an expansion joint or a pinned connection. The beam ends are integrated to a backwall, which can be either prefabricated or cast-in-place during the integration of the beam end. The

backwall is primarily used to retain soils surrounding the abutment, but through the closure pour to integrate it with the beam end also seals the joint between the deck and approach slab of the bridge, where infiltration of water and deicing chemicals can lead to deterioration. An example for the semi-integral abutment using PBES is shown on Figure 2.2 (Culmo, et al., 2013). Since the superstructure and substructure for this system do not have any significant connections, the semi-integral abutment is a prime example of a PBES that can utilize ABC installation methods such as Self-Propelled Modular Transporters (SPMTs) and lateral sliding/skidding and allow for tolerance adjustments into its final location (Culmo M. P., 2011).

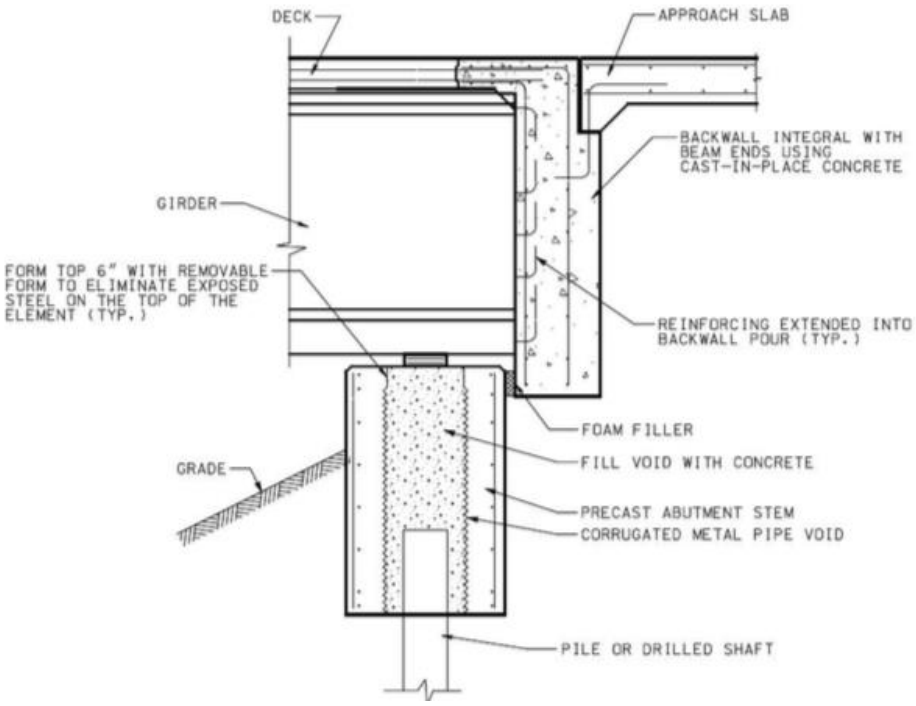

Figure 2.2 *Example of semi-integral abutment design using PBES.* (Culmo, et al., 2013)

The integral abutment connects the superstructure to the substructure and has a moment connection. Like the semi-integral abutment, there is no joint at the deck level but unlike semi-integral abutments, there is no exposed joint between the beam and the abutment

stem since the entire area becomes fully integral with a closure pour. Similar to the semi-integral abutment foundation system, driven piles are connected to the abutment stem through a closure pour. The abutment stem will have reinforcing bars protruding from beams into the area to be connected through a closure pour, or the diaphragm pour. Likewise, reinforcing bars from the deck will protrude into the diaphragm pour, ensuring a complete moment connection. The approach slab will sit on the backwall, which can either be prefabricated separately or with the abutment stem, and the entire area will be sealed off from exposed joints through the closure pour. An example of the integral abutment connection using PBES is shown in Figure 2.3 (Culmo, et al., 2013).

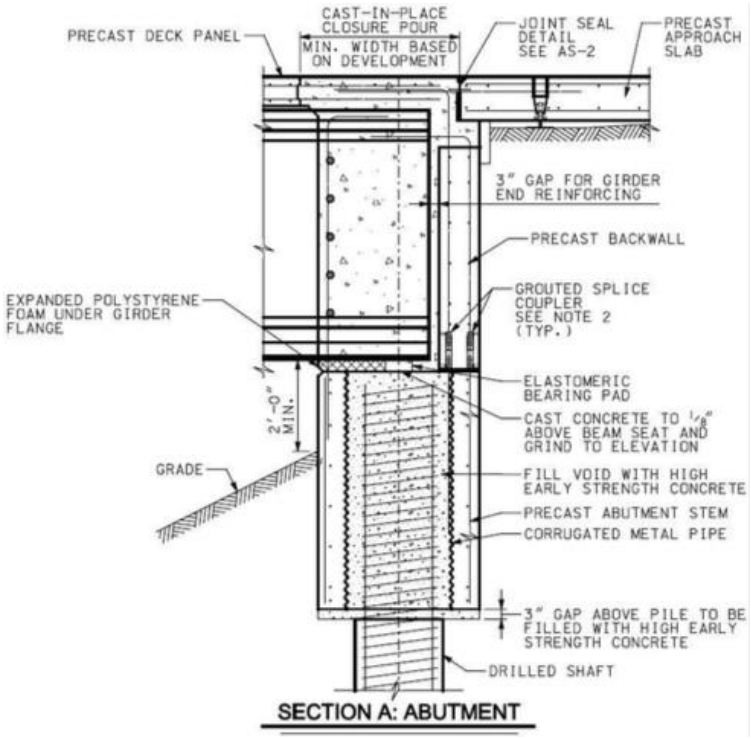

Figure 2.3 *Example of integral abutment design using PBES.* (Culmo, et al., 2013)

There is another type of abutment that benefits from the use of PBES and ABC, the Geosynthetic Reinforced Soil Integrated Bridge System (GRS-IBS). This abutment created by the FHWA integrates the roadway fill to the abutment using geosynthetics allowing for

the systems to act as one whole unit. The geosynthetic walls are direct supports for the superstructure, which allows the superstructure to settle with the approach fill removing the requirement for an approach slab. Ohio implemented this abutment system for a bridge (Figure 2.4) and it was reported that the GRS-IBS abutments could be constructed in one week or less, since there is no curing time for cementitious materials, and resulted in a total construction time of approximately eight weeks (Culmo M. P., 2011).

Figure 2.4 *GRS-IBS bridge in Ohio. GRS Abutment during construction (top). Completed bridge built in 47 days (bottom).* (Culmo M. P., 2011)

One issue with prefabricated abutments is the weight during transportation. To address this issue, some connections were proposed by the University of Wisconsin – Madison. One connection to decrease the weight of the precast abutment cap was the Pile Bent Cap with Hollow Wall Panels (Figure 2.5). The hollow wall panels would be placed to

encapsulate the driven piles, which allows for greater tolerances during pile installation but requires more concrete placement in the field. After the wall placement, the bent cap would be placed and grouted to the hollow wall panel, completing the connection. (Unlu, 2010)

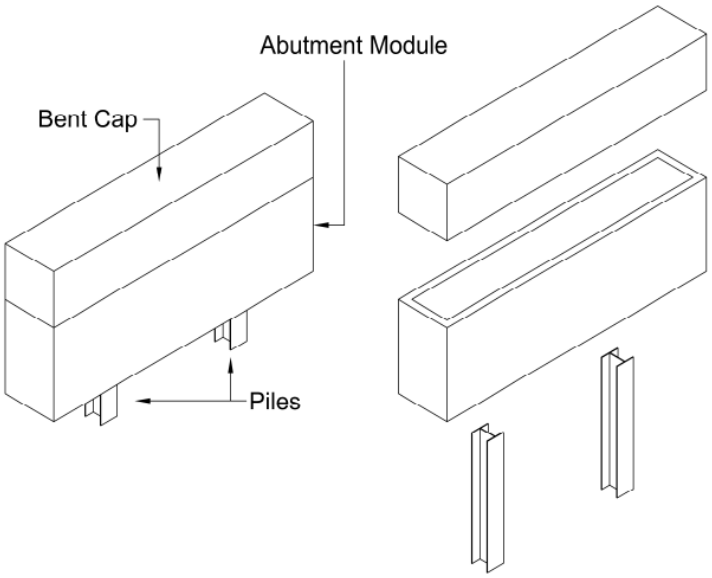

Figure 2.5 *Pile Bent Cap with Hollow Wall Panel*. (Unlu, 2010)

To diminish the amount of excess cementitious material being installed around the piles, another connection was proposed that would use sockets to connect the abutment wall to the driven piles. These sockets encasing the piles would be filled with a cementitious material to complete the connection, and then the bent cap would be placed onto the abutment wall and connected through grouting pockets fabricated within the bent cap. This connection concept was expanded for both a full-length socket and limited length socket, Figure 2.6 and 2,7, respectively (Unlu, 2010).

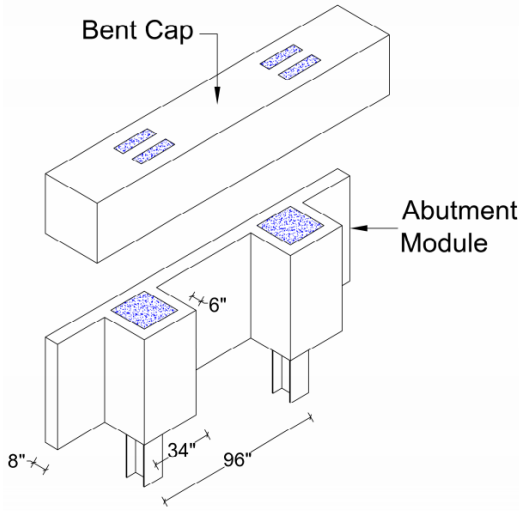

Figure 2.6 *Full Length Socketed Wall with Bent Cap*. (Unlu, 2010)

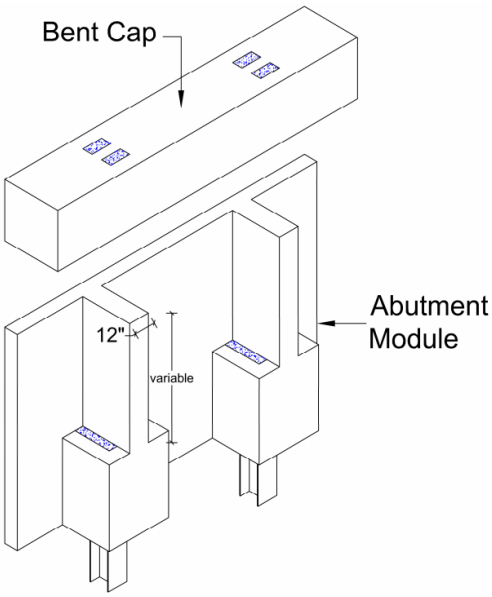

Figure 2.7 *Limited Length Socketed Wall with Bent Cap*. (Unlu, 2010)

Another abutment connection investigated by The University of Wisconsin – Madison was adjacent abutment modules (Unlu, 2010). The use of a shear key was recommended to allow the transfer of shear. The shear key design in the prefabricated abutment modules has a female shear key that results in a void between adjacent modules to be filled with grout (Figure 2.8).

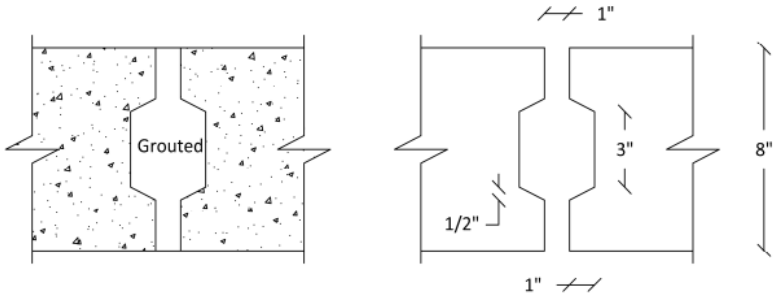

Figure 2.8 *Cross section view showing shear key for abutment module to abutment module connection*. (Unlu, 2010)

Piers also support the superstructure but are away from the ends of the bridge and can be classified as pier bents and wall piers. Pier bents support the superstructure through the use of concrete columns, a singular column for piers and multiple columns for bents, that go down to connect with the foundation system. Wall piers are similar to cantilever abutment systems, as they also use a vertical stem connected to the foundation system. PBES for piers is typically done through having the footing, column, and pile cap be prefabricated and then be connected through mechanical couplers or closure pours. An example of the wall pier design using PBES is shown in Figure 2.9 (Culmo, et al., 2013).

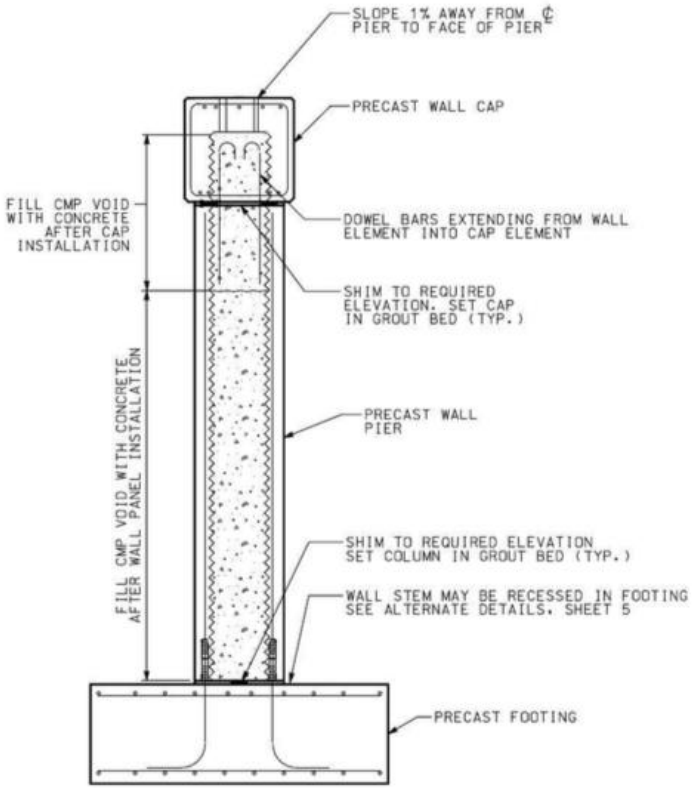

Figure 2.9 *Example of wall pier design using PBES*. (Culmo, et al., 2013)

Another example of PBES for piers is the use of prefabricated open frame bent caps. Projects done in Florida, Utah, and Georgia, shown in Figures 2.10 through 2.12, respectively, have shown successful connections between precast bent caps and precast columns made with grouted sleeve reinforcing bar couplers. The erection of precast concrete piers can be conducted rather swiftly compared to conventional construction practices, some typical pier bents may be installed in two days after the footings are properly placed (Culmo M. P., 2011).

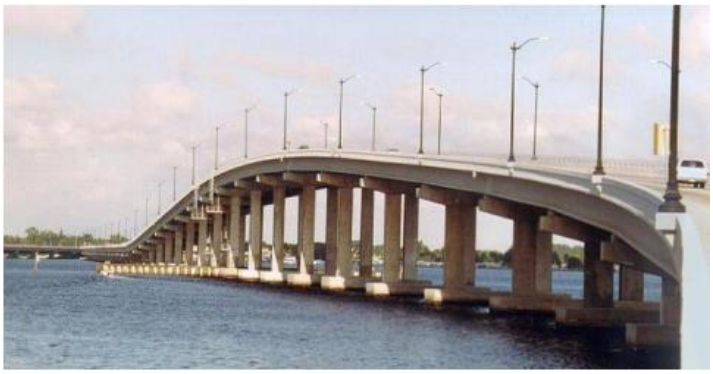

Figure 2.10 *Precast open frame pier bent constructed bridge in Florida*. (Culmo M. P., 2011)

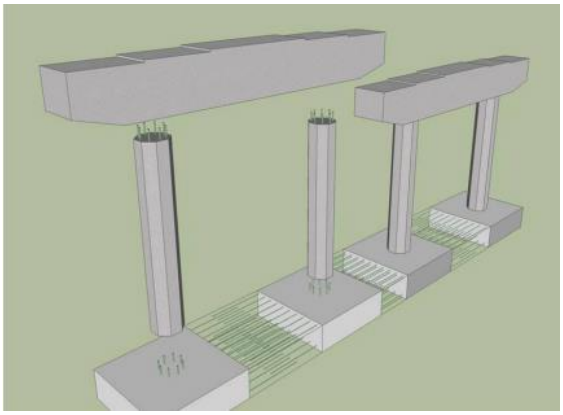

Figure 2.11 *Precast open frame pier bent sketch from Utah DOT*. (Culmo M. P., 2011)

Figure 2.12 *Precast open frame pier bent constructed in Georgia*. (Culmo M. P., 2011)

A study at the University of Wisconsin – Madison investigated some other connections that could be implemented for bent cap and abutment connection with PBES. Three connections were proposed for the bent cap connection, but could also be used as a

pier cap, pile bent cap, or a cap on abutments. The focus of these connections was to connect caps to adjacent caps to allow for shorter lengths to be transported to the construction site, the first being a welded steel plate connection. Steel plates would be embedded into the top of each cap, and then after the caps had been placed, a final drop in splice plate would be welded to the two adjacent embedded steel plates as shown in Figure 2.13 (Unlu, 2010).

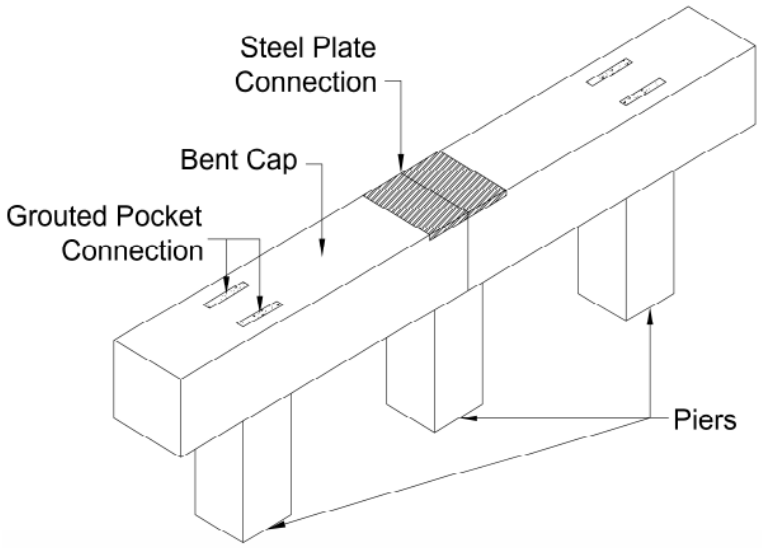

Figure 2.13 *Isometric view of Welded Steel Plate Connection*. (Unlu, 2010)

The Welded Steel Plate Connection would be a fast connection if there was no grouting done between the caps, resulting in a "hinged" connection. If a continuous connection is preferred, grouting would need to be completed below the steel plate. A stainless-steel plate or a masonry cover would need to be used in order to ensure the durability of the connection, but still this can be done in a quick timeline and inexpensive to implement. Grouted pockets would be used to connect piers to the bent caps, which has been shown to be sufficient and simple to construct.

Protruding reinforcement and block outs of prefabricated bent caps was another cap-cap connection proposed. Reinforcing steel bars would protrude out of ends of the caps and would be connected via drop in lap splice bars and a cast in place concrete pour, which

would provide flexural and shear continuity across the joint (Figure 2.14). A few disadvantages of this connection arise, such as the complexity of the formwork for the prefabrication of the caps that require protruding bars and block outs. Also, the use of the cast in place concrete pour requires a curing time that could delay construction (Unlu, 2010).

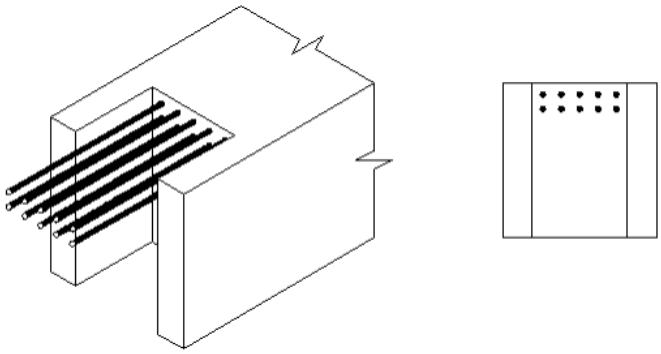

Figure 2.14 *Spliced Reinforcement Connection*. (Unlu, 2010)

The final proposed cap-cap connection for bent caps using ABC was the use of post-tensioning. By fabricating end anchorages and ducts into the precast bent caps, it would be a relatively simple procedure for conducting the post-tensioning process resulting in a favorable connection. Grouting would be done between the prefabricated caps, post-tensioning would be done, and grouting of the ducts would be done to complete the connection. During design of this connection, it would be an important note to account for the pier reinforcement protruding up into the bent cap when designing the post-tensioning ducts (Unlu, 2010).

For some of the substructure designs using PBES, a Corrugated Metal Pipe (CMP) was used to create voids where connections were to be made. A study was conducted by Iowa State University focusing on the constructability and strength of abutment and pier caps using a CMP void to connect to a pile. The strength of this connection was evaluated by subjecting specimens to a moment and punching shear. The moment capacity of the

connection was determined through both positive and negative moments created by different specimen setup. Figure 2.15 and 2.16 show the setups for the single and double pile abutment cap testing, but the same setup was used for the single pile pier cap testing (Wipf, Klaiber, & Hockerman, 2009).

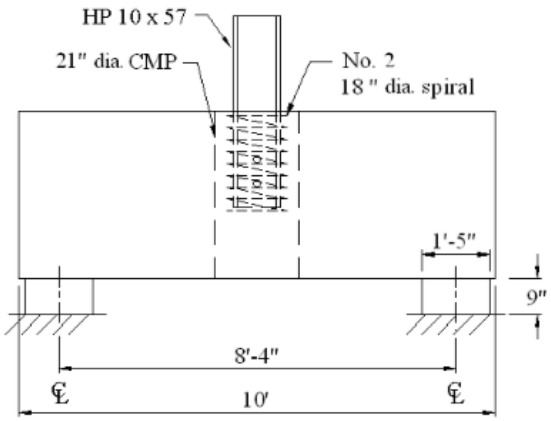

Figure 2.15 *Single pile abutment cap test setup*. (Wipf, Klaiber, & Hockerman, 2009)

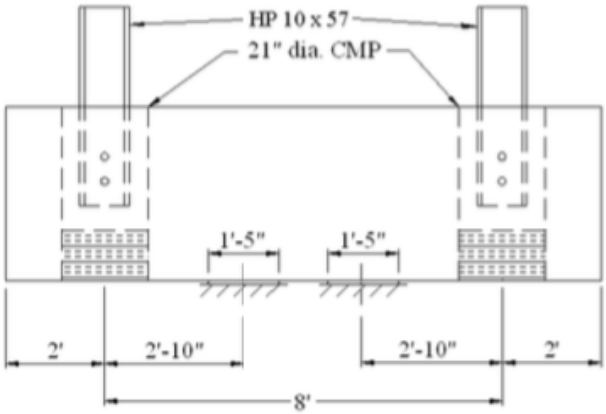

Figure 2.16 *Double pile abutment cap test setup*. (Wipf, Klaiber, & Hockerman, 2009)

Each test setup used a hydraulic pump to load the specimen at the top face of the piles. By doing so, the single pile setup would cause a positive moment reaction within the specimen, and a negative moment reaction within the double pile specimen. After the moment capacity of the specimens were recorded, the punching shear capacity of the connections were tested by loading each pile individually under the hydraulic pump. The

maximum load for the positive and negative moment capacity was around 300 kip and 140 kip, respectively. 400 kip was the maximum load for the punching shear test. The testing of this connection also investigated the possibility of a pile being offset from center within the CMP void, which is shown in Figure 2.17.

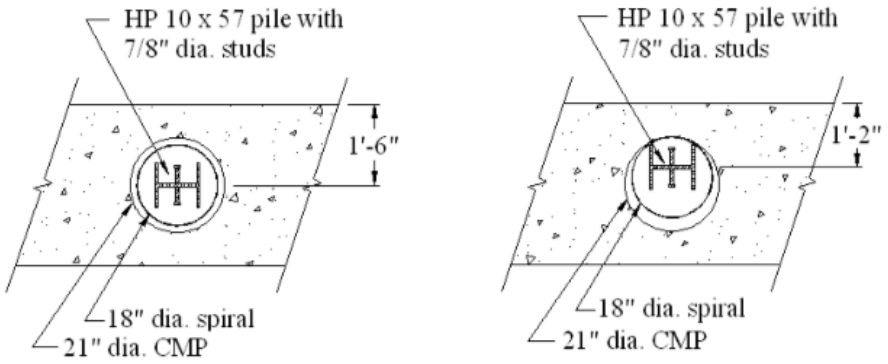

Figure 2.17 *Centered (left) and offset (right) pile location*. (Wipf, Klaiber, & Hockerman, 2009)

The specimens were instrumented with linear variable deflection transducers (LVDT) and strain gauges on the piles and surfaces of the specimen to record stresses and deflections during loadings. The single pile abutment cap specimens were loaded up to 4.5 times their design load, the double pile abutment cap specimens that were already producing more severe loading conditions than would be seen in the field were loaded to twice their design load, and the single pile pier cap specimens were loaded to more than five times their design load (Wipf, Klaiber, & Hockerman, 2009).

Through this testing and instrumentation setup, this connection was deemed to be adequate and cause of no concern for punching shear failure. The differential displacements between the piles, CMPs, and precast caps were not significant, but the presence of the CMP voids did cause tensile stress concentrations along the side of the specimen.

This connection was then documented within the same report by Iowa State University (Wipf, Klaiber, & Hockerman, 2009) during the replacement of a bridge in Boone

County, Iowa. The replacement bridge was designed to use integral abutments using abutment caps with CMP voids for the five H-piles per abutment and used pier caps with CMP voids for the nine pipe piles per pier. After the piles were driven and cut to their final elevation, the caps were delivered to the site and placed in approximately fifteen minutes without any significant issues. Figures 2.18 through 2.22 show the process of placing the caps and filling the CMP voids with concrete.

Figure 2.18 *Abutment cap being lowered in place*. (Wipf, Klaiber, & Hockerman, 2009)

Figure 2.19 *Abutment cap final position (left) H-pile in CMP void (right*). (Wipf, Klaiber, & Hockerman, 2009)

Figure 2.20 *Pier cap being lowered in place.* (Wipf, Klaiber, & Hockerman, 2009)

Figure 2.21 *Pier cap final location (left) Pipe pile in CMP void (right).* (Wipf, Klaiber, & Hockerman, 2009)

Figure 2.22 *Finished abutment cap with CMP voids filled*. (Wipf, Klaiber, & Hockerman, 2009)

After the abutment and pier caps had been finished, the beams were placed onto the caps. With the beams placed at their design elevations, the precast panels were set and post-tensioned. After the panels were finished, the formwork for the cast-in-place concrete around

the beams ends was prepared on the abutment and pier caps. Figures 2.23 through 2.27 show the process of placing the beams, preparing the beam ends to be cast in concrete at the abutment and pier caps, and the final bridge. Unloading the girders and placing them to their final location took approximately ten minutes, each, and all the girders were placed within a day.

Figure 2.23 *Beam end supported by abutment cap by steel beam to provide clearance for concrete placement*. (Wipf, Klaiber, & Hockerman, 2009)

Figure 2.24 *Bridge girders in final locations*. (Wipf, Klaiber, & Hockerman, 2009)

Figure 2.25 *Pier cap diaphragm formwork for beam ends*. (Wipf, Klaiber, & Hockerman, 2009)

Figure 2.26 *Abutment cap diaphragm formwork for beam ends*. (Wipf, Klaiber, & Hockerman, 2009)

Figure 2.27 *Completed bridge*. (Wipf, Klaiber, & Hockerman, 2009)

The precast substructure caps were all set in a short amount of time and without difficulty, but construction had to wait for precast elements to be fabricated and delivered to site. The precast elements worked well for the entirety of the bridge, but some connections, such as the cast in place integral abutment required concrete cure time that delayed construction (Wipf, Klaiber, & Hockerman, 2009).

Another study was done by The University of Washington to determine the seismic adequacy of connections of substructures using corrugate metal ducts, specifically the column to cap beam connection (Figure 2.28 and 2.29).

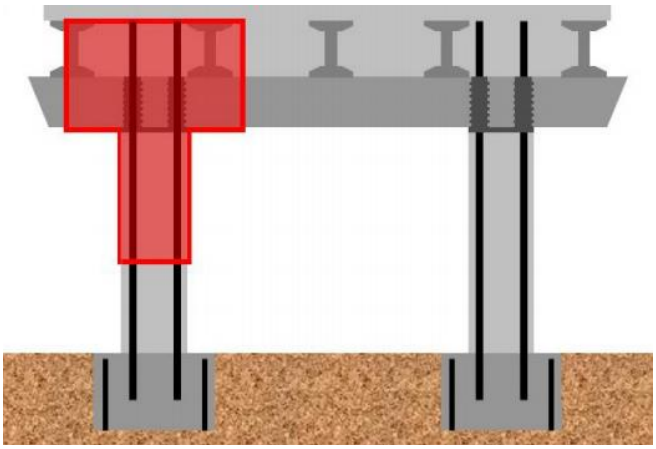

Figure 2.28 *Column-cap beam connection with large diameter bars concept.* (Kapur, et al., 2012)

The design for this test was based on the large-diameter bars anchored in corrugated metal ducts connection used by Florida and was then implemented by the Washington State DOT. An example bridge in Washington State is shown in Figures 2.30 and 2.31. (Kapur, et al., 2012)

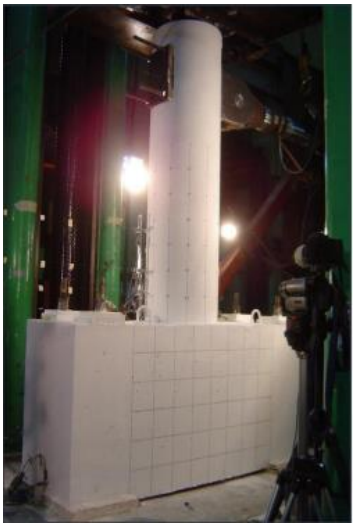

Figure 2.29 *Column-cap beam connection tested at the University of Washington*. (Kapur, et al., 2012)

Figure 2.30 *Corrugated ducts in precast cap beam in Washington State*. (Kapur, et al., 2012)

Figure 2.31 *Placement of cap beam on column bars inserted in corrugated ducts in Washington State*. (Kapur, et al., 2012)

California and Michigan also reported using a corrugated metal duct to provide a void for connecting precast columns and precast crossheads. These ducts were limited in diameter, one design was 1.5 inches, due to the heavy reinforcement within the crosshead and cap beams, which caused very tight tolerances being applied to the column reinforcement cage. To ensure these tight tolerances were met, templates were used to ensure duct locations in the crossheads would align with the column steel. This connection, also known as a grouted vertical duct, has positive factors such as being capable of providing large tolerances, are inexpensive, and can provide less interference with cap beam longitudinal steel. The main disadvantage to the grouted vertical duct is the fact that in order to complete the connection, an exposed top surface will result, which may allow for infiltration of moisture or other chemicals leading to durability issues of the connection (Hewes, 2013).

Another method used to connect precast elements, especially piers to pier caps, is mechanical couplers, such as grouted reinforcing splice couplers. These couplers involve a steel sleeve that connects reinforcing bars from either side of the coupler, typically between elements, and then is filled with a grout material to complete the connection. This load transfer makes the design of these connections simple for designers since it can be assumed to be an "emulative" connection that behaves just as a cast-in-place construction joint.

This assumption of an "emulative" design was investigated by the Michigan Department of Transportation (MDOT) (Jansson, 2008). The scope of this project was to determine the suitability of two grout-filled mechanical couplers, the Lenton Interlok and the NMB Splice Sleeve. The Lenton Interlok is a steel sleeve having one end connection completed via threaded reinforcing bar and the other end is connected through having a reinforcement bar placed into the grout filled sleeve (Figure 2.32). The NMB Splice Sleeve is

a steel sleeve that has both ends being connected to reinforcing bars through the bars being placed into the grout filled sleeve (Figure 2.33).

Figure 2.32 *Lenton Interlok for #6 reinforcing bar*. (Jansson, 2008)

Figure 2.33 *NMB Splice Sleeve for #6 reinforcing bar*. (Jansson, 2008)

Each specimen was to undergo four testing procedures in accordance to procedures for testing mechanical splices of reinforcing bars, which were a slip test, high cycle fatigue test, a secondary slip test, and an ultimate load test.

Both couplers met the AASHTO LRFD requirement of no more than 0.010 inch of slip both for the initial slip test and the secondary test. Both couplers also met the ultimate load requirement by AASHTO LRFD of 125% F_y. Due to the findings of this MDOT

investigation, the use of grouted reinforcing bars couplers was recommended to be implemented in future projects (Jansson, 2008).

Many projects have reported using these grouted reinforcing bar couplers and having the same pros and cons to the connecting device (Hewes, 2013). The pros being a history of use and good performance in the precast building industry as well as the bridge construction industry, continuity of longitudinal reinforcement with full development, and minimal exposed surface resulting in fewer paths for moisture and infiltration. The cons were very tight tolerances, sometimes less than 0.25 inches, and the fact that two grouting operations were required, which were to fill the sleeve and filling the bedding layer. A bridge in Fort Meyers, Florida used grouted reinforcing bar couplers to connect precast columns to the foundation as well as the precast caps. As of 2013, the bridge was in use for eighteen years and had yet to pose any serviceability issues related to the couplers. It was reported that the 55 ft, full height, precast columns were installed at a pace of six per day, which is credit to the ease of installing the grouted reinforcing bar couplers. Another project in Troop County, Georgia also used grouted reinforcing bar couplers to connect precast columns to cast-in-place footings and precast bent caps. Texas, Utah, Alabama, and New Hampshire also reported the use of grouted reinforcing bar couplers to connect precast bent caps to precast columns (Hewes, 2013).

The issue with grouted reinforcing bar couplers though, not only for substructure elements, is the tight construction tolerances that are imposed by the size of the sleeves and the size of the reinforcing bars. To alleviate this issue, it is suggested to use templates to ensure elements to be connected via these couplers will be in their designed locations. Another issue, not necessarily for only grouted reinforcing bar couplers, but for prefabricated

substructure elements is grade control. This can be addressed with grouted reinforcing bar couplers since shims may be introduced to the connection area to provide additional elevation to correct any grade issues due to the presence of precast substructure elements (Hewes, 2013). Figures 2.34 and 2.35 show typical connection details for precast columns and precast footings.

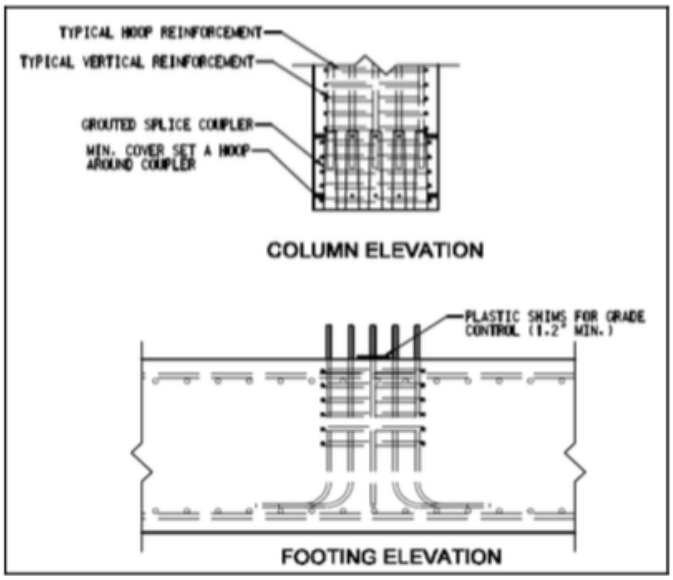

Figure 2.34 *Column/Footing Grout Splice Coupler*. (Hewes, 2013)

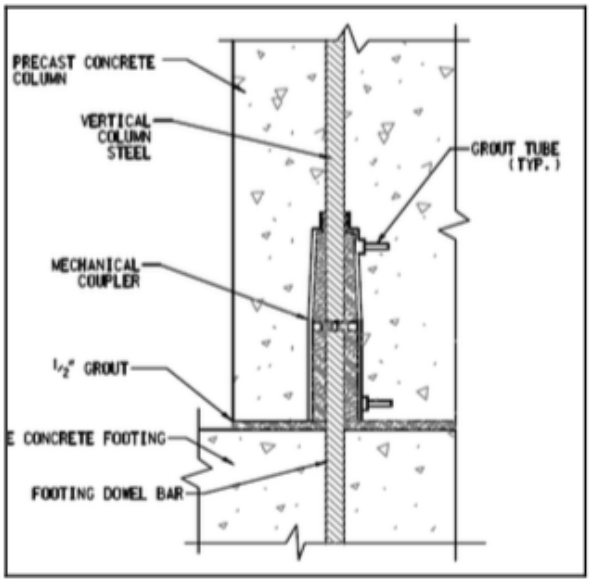

Figure 2.35 *Column/Footing Grout Splice Coupler*. (Hewes, 2013)

Massachusetts has also used the grouted splice coupler to connect precast abutment walls to precast footings (Figure 2.36), but they have also reported using these couplers to connect longitudinal bars in precast superstructure (Figure 2.37) (Kapur, et al., 2012).

Figure 2.36 *Precast abutment wall and footings with grouted coupler connections in Massachusetts.* (Kapur, et al., 2012)

Figure 2.37 *Grouted coupler as continuity splice over pier in Massachusetts*. (Kapur, et al., 2012)

(Hewes, 2013) describes the advantages and disadvantages of connection types such as grout pocket, grouted vertical duct, grouted sleeve coupler, and bolted connection for bridges using precast elements. For the grouted sleeve coupler, the positive constructability

aspect was the fact these couplers have minimal interference with surrounding reinforcement. However, they did have excessively tight tolerances due to product specifications, and the installation of this connection requires high level construction and the constant use of a grout pump. As far as the durability of the grouted sleeve coupler, the advantages were that they are well-protected connectors and can implement the use of epoxy-coated materials as well. No disadvantages for durability were listed. Force transfer was the last facet to judge the grouted sleeve couplers, and the positives listed were the excellent ductility and anchorage of connectors, while the disadvantage was the small rotational stiffness provided by the couplers (Hewes, 2013).

Grouted reinforcing steel couplers were tested for strength and durability in bending, specifically to represent the field application of the connection used in the Keg Creek Bridge located in Pottawattamie County, Iowa (Hosteng, Phares, Abu-Hawash, Bierwagen, & Nelson, 2015). To accomplish this, seven specimens were erected in two parts and connected via two #14 epoxy-coated grouted reinforcing steel couplers in the tension zone of the square columns (Figure 2.38). Five of the seven specimens utilized the W.R. Meadows 588-10K grout to fill the grout bed, while two used UHPC. The specimens were erected, underwent a "dry-fit" for the coupler connections, were grouted together per manufacturer's instructions, and were set up for four-point testing (Figure 2.39).

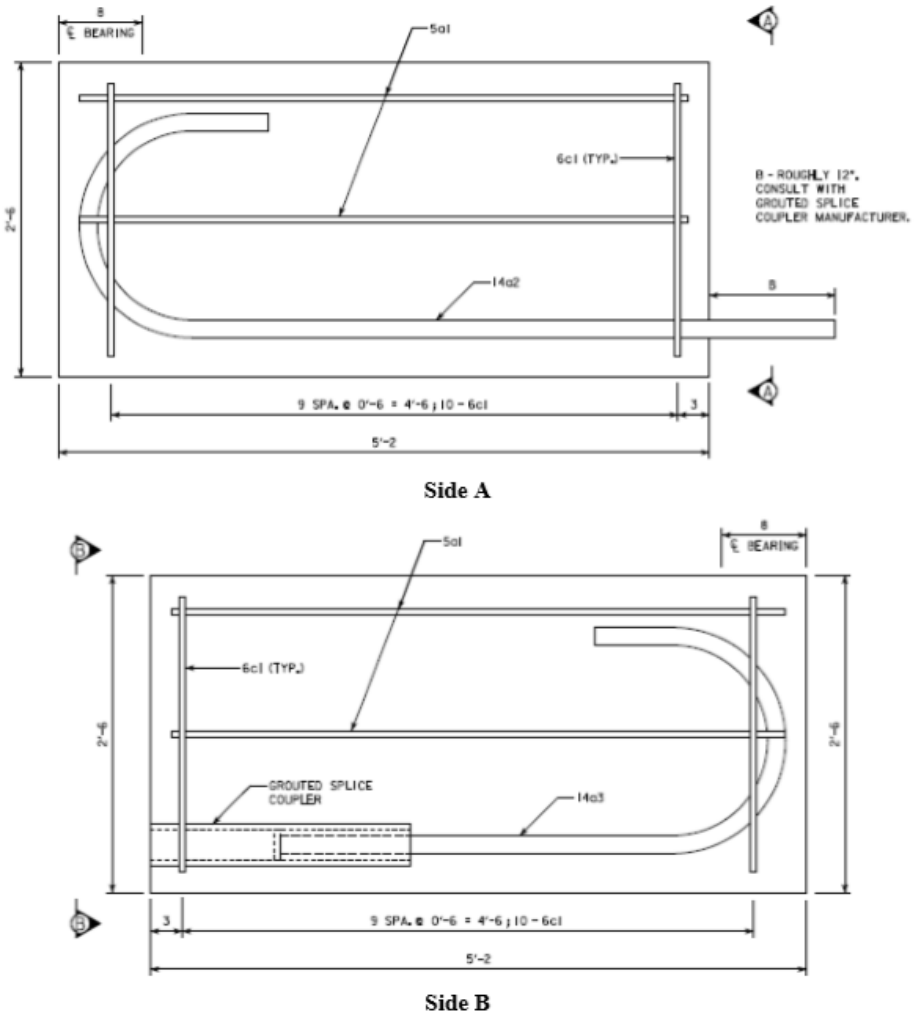

Figure 2.38 *Grouted coupler specimen plan view*. (Hosteng, Phares, Abu-Hawash, Bierwagen, & Nelson, 2015)

Figure 2.39 *Specimen setup for static four-point bending test*. (Hosteng, Phares, Abu-Hawash, Bierwagen, & Nelson, 2015)

Six of the specimens were to undergo static testing to peak loads, while one of the specimens was tested to fatigue under 1 million cycles under a load specifically designed to induce a fatigue stress specified by the American Association of State Highway and Transportation Officials (AASHTO) Load and Resistance Factor Design (LRFD) Specifications when a member is being fatigue-loaded greater than or equal to 1 million cycles.

It was suggested that an axial load be applied to the ends of the specimen to represent the dead load of the bridge on the columns and that these additional loads may have an impact on results of the four-point bending tests (Figure 2.40).

Figure 2.40 *Specimen setup for static four-point bending test with applied axial load.* (Hosteng, Phares, Abu-Hawash, Bierwagen, & Nelson, 2015)

In addition to the four-point bending test, corrosion testing was done on three cylinders with the grouted reinforcing steel coupler to determine if corrosion of the reinforcing steel was probable when submerged in a 3% chlorine bath for six months (Figure 2.41).

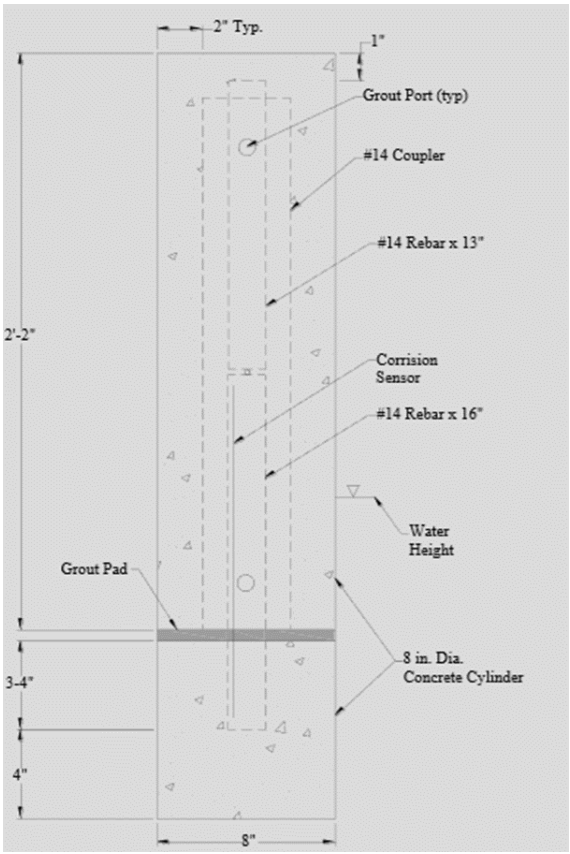

Figure 2.41 *Cross-section view of coupler specimens for chloride penetration tests*. (Hosteng, Phares, Abu-Hawash, Bierwagen, & Nelson, 2015)

The following conclusions were made based on the results of testing the specimens (Hosteng et al. 2015):

- The UHPC grouting material hindered the crack from forming instantaneously upon loading of the specimen, unlike that of the W.R. Meadows 588-10K grout, but there was no apparent gain in reducing the level of cracking during loading and unloading.
- Axially loading of the specimen resulted in minimal effects on the performance of the grouted reinforcing steel couplers subjected to bending, as well as the initiation of cracking at the grout interface.
- Empirical calculations were well correlated to the results of the static four-point bending tests, hence verifying the design assumptions.

- With no cracks present in the three cylinders for the corrosion testing on the couplers, no evidence of corrosion was detected.

Phase I for the research project done for this thesis involved three specimens that were tested to determine the strength, durability, and constructability of two proposed connections for integral abutments under ABC applications compared to a cast-in-place control specimen (Hosteng, Phares, & Redd, 2016). The two proposed connections were: grouted reinforcing bar coupler (GRBC) (Figure 2.42) and pile couplers (Figure 2.43).

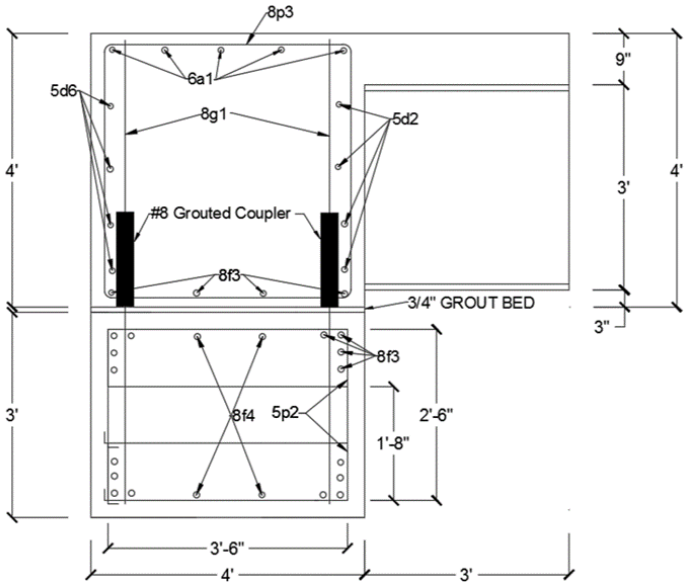

Figure 2.42 *Grouted reinforcing bar coupler*. (Hosteng, Phares, & Redd, 2016)

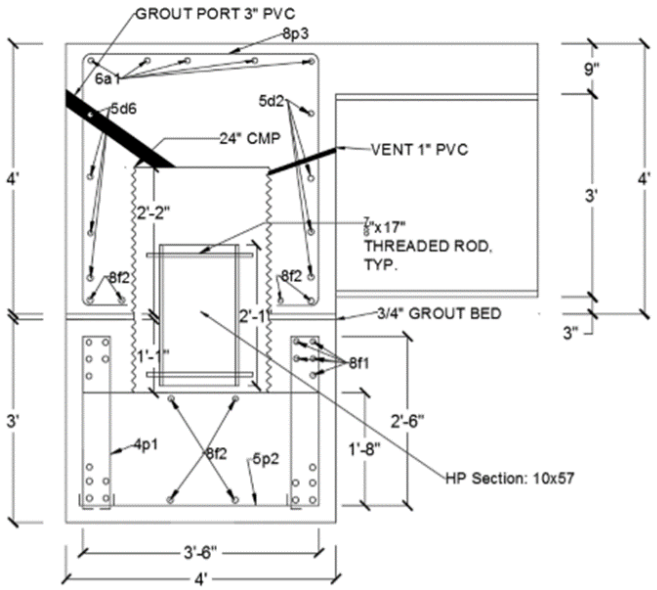

Figure 2.43 *Pile coupler*. (Hosteng, Phares, & Redd, 2016)

The design philosophy behind the two connections was:

- Grouted reinforcing bar coupler
    - Due to previous success with the connection, the need for a closure pour over the integral connection could be eliminated with the presence of the grout-filled mechanical couplers providing the integral connection through protruding reinforcing bars from one element being inserted into sleeves on the other element to be connected, and then filling the sleeve with a grouting material. The ABC application for this connection would likely be suspending the element via crane and placing it in the final location.
- Pile coupler
    - The basis of this design was the previous use of HP-sections being cast in grout within CMP voids in a precast pile cap. The HP-section would be suspended within a CMP void in a precast element and slid into place onto a precast pile cap with matching CMP void locations to receive half of the

suspended HP-section. This void would then be filled with a grouting material just as the previously used precast pile cap/pile connection. This connection allows for the ABC application of "slide-in" construction and alleviates small tolerances that are present in the grouted reinforcing bar coupler connection.

Construction of the three specimens did not pose any significant challenges. The cast-in-place control specimen was erected by forming the steel reinforcement cage (Figure 2.44), and then simply pouring concrete.

Figure 2.44 *Cast-in place integral diaphragm*. (Hosteng, Phares, & Redd, 2016)

The grouted reinforcing bar coupler specimen had the pile cap cast with protruding reinforcing bars (Figure 2.45); it utilized a match-casting procedure (Figure 2.46) to cast the sleeves for the connection in the integral diaphragm element; the integral diaphragm was placed on top of the pile cap via crane (Figure 2.47); and finally the sleeves were filled with grout to complete the connection.

Figure 2.45 *Grouted coupler pile cap*. (Hosteng, Phares, & Redd, 2016)

Figure 2.46 *Grouted coupler template*. (Hosteng, Phares, & Redd, 2016)

Figure 2.47 *Integral diaphragm placement*. (Hosteng, Phares, & Redd, 2016)

The pile coupler was constructed like the grouting reinforcing bar coupler, by having two elements cast with a part of the connection, but instead of protruding reinforcing bars and sleeves, each element had CMP voids. The integral diaphragm had a longer CMP void with the HP section being suspended within the void (Figure 2.48 and Figure 2.49), while the pile cap had CMP voids half the length of the HP section (Figure 2.50).

Figure 2.48 *Side view of CMP void*. (Hosteng, Phares, & Redd, 2016)

Figure 2.49 *Suspended HP sections*. (Hosteng, Phares, & Redd, 2016)

Figure 2.50 *CMP void in pile cap*. (Hosteng, Phares, & Redd, 2016)

The elements were cast with the CMP voids and then placed together, then the HP-section was lowered into place via a pulley system, and then the CMP void was filled with grout to complete the connection.

To test the strength and durability of the connections, the specimens were tested in the structural laboratory with the setup shown in Figure 2.51.

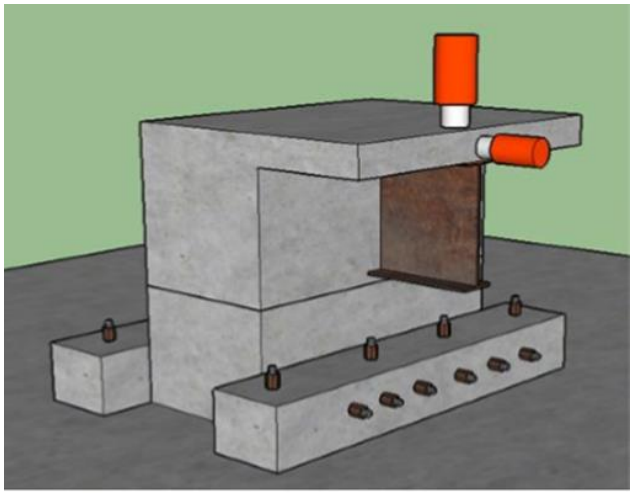

Figure 2.51 *Three-dimensional drawing of laboratory test setup, front*. (Hosteng, Phares, & Redd, 2016)

The actuators were placed on the specimen to resemble live and thermal loads typically induced on a bridge abutment. The horizontal actuator was set to apply a load of 100 kips onto the face of the steel beam to relate to loading induced by thermal contraction of the bridge superstructure, while the vertical actuator was designed to apply a load of 400 kips to simulate both live loading on the abutment, as well as loading from thermal expansion. The results of this study led to the following conclusions (Hosteng, Phares, & Redd, 2016):

- Tight tolerances typically seen with grouted reinforcing bar couplers were alleviated through a match-casting procedure.
- Strength and durability of the grouted reinforcing bar coupler specimen were similar to the cast-in-place control specimen. The crack width of the back face of the integral abutment was measured at the precast joint to be 0.035 in. for the grouted reinforcing bar coupler, and 0.019 in. for the cast-in-place control specimen, which means the grouting reinforcing bar coupler's resulting crack width was about 1.8 times greater than the control specimen.

- Strength and durability of the pile coupler was less favorable than the grouted reinforcing bar coupler, with a crack width measured to be approximately 1.75 in., which was significantly greater than the control specimen.
- The constructability of the pile coupler was more ideal than the grouted reinforcing bar coupler simply due to the ability of the pile coupler allowing for the slide-in application of ABC, while the grouted reinforcing bar coupler would have to be suspended via crane and lowered into place.
- Improvements to the pile coupler would be:
    - Increasing the length of the HP-section.
    - Increasing the number of threaded rods/shear studs on the steel section.
    - Increasing/revising the amount of reinforcing steel in the abutment.
    - Using two HP-sections to act as a force couple.

Since its first appearance in Colorado in 1920, the integral abutment bridge has been on the rise in the United States bridge engineering community. A survey conducted by The University of Maryland in 2009 resulted in 41 state department of transportation reporting their use of integral abutment bridges (Figure 2.52); while out of the nine that do not, three states (Alabama, Delaware, and Louisiana) have never put the integral abutment to use, three states (Alaska, Arizona, and Mississippi) discontinued the connection due to serious problems encountered, and three states (Florida, Texas, and Washington) discontinued the use of the connection for other reasons (Paraschos & Amde, 2011).

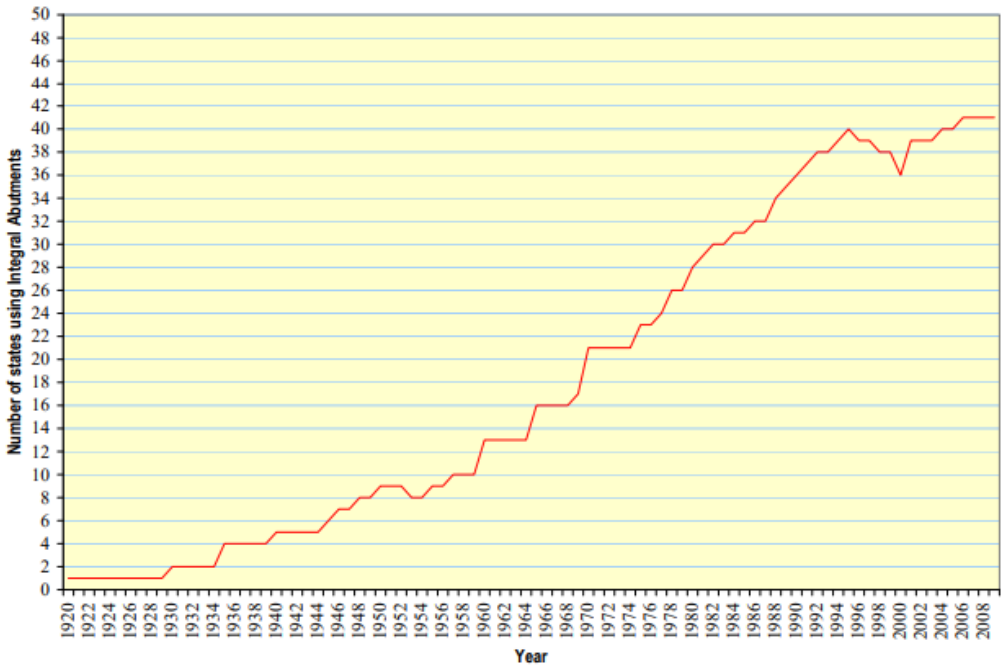

Figure 2.52 *Evolution of integral abutment bridges in the United States*. (Paraschos & Amde, 2011)

Some of the serious problems causing the discontinuation of the integral abutment bridge in some states were derived from soil issues, such as extreme temperature variation, frozen soil, and soil liquefaction. Less serious problems that caused the discontinuing of integral abutment bridges were some states found no benefit to their use opposed to conventional construction, or that the cost for installing the integral abutment system was uncompetitive from a cost perspective. One state, Washington, decided to continue with the semi-integral abutment bridge system instead due to the ability for the structure to move during seismic events, decreasing the seismic forces within the structure.

The survey also questioned the comparison of construction and maintenance costs between integral abutment bridges and conventional bridges. The results of this part of the survey are shown in Figures 2.53 and 2.54 (Paraschos & Amde, 2011).

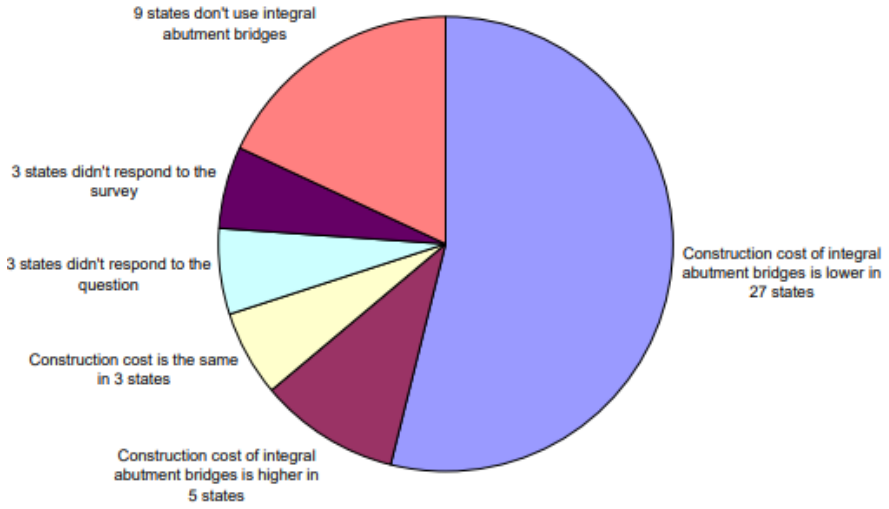

Figure 2.53 *Status of comparative construction costs of integral abutment and conventional bridges*. (Paraschos & Amde, 2011)

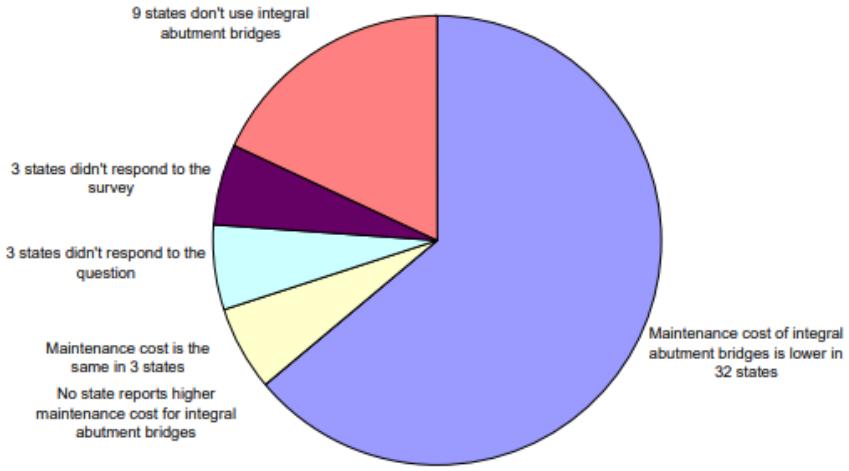

Figure 2.54 *Status of comparative maintenance costs of integral abutment and conventional bridges*. (Paraschos & Amde, 2011)

Since AASHTO had yet to explicitly address any design of integral abutment bridges, an investigation into state department of transportation bridge design manuals was conducted by the University of Wisconsin – Milwaukee to understand and compare the design criteria and parameters used by various states during the design of integral abutment and jointless bridges (Tabatabai, Magbool, & Fu, 2017).

(Tabatabai, Magbool, & Fu, 2017) provides a few example definitions for integral bridges or integral/semi-integral abutments, and they all have a similar definition as a bridge that has the superstructure cast integrally to the substructure. The definitions also delve into the fact that integral bridges are supported by a single row of flexible vertical piles, rigidly connected to the superstructure, which allow for the longitudinal movement. The University of Wisconsin – Milwaukee also reported the states that do and do not specifically consider integral or semi-integral abutment bridges (Figure 2.55) and if states had preference of using integral abutment bridges rather than traditional designs (Figure 2.56).

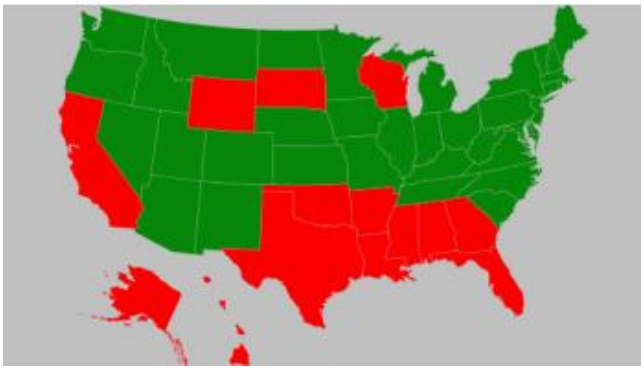

Figure 2.55 *Graphical representation of states specifically considering integral/semi-integral bridges (green*). (Tabatabai, Magbool, & Fu, 2017)

Figure 2.56 *Graphical representation of states preferences: Integral over traditional? Yes (green), No (semi-integral preferred) (yellow), Not mentioned (red*). (Tabatabai, Magbool, & Fu, 2017)

For the states that implement integral abutment bridges in their bridge design manuals, the maximum skew angle (Figure 2.57), pile type (Figure 2.58), maximum permissible length of steel and concrete bridges (Figure 2.59) pile orientation (Figure 2.60), and pile minimum embedment length (Figure 2.61) were reported.

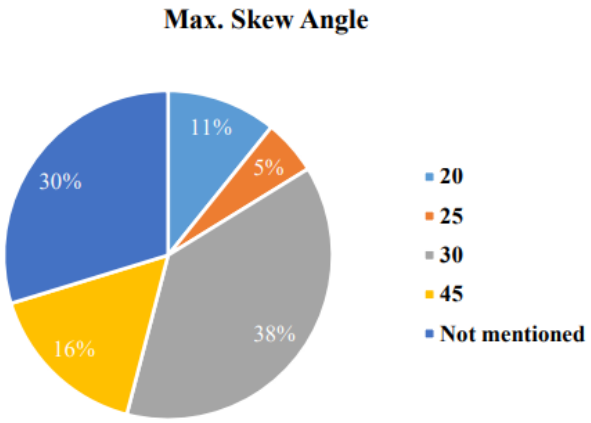

Figure 2.57 *Graphical representation of states preferences: Integral over traditional? Yes (green), No (semi-integral preferred) (yellow), Not mentioned (red*). (Tabatabai, Magbool, & Fu, 2017)

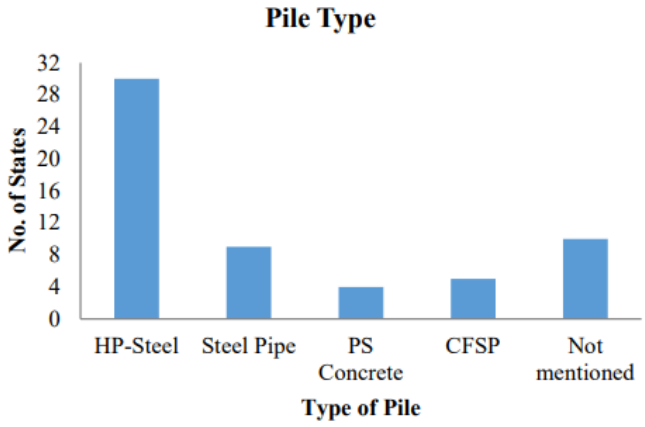

Figure 2.58 *Pile types for integral abutment bridges*. (Tabatabai, Magbool, & Fu, 2017)

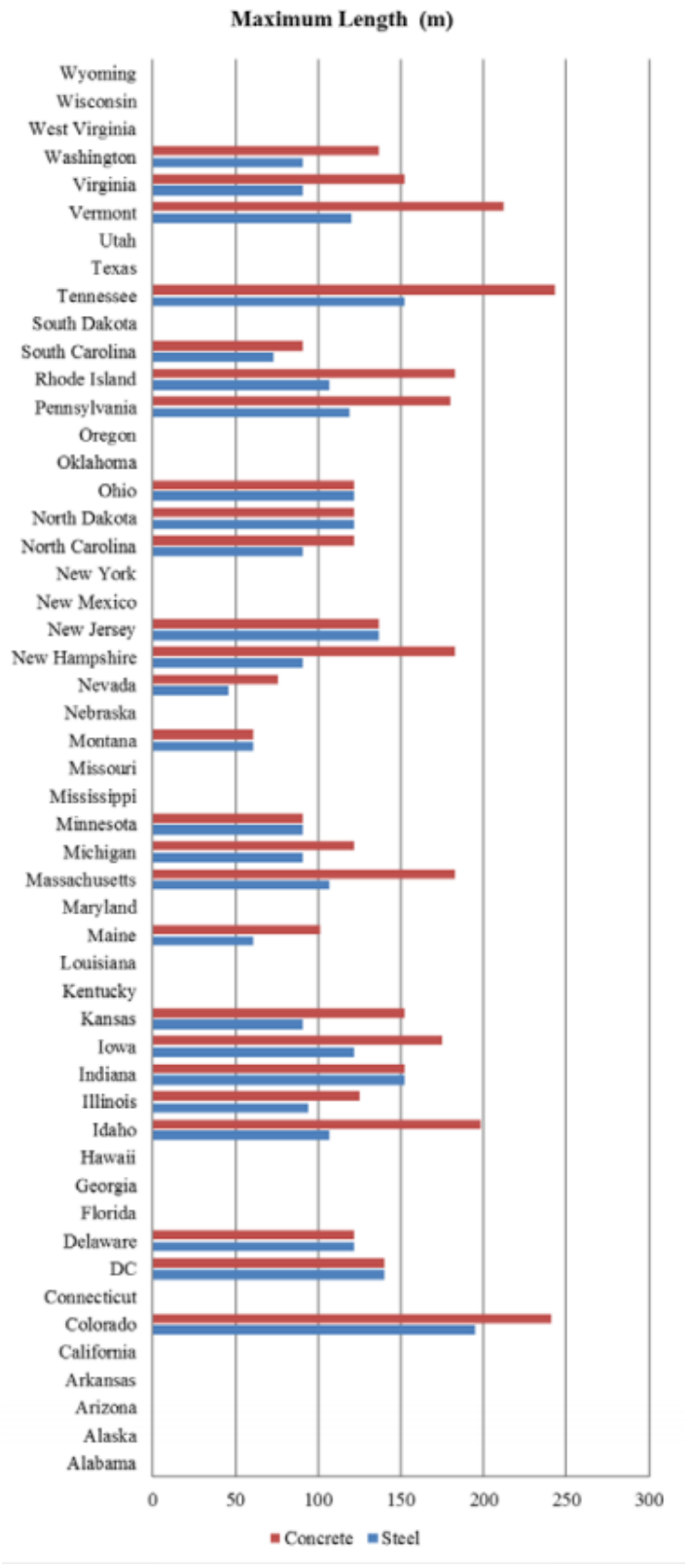

Figure 2.59 *Maximum permissible length of steel and concrete integral abutment bridges.* (Tabatabai, Magbool, & Fu, 2017)

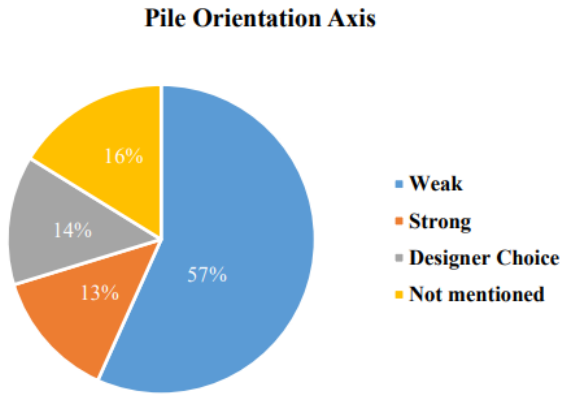

Figure 2.60 *Pile orientation (bending axis) in integral abutment bridges*. (Tabatabai, Magbool, & Fu, 2017)

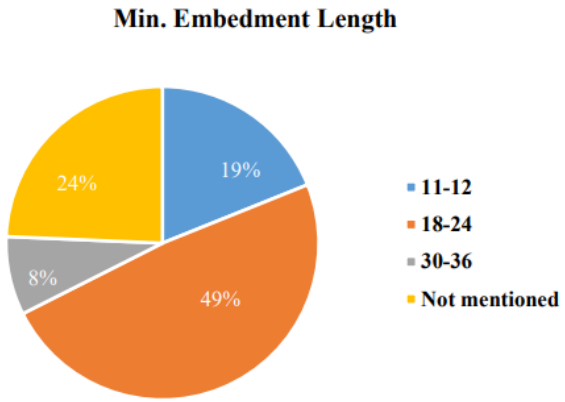

Figure 2.61 *Pile minimum embedment length in integral abutment bridges*. (Tabatabai, Magbool, & Fu, 2017)

The behavior of integral abutment bridges had been shown to be different from predictions made during the design process for the bridge, sometimes displacements due to thermally induced loads differed in the order of 10% to 25%. For this reason, a long-term, seven years, field monitoring of four integral abutment bridges (Figure 2.62) was conducted in Pennsylvania (Kim & Laman, 2012).

Figure 2.62 *Instrumented bridges. (a) Bridge 109; (b) Bridge 203; (c) Bridge 211; (d) Bridge 222* (Kim & Laman, 2012)

The monitoring of PennDOT Structures 203, 222, 211, and 109 started in November 2002, September 2004, November 2003, and September 2005, respectively. Traffic was delayed until December 2007 for all four bridges due to a severe environmental issue. Data collected from weather stations started in August 2002, and consisted of solar radiation, temperature, rainfall, wind speed, and wind direction. The field monitoring data recorded for the integral abutment bridges was abutment displacement, backfill pressure, abutment rotation, girder rotation, girder bending moment, girder axial force, pile moment, pile axial force, and strain in approach slab.

All four bridges have four precast prestressed concrete girders with a cast-in-place deck, and the integral abutments are supported by a single row of weak-axis oriented HP12X74 steel piles. The instrumentation used was backfill pressure cells, abutment

displacement extensometers, girder axial force and moment strain gauges, girder tiltmeters, abutment tiltmeters, pile moment and axial force strain gauges, and approach slab sister-bar strain gauges.

(Kim & Laman, 2012) made the following conclusions after deducing the seven-year monitoring results for the four integral abutment bridges:

1. The abutment moves significantly over time; hence the displacement of the abutment should be considered during design. These displacements for all four bridges underwent increasing nonlinear displacements due to thermal loading during the monitoring timeframe.
2. The time-dependent effects in precast concrete integral abutment bridges should be considered in the unrestrained expansion design calculation of the bridge.
3. Pressures due to backfill on the abutment fluctuate with temperature change. Initially there is a discernable difference between pressures on the top and bottom of the abutment, but these differences diminish over time. All four bridges had their backfill pressures reach passive pressures, which validates this assumption during design.
4. The AASHTO design assumption of a rigid connection between the girders and abutments should be reconsidered due to recorded differential rotation between the girders and abutments at the abutment-to-backwall construction joint. This flexibility of the connection could affect integral abutment bridge behavior and should be considered during pile design.
5. The bending moments and axial forces from the girders caused by thermal loading should be an additional design consideration.

6. Superstructure temperature can be represented by ambient temperature since the differences recorded during the monitoring period were negligible. The range of temperatures recorded for the 7-day mean temperature range shows the AASHTO LRFD temperature range is conservative.
7. The monitoring results showed the introduction of traffic loading insignificantly changes the responses recorded for the integral abutment bridges.

Another bridge was field monitored by the Utah State University (Huffaker, 2013). The bridge under investigation was the 400 South Street Bridge in Salt Lake City, Utah (Figures 2.63 and 2.64). This four-lane bridge would typically see 29,447 vehicles for an Average Daily Traffic (ADT), and an Average Daily Truck Traffic (ADTT) of 6%.

Figure 2.63 *Aerial view of the 400 South Street Bridge*. (Huffaker, 2013)

Figure 2.64 *Photograph of 400 South Street Bridge in elevation view*. (Huffaker, 2013)

The curved deck is supported by three spans of eight prestressed girders that are divided in three straight segments of 84.5-ft, 150.4-ft, and 84.5-ft placed at skewed angles of 0.2 degrees, 5.6 degrees, and 11.7 degrees to accommodate the 8-inch curved deck. The bridge is supported at the ends by integral abutments that are 3.0-ft thick and 11.0-ft tall (Figure 2.65), and each abutment is supported by twelve 12-in diameter piles spaced at 6-ft.

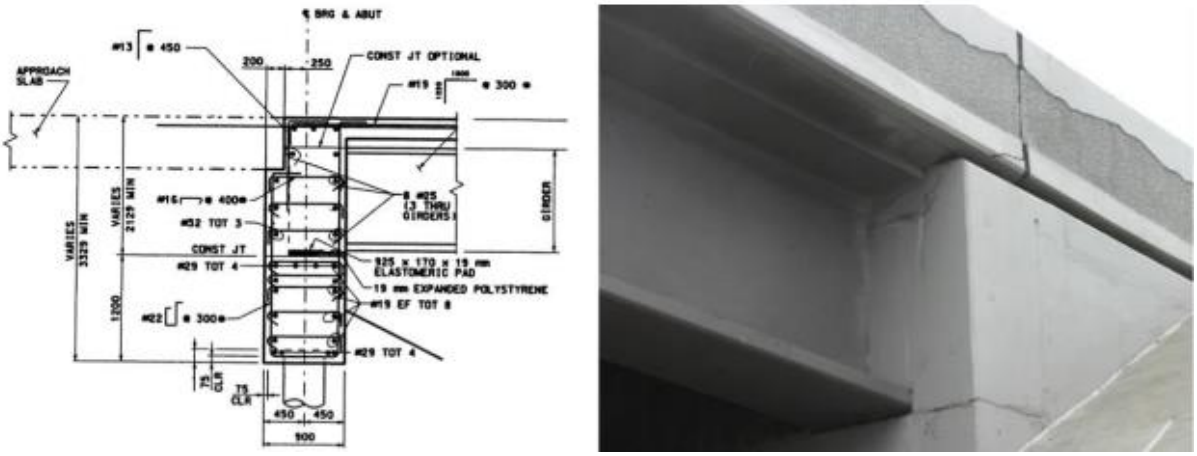

Figure 2.65 *Detail view of abutment with reinforcing shown along with photo of actual abutment*. (Huffaker, 2013)

The bridge was monitored for variations in displacement due to temperature, primarily changes in the length of the bridge and how those changes affected the expansion joint gaps. Monthly surveys done at approximately the same time of morning, in addition to one full-day survey, utilized markers placed on various points along the abutments, girders, and approach slabs (Figure 2.66) of the bridge and surveying equipment to measure the changing length of the bridge, and a conventional tape measure was used to measure the expansion joint gaps.

Figure 2.66 *Survey targets at approach slab*. (Huffaker, 2013)

Evaluating the results of the year-long study, (Huffaker, 2013) made the following conclusions regarding the 400 South Street Bridge in Salt Lake City, Utah:

- Small movements due to changes in temperature were recorded, but movements were enough to cause damage to one abutment.
- There were differences in longitudinal movement on either side of different spans of the bridge, and opposite corners of the bridge expanded and contracted differently, leading to the conclusion there is a twisting motion throughout thermal loading which could lead to moments being applied to abutments.
- Temperature design averages and gradients from AASHTO LRFD Specifications were near what was recorded during the monitoring period.

To do a parametric study of the 400 South Street Bridge in Salt Lake City, Utah, a finite element model was required. Two models were created to simulate the bridge, a detailed solid model and a simplified model. The detailed solid model (Figure 2.67) was created using SAP2000 software. Solid elements were used for the girders, abutments, bents, and bridge deck, while the columns and piles were modeled through frame elements.

Surface springs to simulate soil interaction were placed on the abutment face, and the stiffness of these springs were tabulated on typical properties of granular backfill.

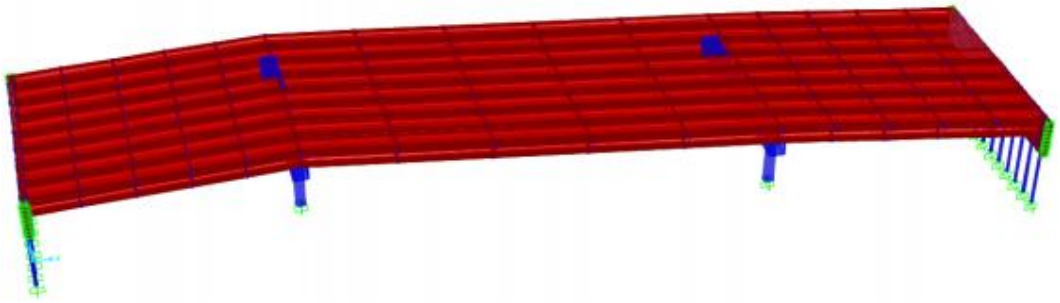

Figure 2.67 *3D view of solid SAP model*. (Huffaker, 2013)

A uniform temperature load of 50 °F was applied to the concrete girders and deck, and changes in stress between the girders and abutment were plotted in contours. Figure 2.68 shows the principal stress levels of the abutment, with the highest concentrations being the purple and red contours which validated the spalling observed during the monitoring process. Figure 2.69 shows the difference in stress between girders along the north abutment for the bridge, which were more than double from one exterior girder to the other.

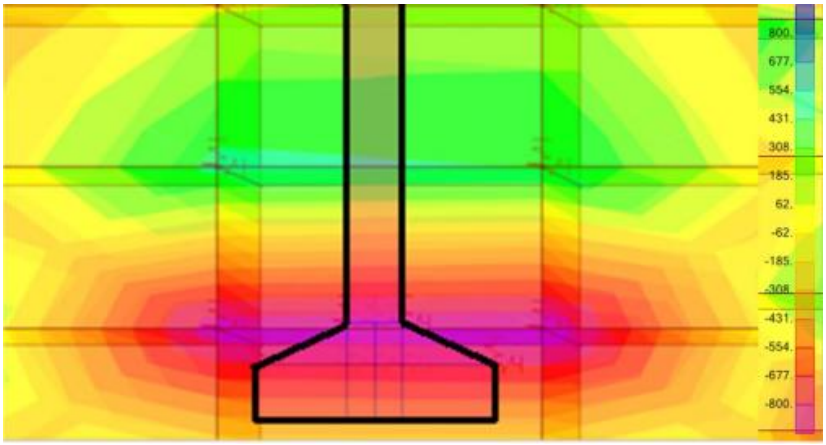

Figure 2.68 *View of model abutment with stress contours around girder bottom*. (Huffaker, 2013)

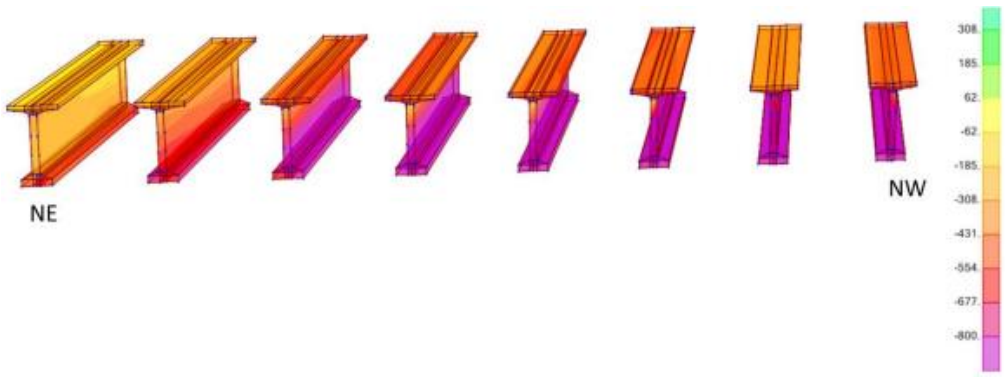

Figure 2.69 *View of stress contours on model girders*. (Huffaker, 2013)

To do a parametric study of how different bridge properties affect resulting stress concentrations, a simplified model was created using SAP2000 software (Figure 2.70). This model used frame elements for all components of the bridge, except the deck which used solid elements. The model was validated through the results of the detailed solid model and measurements recorded during the monitoring period, and then the parametric study was conducted to investigate how the following changes to bridge properties affect resulting stress concentrations for the integral abutment bridge: abutment and pier offset, skew, span length, and temperature gradient.

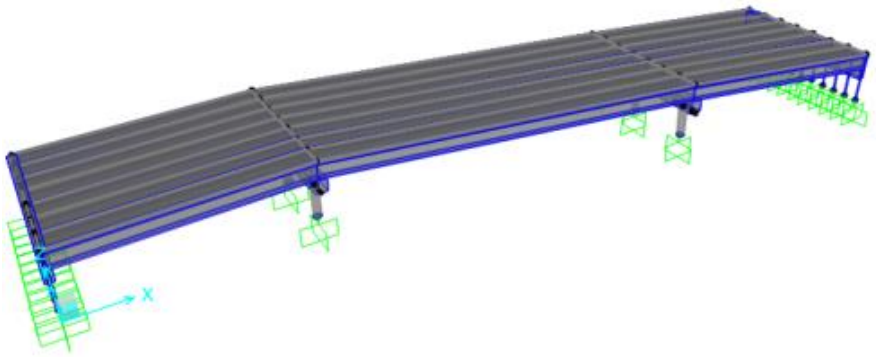

Figure 2.70 *View of simplified SAP model using frame elements*. (Huffaker, 2013)

The results of the parametric study led to the following conclusions (Huffaker, 2013):

- The simplified model displayed the effects of length, skew, and temperature gradient cause the bending moment about the weak-axis of the abutment to approach tabulated cracking moment.
- For every five degree increase in skew, an increase of approximately 50% to 65% of weak-axis bending moment applied to the abutment was recorded.
- An increase in the weak-axis bending moment applied to the abutment of approximately 60% was calculated by doubling the span length.
- A substantial increase in the weak-axis bending moment applied to the abutment, approximately 200%, was the result of a 20 °F increase in the temperature gradient between the girders and bridge deck.

Is was concluded by (Huffaker, 2013), after studying monitoring results and finite element analyses, that the unequal changes in length of the bridge are likely due to the lateral movement of the skewed support of the north abutment. Also, the different aspects of the bridge properties present at the 400 South Street Bridge such as skew, curvature, span length, and detailing could be the cause for the abutment cracking; it was recommended that additional design checks be done for integral abutment bridges with multiple unique bridge properties and the demand of these abutments can be better predicted through the use of finite element models.

Two integral abutment bridges were monitored in Illinois, a four-span continuous bridge with span lengths of 125 ft, 152 ft, 152 ft, and 120 ft and a single-span bridge with a length of 184.5 ft. The four-span bridge was, at the time of construction, near the Illinois Department of Transportation (IDOT) maximum permissible length of 550 ft at a length of

549 ft, and the single-span bridge is near the skew limit of 45° at a skew of 42.5°; for these reasons, these two bridges were chosen to be instrumented and monitored for more than a year (LaFave, et al., 2017). The instrumentation goals for the field monitoring of the integral abutment bridges was to validate design assumptions made during a parametric study for an earlier phase of this project (LaFave, et al., 2016).

The first phase of this project performed by the University of Illinois at Urbana – Champaign was to perform a parametric study of integral abutment bridges under various bridge parameters. Organization of the simulations was in such a way to maintain efficiency of the study, and went from initially changing span lengths for a pile section, then repeating this for different pile sections, after that different values of skew were investigated, and finally other parameters were investigated (LaFave, et al., 2016). Bridge parameters to be investigated were categorized as primary or secondary. Abutment skew, pile size, span length, and number of spans, or overall bridge length, were deemed primary parameters and underwent a detailed parametric study.

The secondary parameters had a less detailed parametric study conducted, and were analyzed with 100 ft spans, ranging from one to six spans, with HP14X73 piles unless otherwise noted. The secondary parameters investigated were, but are not limited to, end-span ratio, bridge width, extreme skew (60° for example), soil type, abutment height, number of piles, pile relief, pile orientation, and pipe piles of different thicknesses.

Modeling for the study was done in SAP2000 and designed per IDOT and AASHTO standards. A typical configuration is shown in Figure 2.71. Thin and thick shell elements were used for the deck and abutment, respectively. Girders used frame elements that were made composite to the deck thin shell elements. Piers, like the abutments, were modeled

using thick shell elements, piles were modeled as frame elements, and soil for the piles and abutment backfill was input as springs with stiffnesses tabulated per soil properties.

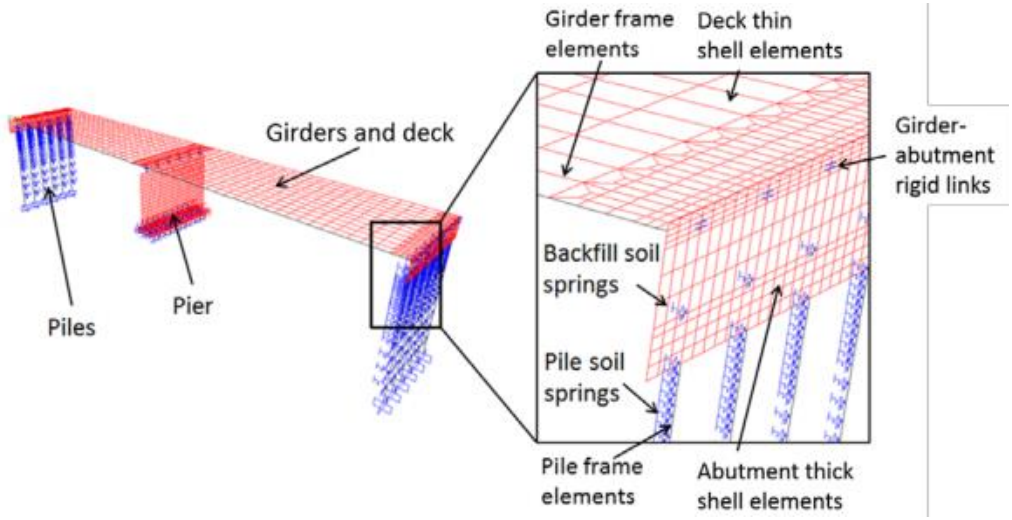

Figure 2.71 *Finite element model of integral abutment bridge*. (LaFave, et al., 2016)

Results of the study showed that longitudinal movement of the bridge can be estimated as 90% of free expansion of the superstructure, regardless of superstructure rotational stiffness, pile stiffness, or abutment skew. For bridges with increased skew, amplification of displacements is seen at the acute corner, and along with increasing bridge length extreme fiber strains of the pile head increase. For cases where pile stain limits are allowed to be surpassing yield strain, integral abutment bridge permissible lengths can be increased, especially if larger piles such as HP16s or HP18s are implemented. The demand on piles can also be increased if the width of the integral abutment bridge is increased, but demand can be decreased by stiffer backfill, softer pile foundation soils, pile top relief, double piles, and deeper abutments (LaFave, et al., 2016).

With the knowledge acquired through the parametric study done for the first phase of the project (LaFave, et al., 2016), the second phase could validate design assumptions made during the parametric study through instrumentation and field monitoring of integral

abutment bridges for the second phase of the project (LaFave, et al., 2017); a schematic of the instrumentation plan is shown in Figure 2.72. Integral abutment bridge superstructure behavior, such as additional buildup of thermal stresses in the superstructure due to integral abutment construction and the overall displacement at the deck level caused by thermal and other loading effects, was at the primary concern. Validation of the fixity of the girder to abutment connection and the upper-diaphragm and lower-footing portions of the abutment connection was to be done by measuring any differential rotation of the girder to the abutment and any differential rotation above and below the cold-joint.

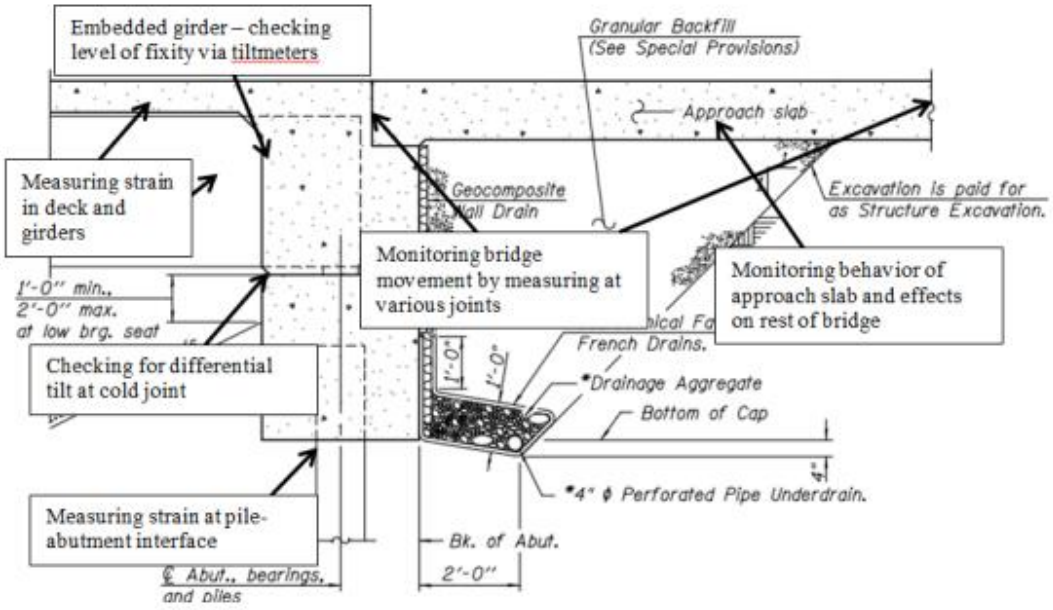

Figure 2.72 *Schematic of instrumentation goals*. (LaFave, et al., 2017)

Since the approach slab was neglected in the parametric study since they were assumed to have minimal impact on the integral abutment bridge behavior, embedded strain gauges were placed in the approach slab to record any stress buildup and major axial force applied to the integral abutment bridge superstructure. Also, to verify pile behavior previously investigated, strain gauges were placed on the H-pile steel sections for the abutment foundation at the pile-abutment interface. Data collection on the four-span bridge

began May 24, 2014 and ended May 26, 2016 measured at 15-minute intervals until March 2015 when the intervals were decreased to 5 minutes. Data collection on the single-span bridge began June 18, 2014 and ended on September 10, 2015 measured at 15-minute intervals.

Observations of abutment rotation were made from the monitoring results to either validate design assumptions, or to propose changes. Instrumentation to capture these results were tiltmeters installed on the abutment face on the top and bottom portions of the abutment and on the embedded girder (Figure 2.73).

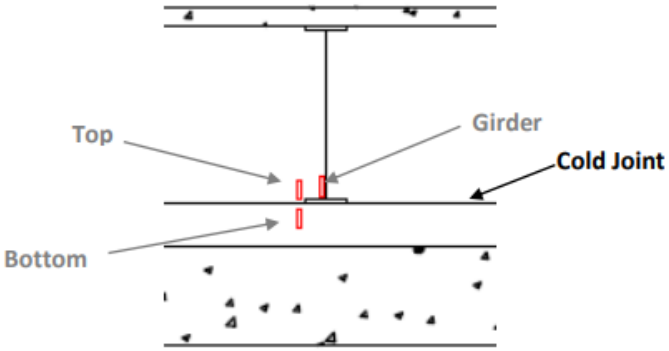

Figure 2.73 *Tiltmeter labeling convention at an abutment*. (LaFave, et al., 2017)

To verify the rigidity of the abutment cold-joint connection the differential rotation of the upper-diaphragm (top tiltmeter) and pile cap/lower-footing (bottom tiltmeter) of the abutment was to be investigated. Figure 2.74 shows the differential rotation about the cold-joint of the integral abutment for both the four-span (Kishwaukee) bridge and the single-span (UPRR) bridge, and there seems to be zero difference in rotation. Therefore, the assumption of a fully continuous moment-resisting connection was validated.

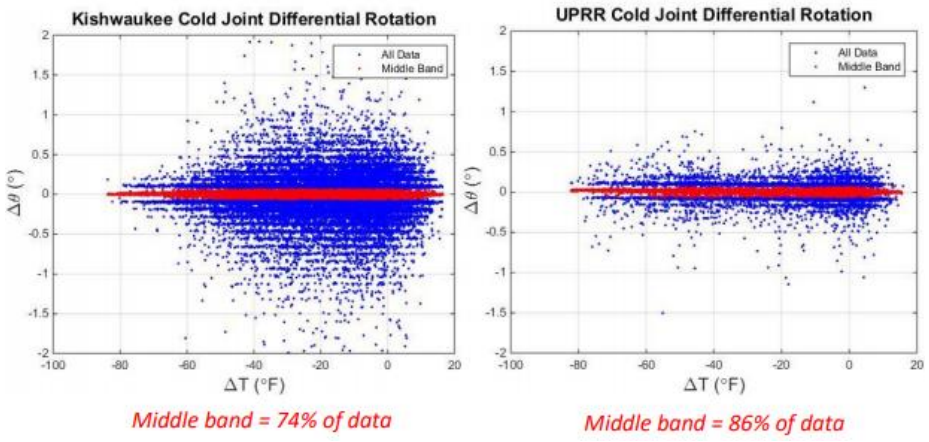

Figure 2.74 *Cold-joint differential rotations for the south side of the Kishwaukee and UPRR abutments.* (LaFave, et al., 2017)

Validation of the rigidity of the connection between the abutment and girders was conducted in the same fashion as the cold-joint connection, in that the differential rotations recorded by tiltmeters on the top portion of the abutment and the adjacent tiltmeter on the girder were tabulated. Figure 2.75 shows this differential rotation, which did result in a non-zero difference, but maximums were not above 0.33°.

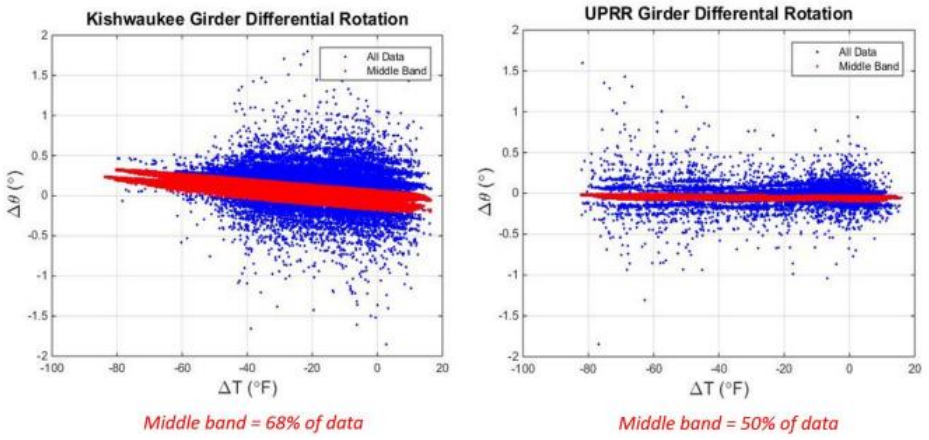

Figure 2.75 *Differential rotation between the abutment and girders at the north side of the Kishwaukee and UPRR abutments*. (LaFave, et al., 2017)

Simple hand calculations were done to the UPRR bridge to investigate the differential rotation at the yield moment for a composite and non-composite section under pinned-pinned connections. Comparing the results of those hand calculations, 1.06° and 1.92°, respectfully, to the maximum differential rotation recorded in the field on the single-span bridge, 0.1°, it was apparent that the connection acted as a continuous, rigid connection rather than a pinned connection. This concept was extrapolated to the four-span bridge and the same conclusion was deduced. Therefore, even though there was slight differential rotation recorded during the field monitoring of the connections, assuming a rigid connection can be allowed.

Demand on the weak-axis orientated piles were also investigated through the field monitoring using strain gauges being installed at the pile-abutment connection interface. The results show flanges on either side of the web underwent both tensile and compressive stresses along with decreasing and increasing temperatures not only throughout the year, but even within a day. The maximum strains recorded for all piles in the monitoring period were significantly less than the yield strain of 1724 microstrain, therefore there is some additional remaining elastic pile-deformation capacity for these integral abutment bridge connections.

Strain gauges were also used to capture strains due to axial force and strong-axis bending moment in addition to weak-axis bending moment, which was the primary source of stress to the piles. While weak-axis bending moment and strong-axis bending moment were consistent throughout the piles being monitored, axial force did result in higher strains at the exterior piles. Another observation made from the results of pile strains was the difference in magnitude of either compressive or tensile strains between an acute and obtuse end of an abutment for the four-span bridge that had a skew. The difference, increasing from the acute to obtuse corner, in compressive or tensile strains between flanges on the same side of the

web were most likely the result of strong-axis bending moment and axial forces being increased due to the geometry of the skew (LaFave, et al., 2017).

Finite element models were made to simulate the field monitored results of both bridges. The same modeling assumptions and methodologies from the first phase of the project, (LaFave, et al., 2016), were used for the models to be done in the second phase in addition to more precise properties for bridge geometry and materials.

Displacements of the abutments tabulated through the finite element modeling were compared to what was recorded in the field (Figures 2.76 and 2.77). It is apparent that there is a strong correlation between the model and the field, which is validation of the modeling techniques used. Another comparison done for the abutment displacements was the magnitude of the displacements for the acute corner and obtuse corner for the skewed bridge. As shown in the findings of the parametric study, the displacement was larger near the bridge's acute corner due to the unsymmetrical global bridge movement seen in higher-skew bridges.

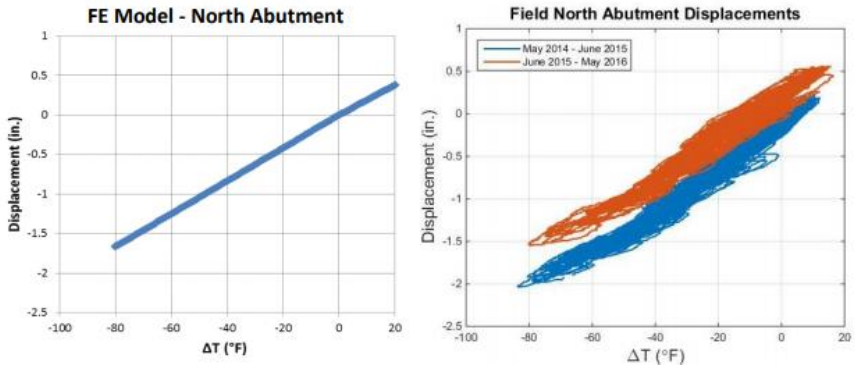

Figure 2.76 *Comparison of Kishwaukee east-abutment north side longitudinal displacement.* (LaFave, et al., 2017)

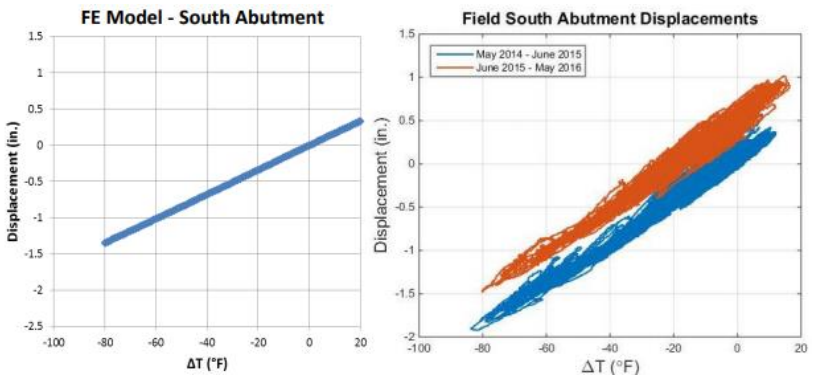

Figure 2.77 *Comparison of Kishwaukee east-abutment south side longitudinal displacement.* (LaFave, et al., 2017)

In addition to abutment displacements, abutment rotations were calculated by the finite element model and compared to field monitored results (Figure 2.78). The model resulted in abutment rotations less than was what seen in the field. This was assumed to be the result of the model overestimating the pile strains. If the abutment rotation were to be increased, the pile strains would then be reduced (LaFave, et al., 2017).

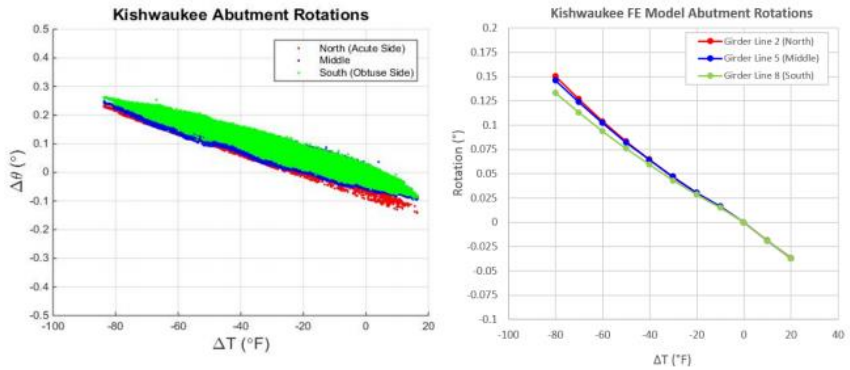

Figure 2.78 *Kishwaukee field and FE model abutment-rotation measurements*. (LaFave, et al., 2017)

Regarding the differential displacement recorded between the girders and abutment, a sensitivity analysis was done to investigate how changing the fixity of this connection affected results. Two models were created in addition to the model already discussed for the Kishwaukee bridge, one with partially rigid girder-abutment connection, and one with a nearly pinned girder-abutment connection. The results of this sensitivity analysis showed that

the girder stresses at the abutment decreased in magnitude as the connection flexibility increased. Bottom-flange girder stresses decreased along the length of the middle girder, and the peak pile strains were a smaller magnitude as the girder-abutment connection increased in flexibility. Thus, assuming a rigid girder-abutment connection for modeling purposes will result in conservative predictions of stresses induced on the structure, as found in the parametric study as well.

Pile strains recorded in the model matched those reported from the field monitoring. As shown in Figures 2.79 and 2.80, it can be seen the model slightly overestimates the pile strains, which can be determined as a slightly conservative results since the model neglects possible softening effects of the pile soil system.

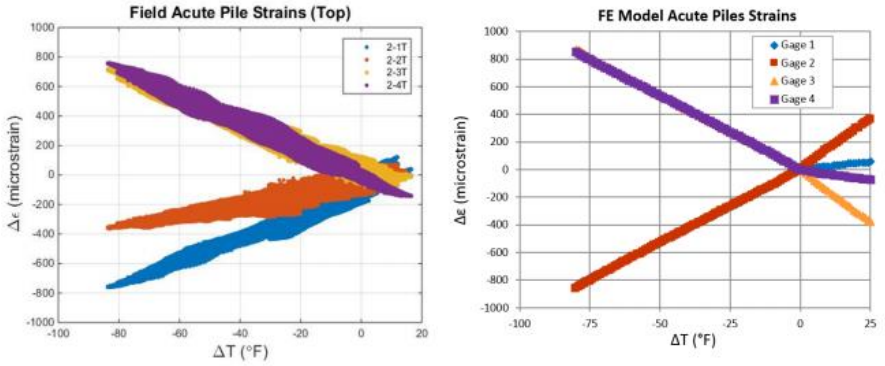

Figure 2.79 *Comparison of Kishwaukee field-measured and FE-model acute pile strains at the pile-cap boundary*. (LaFave, et al., 2017)

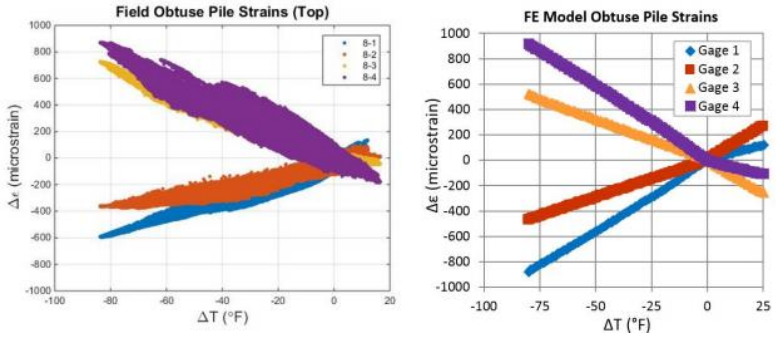

Figure 2.80 *Comparison of Kishwaukee field-measured and FE-model acute pile strains at the pile-cap boundary*. (LaFave, et al., 2017)

Another potential reason for the difference in pile strains between the model and field monitoring results could be the rigidity of the pile-abutment connection. Each pile was embedded 2 ft into the abutment, essentially creating a rigid connection. This was the assumption for the models, but it could be possible to introduce some flexibility in the connection, for example if cracks propagated in the concrete surrounding the piles. To investigate this, another sensitivity analysis was done using the original UPRR bridge model, in addition to one model with a semi-rigid connection and one with a completely released (pinned) pile-abutment connection. A decrease in the peak pile-strain magnitudes resulted for both alternative connections, with the pinned connection having an average 90% decrease. Increased connection flexibility reduces the demand imposed to the piles, therefore the assumption of a rigid pile-abutment connection will result in conservative models (LaFave, et al., 2017).

An integral bridge in western New Jersey was the focus of a study on rigidity of abutments in integral abutment bridges. The Scotch Road bridge over I-295 has integral stub abutments supported by 19 HP360X152 (HP14X102) steel piles oriented to have weak-axis bending embedded 0.6 m (2 ft) within the abutment. Compacted porous fill was used behind the abutment and below the approach slab, the steel piles were encased in concrete from their bottom up to a depth of 5.18 m (17 ft) below the abutment and then encased in sand up to the base of the abutment. The concrete surrounding the base of the piles was intended to ensure a full fixity of the piles at that level, and the sand was designed to help absorb stresses imposed to the piles from the cyclic loading due to thermal movements of the bridge (Khodair & Hassiotis, 2013).

The bridge was instrumented with soil pressure cells, strain gauges, displacement gauges, tiltmeters, and temperature gauges to field monitor the thermal movements of the integral abutments. The results of this monitoring period would provide data to validate a finite element model made in ABAQUS, as well as a finite difference model performed in LPILE. The initial approach to modeling the piles and abutments was to apply a tabulated load and recorded displacements from the superstructure and impose the soil conditions in the field to analyze and compare results. However, it was reported the bending stress curves and displacements for the piles developed from the modeling did not match that from the field monitoring. This was deemed to derive from the modeling not accounting for the resistance provided by the backfill soil as well as neglecting the rotation of the abutments.

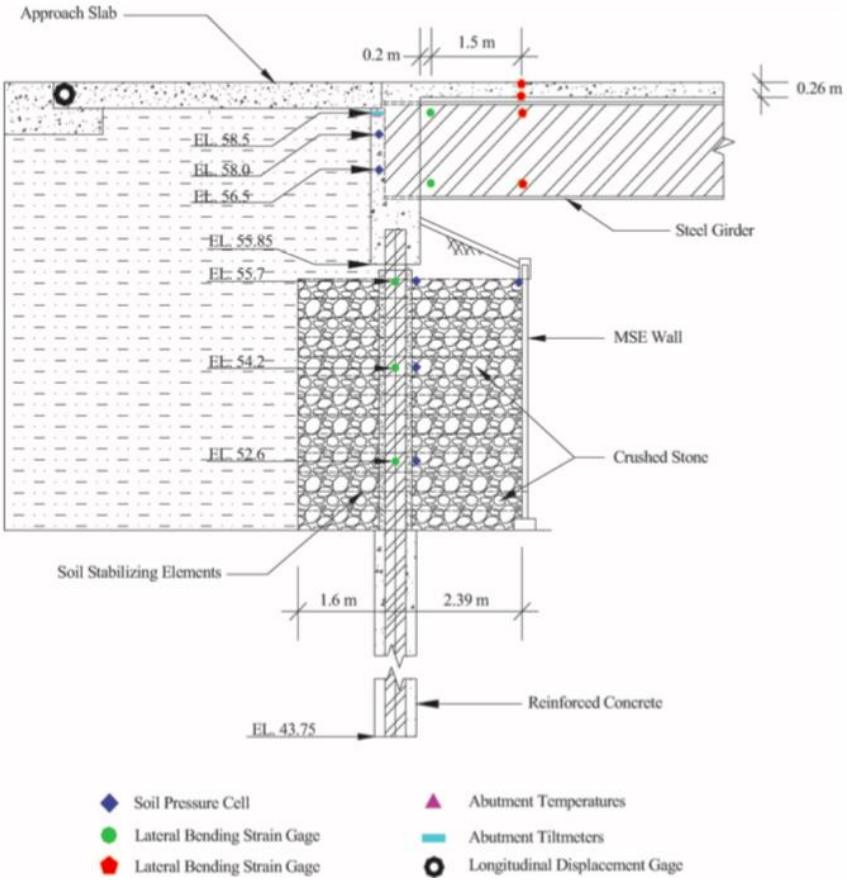

Figure 2.81 *A schematic diagram of the cross-section elevation of the instrumented bridge.* (Khodair & Hassiotis, 2013)

A few considerations were investigated for the finite element model made in ABAQUS, primarily differing boundary conditions for the piles. These options were: fixed pile base with fixed surfaces along the length of the pile embedded in concrete, fixed surface along exterior surface of sand embedding pile to simulate steel void around sand, fixity of top of pile to bottom of abutment.

Loading was applied under the assumption that the abutment would react rigidly, which was not the result of the analysis. The results of the ABAQUS and LPILE model both failed to provide reasonable predictions for the field conditions, hence the conclusion was made that the abutments do not act rigidly and cause a significant need to account for the soil resistance and the differential displacements of the top and bottom of the abutment. Therefore, to validate models, the loading approach was changed to impose field bending moment values to the top of the piles, as well as inputting the field monitored deflections of the approach slabs to the top of the pile that would be changed to match the bending stress curves tabulated by the field monitoring data.

Through validating models, the following conclusions were made by (Khodair & Hassiotis, 2013): the abutment does not act rigidly and rotations along the depth of the abutment vary, soil resistance needs to be accounted for since it greatly affects the rotation and displacement of the abutment, displacements recorded for approach slabs are much greater than displacements imposed on the piles, the connection between the top of the pile and the bottom of the abutment is adequate since the displacement required to cause a plastic hinge at the connection was approximately 2.6 times greater than the displacement recorded during bridge thermal movements.

A study was done by researchers in China on developing a new connection for the beam-pier-beam connection seen with integral abutment bridges. The joint was designed to use shear studs at the ends of the beams to transfer shear forces and provide tensile strength when the connection would be under a "sagging" moment, which would also be resisted through compression of the concrete slab. The "hogging" moment put onto the connection was designed to be resisted in compression by the steel end plate at the end of the beams in contact with the concrete pier and resisted in tension by the reinforcing steel in the slab (Figure 2.82) (Briseghella & Zordan, 2015).

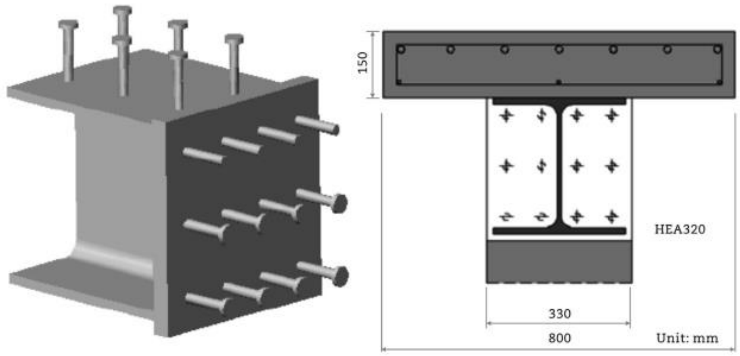

Figure 2.82 *Joint under investigation*. (Briseghella & Zordan, 2015)

Requirements for this joint were that it needed to achieve the connection between a composite steel and continuous concrete beam (part of a composite deck or floor) or a concrete pier (or column); minimization of the joint components; minimization of installation time; minimization of tolerance problems due to the connection between steel and concrete; appropriate stiffness under hogging and sagging moment conditions (Briseghella & Zordan, 2015). These requirements were deemed to be met, hence there was a real-world application of the joint in Differdange, Luxembourg that had acceptable results in construction time and cost.

To create a finite element model to capture the response of the connection under loading, an experimental test of the connection was performed by the University of Trento in Italy to capture the response of the connection under monotonic and symmetric loading until failure (Figure 2.83).

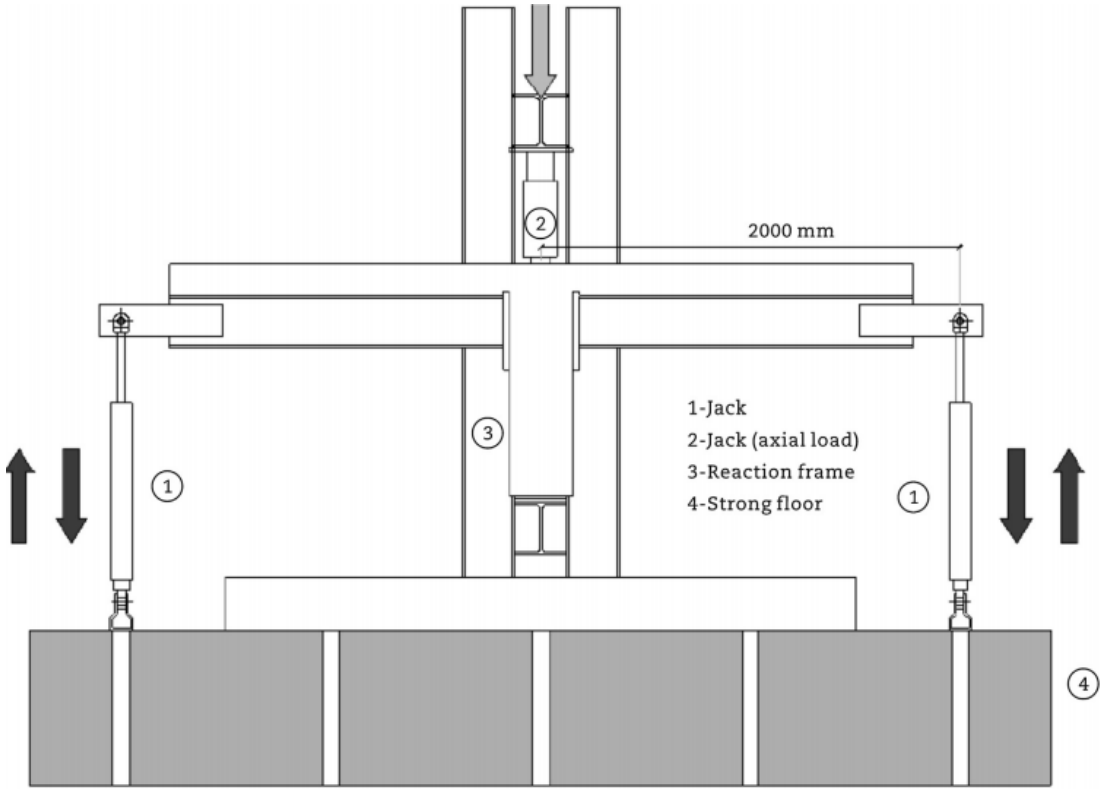

Figure 2.83 *Experimental test setup scheme*. (Briseghella & Zordan, 2015)

With the results of the experimental testing known, finite element models were created to replicate what was seen in the laboratory. Two models were created, a 3D global model and a 2D local model intended to focus on the area of the connection itself (Figure 2.84). The global model used the same dimensions, boundary conditions, and loading setup as was done for the experimental testing setup; but the local model used a fixed boundary condition on the lower flange of one beam and applied the experimental loading to the lower flange of the opposite beam.

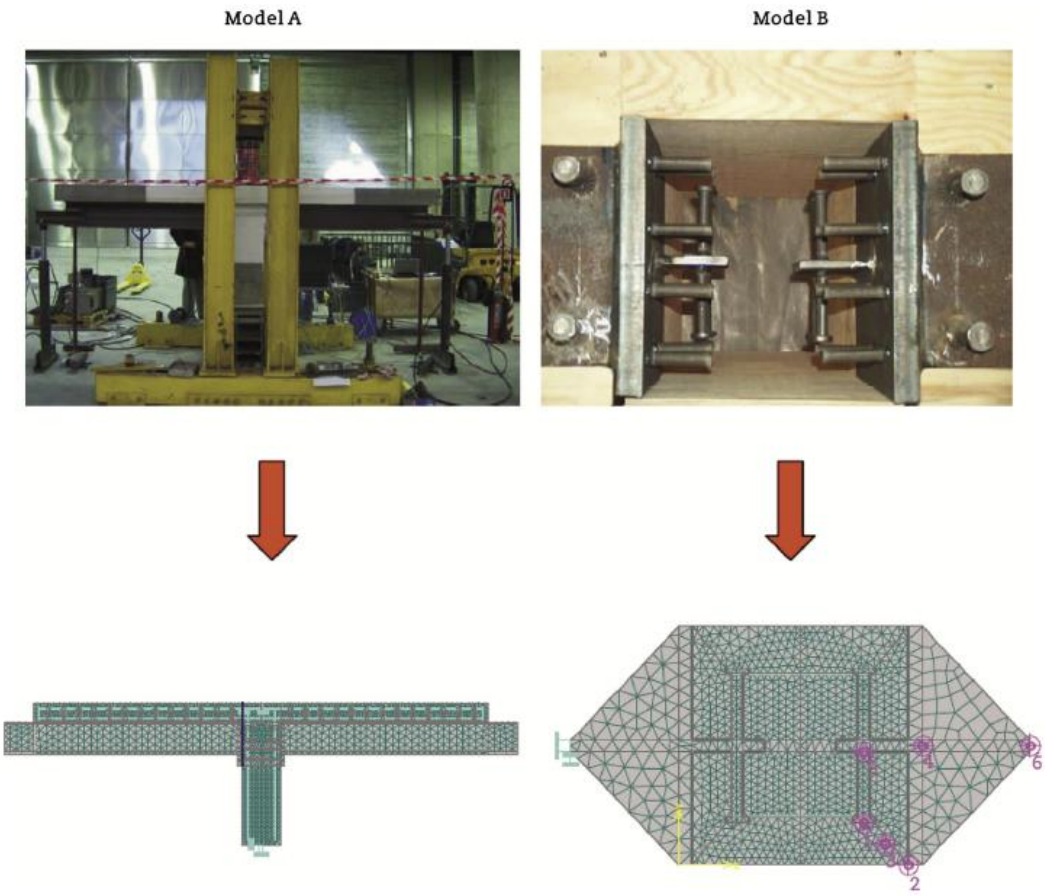

Figure 2.84 *Two finite element models of the specimen*. (Briseghella & Zordan, 2015)

Analysis of the experimental and finite element results led to the conclusions that the proposed joint investigated would be a good option for the beam-to-pier connections for integral abutment bridges not only due to the results seen through loading, but also due to its simplicity for fabrication and installation. The failure mechanism seen under the cyclic loading was the degradation of the concrete in the pier, but this response could be improved by revising the joint to have the stirrups crossing the joint be close to the base of the shear studs rather than having them attached near the top of the studs; this would lead to the failure mechanism being the failure of the shear studs, not the tensile failure of the bond between the studs and pier concrete (Briseghella & Zordan, 2015).

The connection between a steel girder and integral abutment was investigated to address the issue with cracking due to tensile stresses at the upper surfaces of the abutment at the location of the embedment of the steel girder since these cracks could lead to durability issues propagated by infiltration of water and other chemicals. To do this, the designs created were intended to increase the shear and moment capacity of the connection using shear studs and rib shear connectors. Two empirically designed connections were used as control specimens for the four proposed connection designs that used different layouts of shear studs and perfobond rib shear connectors (Kim, Yoon, Kim, Choi, & Ahn, 2011). Figures 2.85 through 2.90 show the specimens that underwent the experimental investigation.

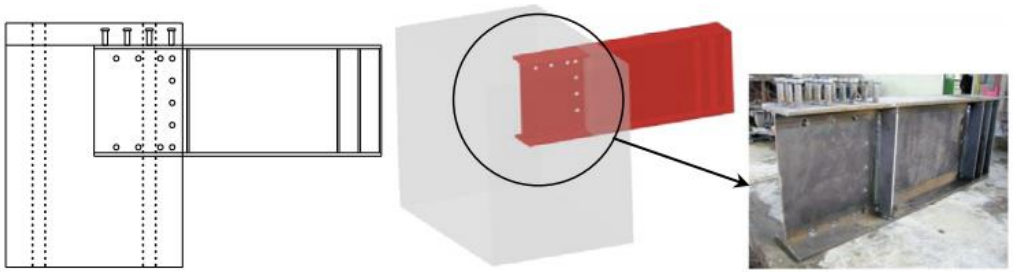

Figure 2.85 *Empirically constructed joint-1 (Reference type*). (Kim, Yoon, Kim, Choi, & Ahn, 2011)

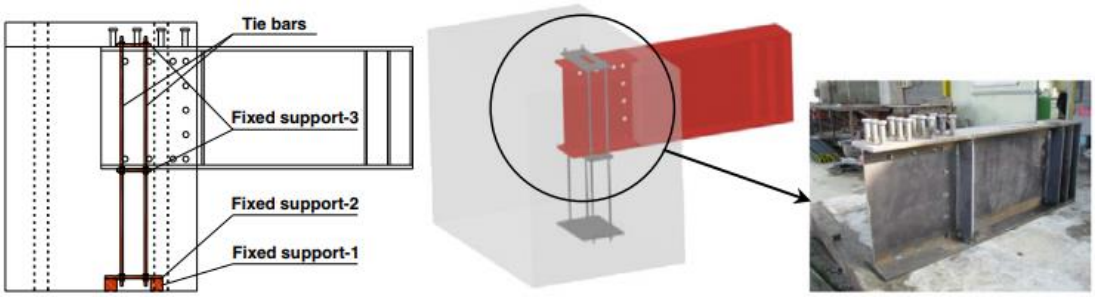

Figure 2.86 *Empirically constructed joint-2 (Joint with thread bars and fixed supports).* (Kim, Yoon, Kim, Choi, & Ahn, 2011)

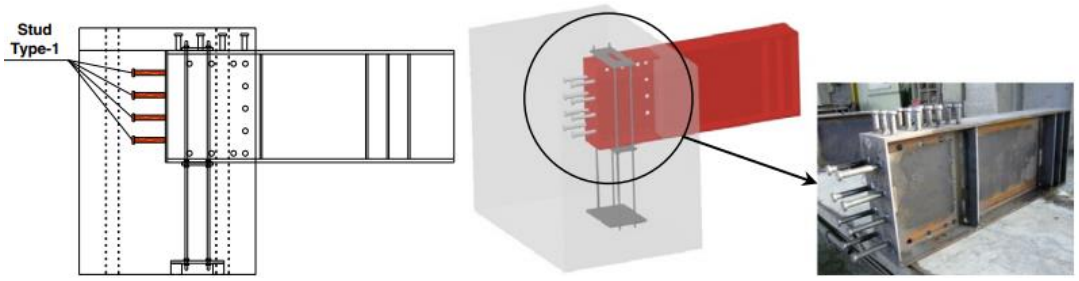

Figure 2.87 *Joint with stud Type-1 (Proposed joint-1*). (Kim, Yoon, Kim, Choi, & Ahn, 2011)

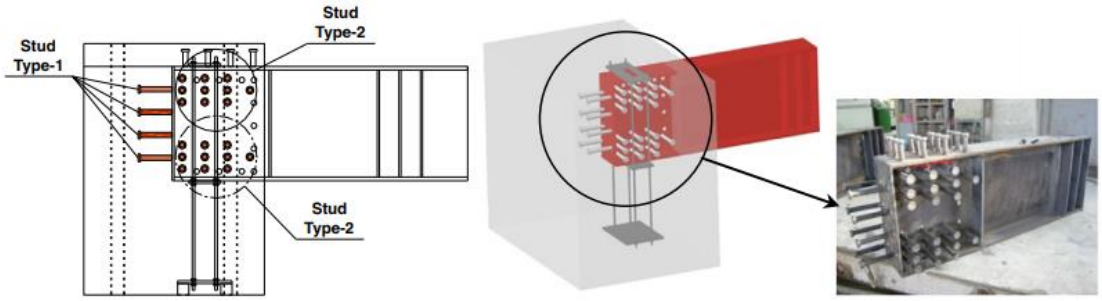

Figure 2.88 *Joint with stud Type-1 and Type-2 (Proposed joint-2).* (Kim, Yoon, Kim, Choi, & Ahn, 2011)

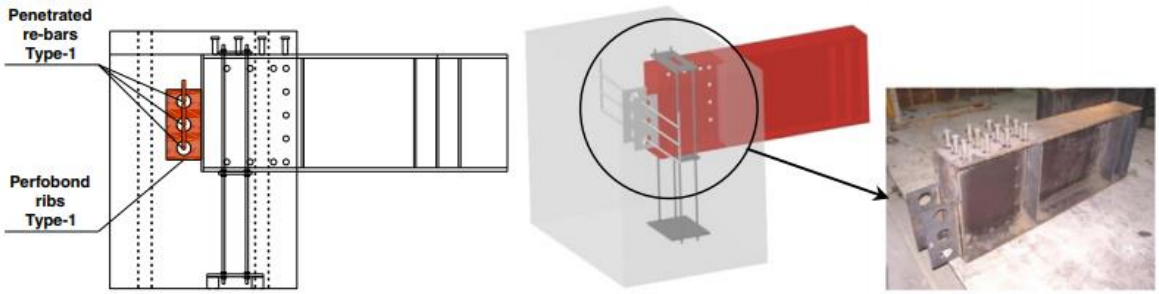

Figure 2.89 *Joint with perfobond ribs Type-1 and penetrated re-bars Type-1 (Proposed joint-3).* (Kim, Yoon, Kim, Choi, & Ahn, 2011)

Strain gauges were installed on the reinforcing bars, shear connections, and on the surfaces of the H-beam and abutment to measure development of the specimen; linear variable differential transformers were also installed to measure displacements of the joint as

well. The small-scale specimens were loaded to a static load of 1,000 kN that was incrementally loaded at 0.02 mm/s to prevent sudden failure of the specimens.

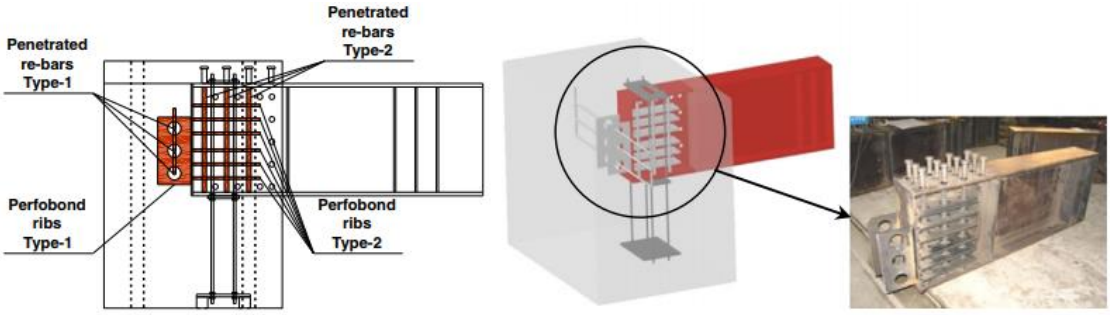

Figure 2.90 *Joint with perfobond ribs Type-1, 2 and penetrated re-bars Type-1, 2 (Proposed joint-4).* (Kim, Yoon, Kim, Choi, & Ahn, 2011)

Figure 2.91 shows the load-displacement curves for all specimens. All specimens recorded linear and elastic behavior under the design load of 230 kN and yield load of 460 kN and had similar elastic behavior until limits of 584-650 kN, after then the stiffness and rigidity of each specimen varied but were all sufficient. The load-displacement curves also show the initial stiffness of the proposed joint details was about 11% greater than that of the empirically construction specimens (Kim, Yoon, Kim, Choi, & Ahn, 2011). The preferred structural response of the proposed joints was also proven superior to the empirically constructed specimens through the analysis of the cracking pattern of the specimens. All specimens had yet to show cracking at the design load of 230 kN, but around the load of 450 kN, near the yield load of 460 kN, cracks were beginning to form for all specimens. The cracks for the empirical specimens were greater in amount and larger in propagation compared to those of the proposed joint specimens.

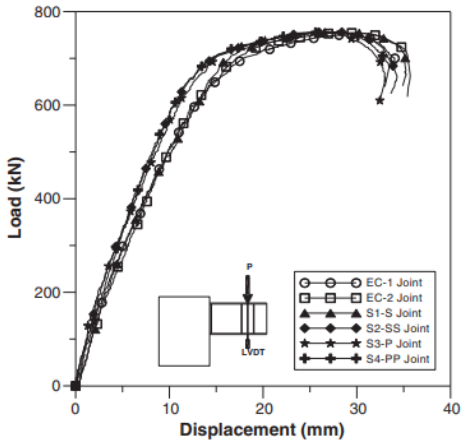

Figure 2.91 *Load-displacement curves*. (Kim, Yoon, Kim, Choi, & Ahn, 2011)

Analysis of the load-strain history of the specimens shows, again, the proposed joint specimens had superior stiffness and crack-resistance capacity compared to the empirical specimens, with the cracking strains being taken from strain gauges placed along the top concrete surface of the specimens. Also, it was reported that the main reinforcing steel for the concrete slab parts underwent yielding in the empirical specimens prior to those of the proposed joint specimens, and the main reinforcing steel for the abutment parts of all specimens remained elastic providing steady stiffness. The presumed failure mode for the experimental testing, which was the yielding of the H-beam, was proven to be valid since the upper and lower flanges of the H-beam displayed strains greater than their yield strain.

A nonlinear finite element model was created in ABAQUS to capture the response seen in the experimental investigations of the empirically constructed specimen shown in Figure 2.84. The abutment concrete was modeled with C3D8R elements and the H-beam steel was modeled with S4R elements (Figure 2.92). Nonlinear material properties, concrete damaged plasticity and classical metal plastic model, were input and contact interaction was defined for the girder-abutment joint interface for a partially connected model, but an embedded option was used for the assumption of a rigid connection at the same interface.

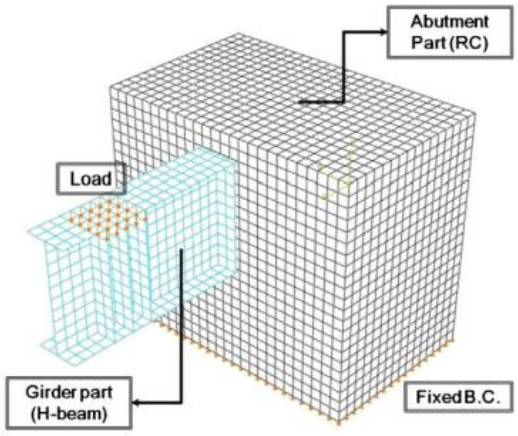

Figure 2.92 *Finite element model of steel girder-abutment joint specimen.* (Kim, Yoon, Kim, Choi, & Ahn, 2011)

Figure 2.93 shows the load-displacement curves from the experimental investigation as well as the finite element investigation into how to model the girder-abutment interface. It can be seen the contact interaction version of the modeling caused the experimental results to be conservative, and the embedded version of the modeling resulted in having greater capacity in initial stiffness than the experimental investigation. Also, the yielding load of the contact interaction model (562.02 kN) was less than that of the experimental specimens, but still was above the required load of 460 kN. Therefore, it was recommended by (Kim, Yoon, Kim, Choi, & Ahn, 2011) to use contact interaction to define the girder-abutment interface rather than defining it using the embedded constraint available in ABAQUS to ensure that the comparison between modeling and real-world applications will result in conservative designs.

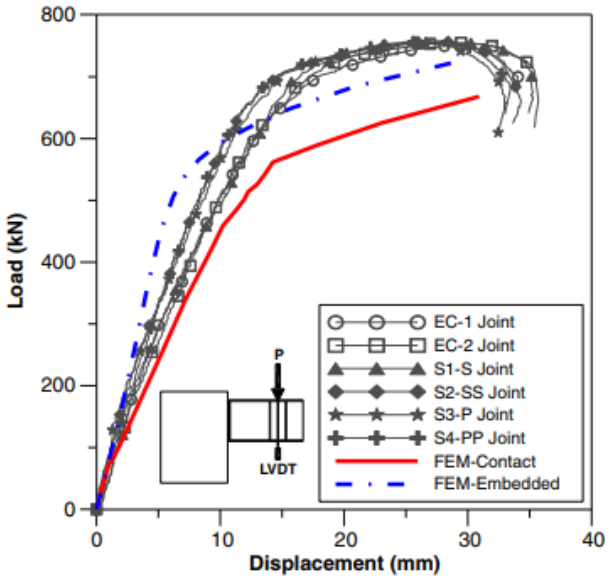

Figure 2.93 *Comparison of experimental loading test results with FE analysis results*. (Kim, Yoon, Kim, Choi, & Ahn, 2011)

A study was done in Korea to investigate the adequacy of abutment-pile connections for integral abutment bridges, specifically if new detailing could pose benefits to the response of the connection. The investigation included experimentally testing five connection details between a half-scale pile and abutment for integral abutment applications. The details were the conventional connection using a weak-axis oriented H-pile with reinforcing steel around it; reinforcing steel around the H-pile and passing through the flanges of the pile; shear studs along the flanges of the H-pile; and two orientations of perfobond connectors and reinforcing steel (Figure 2.94) (Ahn, Yoon, Kim, & Kim, 2011).

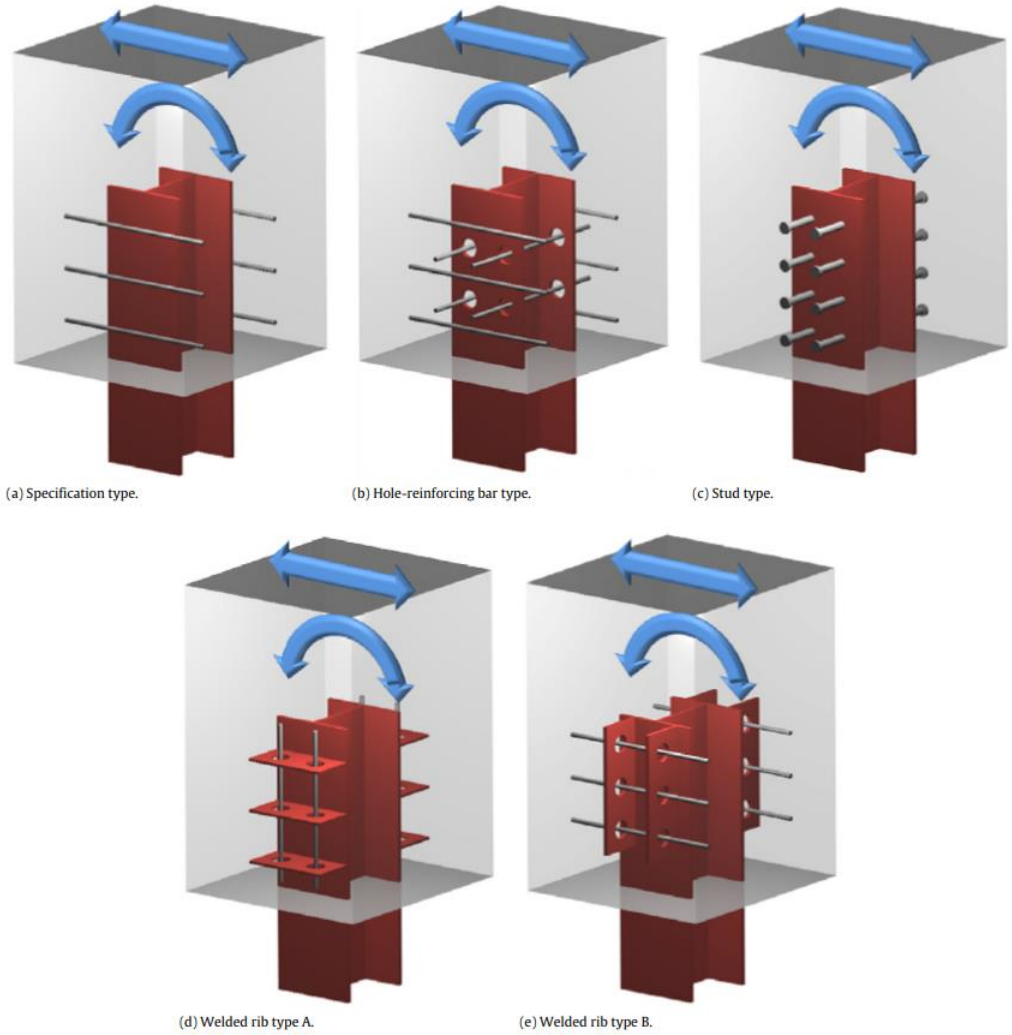

Figure 2.94 *Proposed abutment-pile connections*. (Ahn, Yoon, Kim, & Kim, 2011)

Half-scale specimens were designed in a way to allow for the connection to be subjected to axial force, shear force, and bending moment (Figure 2.95). To evaluate the performance of each connection details, the crack patterns, load deflection, and load-rotation correlations were monitored under the applied static load which had a maximum value of 1,000 kN and was applied at 0.02 mm/s.

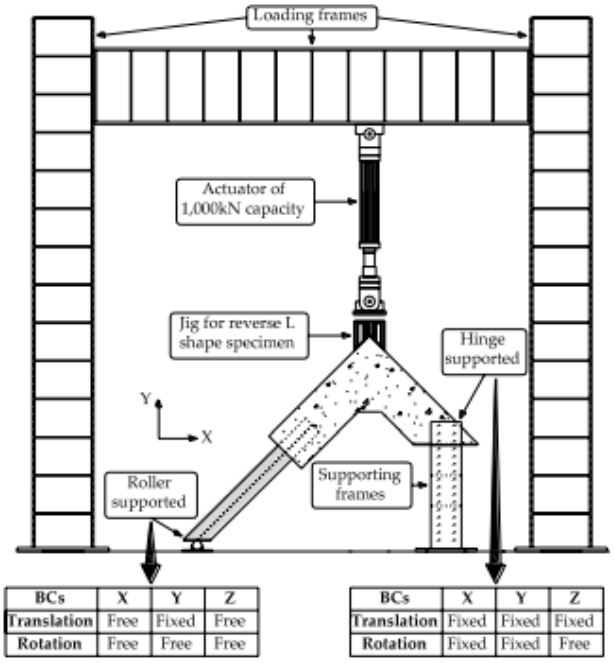

Figure 2.95 *Set-up of test specimens*. (Ahn, Yoon, Kim, & Kim, 2011)

The cracking pattern of the proposed connections was reported to initiate at a load 33%-67% higher than that of the control specimen, and the ultimate load of the proposed connections was approximately 31%-63% greater than the control specimen. Cracking of the proposed connections were smaller and less numerous than the control specimen, but initiation of some cracks in specimens with shear studs and perfobond connectors occurred at lower or similar loading levels as recorded for the control specimen. The reasoning behind this is due to how these connections distribute force from the concrete to the H-pile. These connections tend to decrease the bearing stress of concrete on the H-pile by resisting deformations and rotations of the entire abutment-pile connection, but once this bearing stress approaches a certain threshold a crack will appear (Ahn, Yoon, Kim, & Kim, 2011).

The load-displacement (Figure 2.96) and load-rotation (Figure 2.97) relationships of the connection were another method used to analyze the adequacy of the proposed connections versus the control specimen. All the specimens had an elastic limit of

approximately 250-540 kN, and all the stiffnesses of all the proposed connection was deemed to be enough to resist the rotational and translational deformations of an integral abutment compared to the control specimen. The yielding load of the proposed connections increased in the range of 11%-106% compared to the control specimen, with the lower end being the additional reinforcing steel connection and the higher end being the perfobond connectors, and the ultimate load of the proposed connections was also higher than the control specimen. The same conclusions were drawn for the rotational deformation of the specimens, in that after the elastic limit and yield load, the deformations of the specimens increased rapidly under loading. But, for both deformation and rotation displacements, the proposed connections resulted in adequate designs when compared to the results of the control specimen.

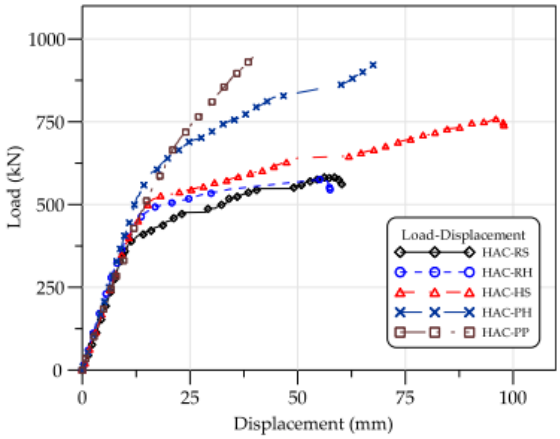

Figure 2.96 *Load-displacement relationships*. (Ahn, Yoon, Kim, & Kim, 2011)

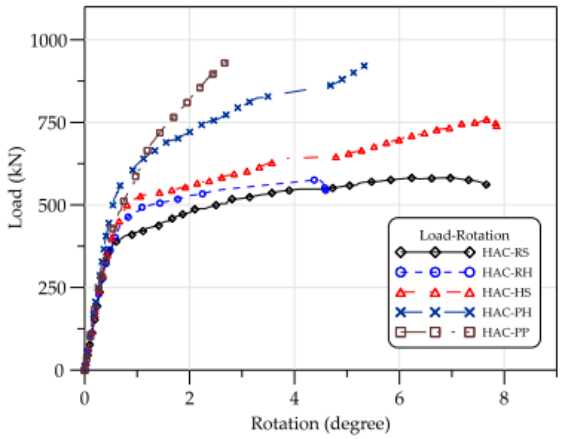

Figure 2.97 *Load-rotational angle relationships*. (Ahn, Yoon, Kim, & Kim, 2011)

Finite element models were created in LUSAS to compare the experimental investigation to structural analysis. Solid elements were used for abutment concrete, thin shell elements were used for the H-pile, and bar elements were used for the reinforcing bars. The connection interface between the abutment and H-pile was modeled as full composition. The reported comparison of the models to the experimental specimens was the load-displacement relationship (Figure 2.98), which showed the models having a higher initial stiffness than the laboratory test results and experimental results being higher than the finite element results after yielding occurred. This is most likely due to the modeling assuming a fully rigid connection between the H-pile and abutment, when in reality the different connection details caused some discrepancies of the fixity of the connection, but the structural strength of the experimental specimens was greater than that of the finite element models, therefore the results of the modeling are conservative.

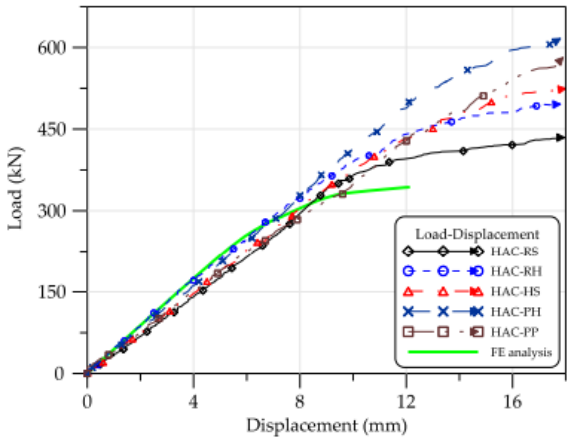

Figure 2.98 *Comparison of test results with FE analysis results*. (Ahn, Yoon, Kim, & Kim, 2011)

Upon the completion of testing, both experimental and numerical, and compilation of the results, (Ahn, Yoon, Kim, & Kim, 2011) made the following concluding remarks about the study:

- The connection with reinforcing steel passing through holes in the H-pile flanges resulted in a similar ultimate load but increased the elastic stiffness and yield load when compared to the conventional connection detail.
- The connection utilizing shear studs installed on the flanges of the H-piles had a similar elastic stiffness compared to the control specimen, but had a higher yield load, ultimate load, and ductility.
- Perfobond rib connectors increased the bearing resistance and sectional properties of the H-pile resulting in higher elastic limit, rotation stiffness, yield load, and ultimate strength compared to the control specimen.
- Upon the conclusions of this report, the proposed abutment-pile connections should be allowed to be implemented to integral abutment bridge designs using H-piles orientated for weak-axis bending.

In addition to the numerous experimental efforts made in researching integral abutments and their connections, many researchers have also investigated aspects of integral abutments using numerical analysis. One such study was conducted to investigate the behavior of slab-type concrete integral bridges under cyclic expansion and contraction due to thermal changes and how these cyclic changes affected soil pressures of the abutment backfill and abutment rigidity (Abdel-Fattah, Abdel-Fattah, & Hemada, 2017).

A multiple-span, slab-type, reinforced concrete bridge (Figure 2.99) was chosen as the geometry for the investigation with varying span lengths of 20, 60, 100, 140, 180, 220, and 260 m (BR1 through BR7). The 13 m wide bridge deck is cast integrally with the 6 m tall abutment, which is supported by a single row of H-piles orientated for weak-axis bending.

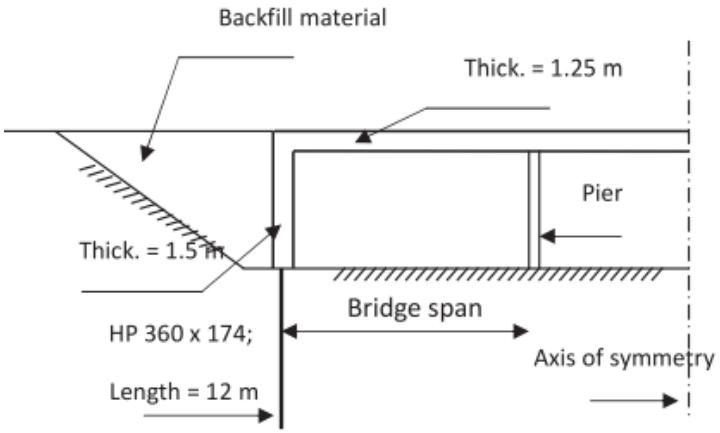

Figure 2.99 *Geometric properties of example bridge*. (Abdel-Fattah, Abdel-Fattah, & Hemada, 2017)

The finite element analysis was done as a 2D model, so plane-strain FE modeling methodologies were used to represent the geometry of the bridge as well as the soil. The bridge deck, abutments, and piles were modeled using three-noded beam elements, and the foundation layers and backfill soil were modeled as six-noded triangular solid elements. The interaction between the soil, abutments and piles was defined using interface elements, which were defined as conditions from smooth to rough.

The procedure for analysis and loading of the model was done to resemble the construction of the bridge as well as the various loadings imposed to the bridge, such as self-weight, soil pressure on the abutments, and thermal loadings. Live load, concrete creep and shrinkage, and other loads of the like were not considered for this investigation.

For discussion of the analysis results, a stage numbering system was created to describe what version of bridge life was being analyzed. Stage 1 represented the completion of placement of the backfill behind the abutment, Stages 2 and 3 represent the first and second cycles of temperature variation, and Stages 4 and 5 represent the third and fourth cycles of temperature variation. The soil backfill pressures along the abutment were plotted for the height of the 6 m abutment for each stage as well as for at-rest and passive Rankine earth pressure calculations and DMRB calculations which come from highways agency. From the analysis, maximum bending moment and shear forces were reported for both the abutment and piles of each bridge setup (Figures 2.100 and 2.101).

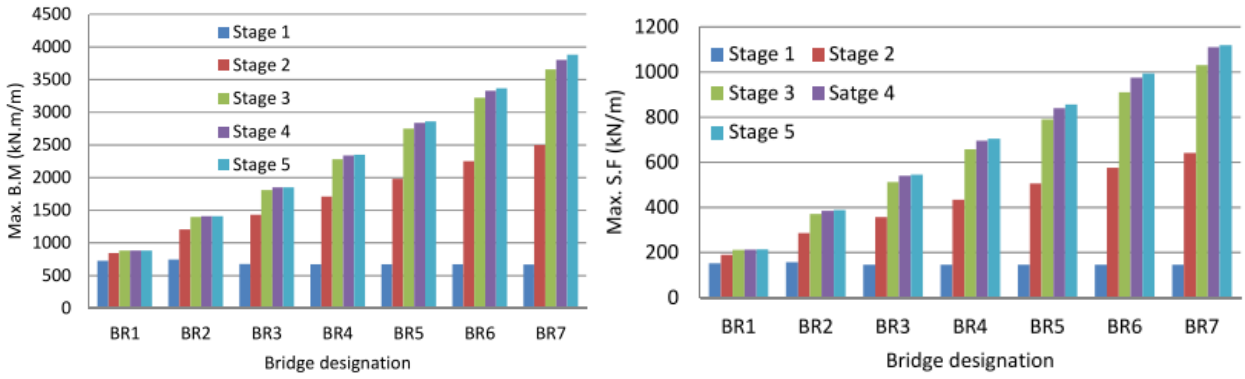

Figure 2.100 *(Left) Maximum bending moment and (Right) Maximum shear force in abutment*. (Abdel-Fattah, Abdel-Fattah, & Hemada, 2017)

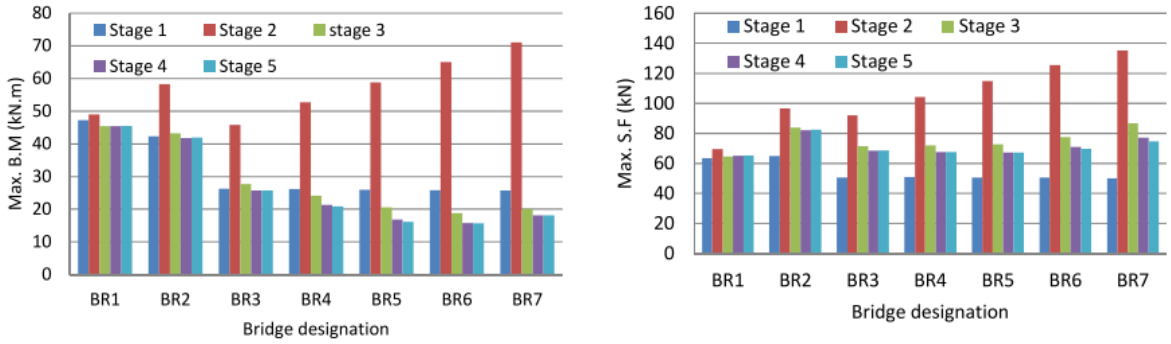

Figure 2.101 *(Left) Maximum bending moment and (Right) Maximum shear force in pile.* (Abdel-Fattah, Abdel-Fattah, & Hemada, 2017)

In addition to the results of forces within the abutment and piles during thermal loading and backfill soil, other conclusions were made by (Abdel-Fattah, Abdel-Fattah, & Hemada, 2017). The effect of soil pressure on the abutment causes notable forces within the abutment and are due to the expansion of the bridge due to thermal increase, but these soil pressures become less significant after the first few cycles of thermal loading due to the densification of the soil during bridge expansion and contraction. The maximum earth pressures on the abutment are dependent on the bridge length and the order of cycle of thermal increase, and these pressures that are calculated through approximate tabulations from guidelines are acceptable for short span bridges (lengths up to 100 m) but for longer spans this tabulated value was deemed to negate the effect of cyclic thermal loading.

Also, the higher the backfill stiffness, the pressures imposed to the upper portion of the abutment increase as well; for the approximately the lower 25% of the abutment height, the relationship is opposite. This comparison was also viewed for increasing abutment stiffness (i.e. increase in abutment thickness), which caused an increase in maximum soil pressures especially for longer span bridges.

A numerical study was done into the pile-pile cap connection for stub-type integral abutment bridges, specifically how cracking patterns propagate and how certain reinforcing

steel details could help mitigate those cracking patterns. 3D nonlinear solid elements were used to model a pile cap and pile typically seen for stub-type integral abutments and equivalent cantilever pile length to ignore nonlinear soil conditions (Figure 2.102).

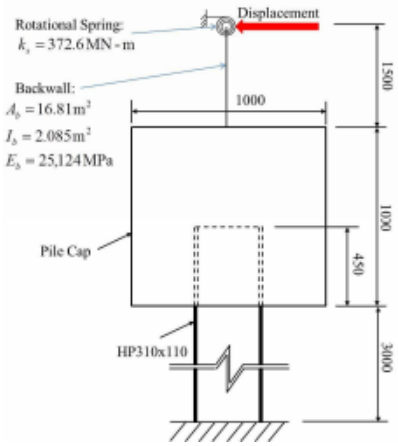

Figure 2.102 *Schematic of numerical model setup*. (Lee, Kim, & Jeoung, 2013)

Three analysis cases were conducted for the modeling: (1) translation only, (2) rotation only, and (3) simultaneous translation and rotation. Although previous knowledge of integral abutment bridges shows that case (3) is the actual movement of the integral abutment, cases (1) and (2) were done merely to investigate their individual contribution to cracking patterns; the cracking patterns for case (1) and (2) are shown in Figure 2.102. It was reported that the cracking pattern for case (3) was a 4-way cracking pattern, but had the same results as case (1) or (2). The propagation of cracking in case (3) was delayed resulting that the combined actions of translation and rotation lead to an increase in pile cap performance and that reinforcing should be able to resist the 4-way cracking pattern.

Two reinforcing details were investigated under the same modeling setup used for the three deformation cases. One reinforcing detail came from PennDOT (Figure 2.103) which utilizes a single reinforcing steel bar passing through the web of the H-pile as to compensate down-drag force in the supporting piles. The other reinforcing detail is the use of a spiral

reinforcing cage that surrounds the H-Pile throughout the length of embedment of the pile into the pile cap (Figure 2.104). This design is intended to confine the concrete within the spiral as to increase the strength of the concrete, but due to the complexity of the spiral and geometric limitations this connection can be complicated to install.

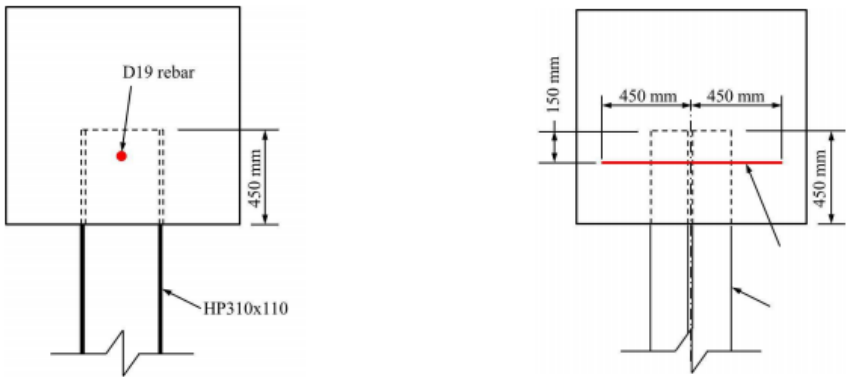

(a) Front View (b) Side View

Figure 2.103 *PennDOT rebar detail.* (Lee, Kim, & Jeoung, 2013)

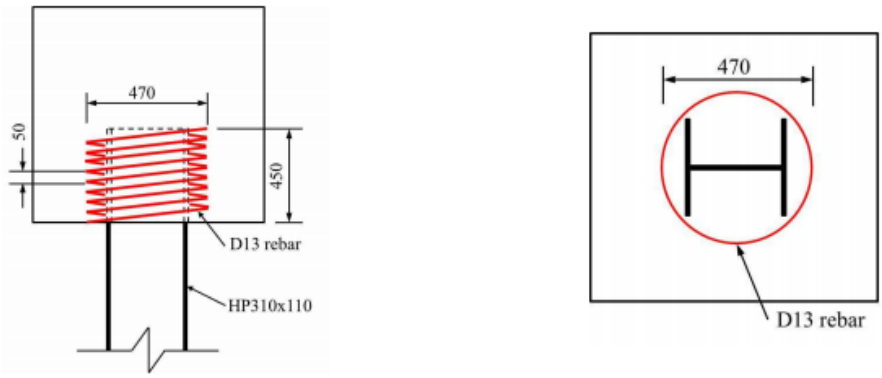

(a) Front view (b) Plan view

Figure 2.104 *Spiral steel rebar detail.* (Lee, Kim, & Jeoung, 2013)

The analysis of the two reinforcing details resulted in the PennDOT detail having the same crack propagation as seen from case (3) analysis. The stress in the single reinforcing bar passing through the H-pile was approximately a maximum of 11% of its yield strength at crack propagation, and a maximum of 68% of yield strength after the pile cap had completely cracked; this leads to the conclusion that the PennDOT reinforcing detail for pile-pile cap

connection is not effective for mitigating crack propagation in the pile cap for an integral abutment bridge. The same analysis was conducted for the spiral steel reinforcing detail, and the results were improved. The detail sufficiently delayed pile cap crack initiation and propagation, and the stress within the spiral reinforcing was stable until concrete cracking when it suddenly gained to 352 MPa, which leads to the conclusion that the spiral steel reinforcing detail is much more effective than the PennDOT reinforcing detail for pile-pile cap connections for integral abutments. This conclusion is best shown in the load-displacement curve shown in Figure 2.105 (Lee, Kim, & Jeoung, 2013).

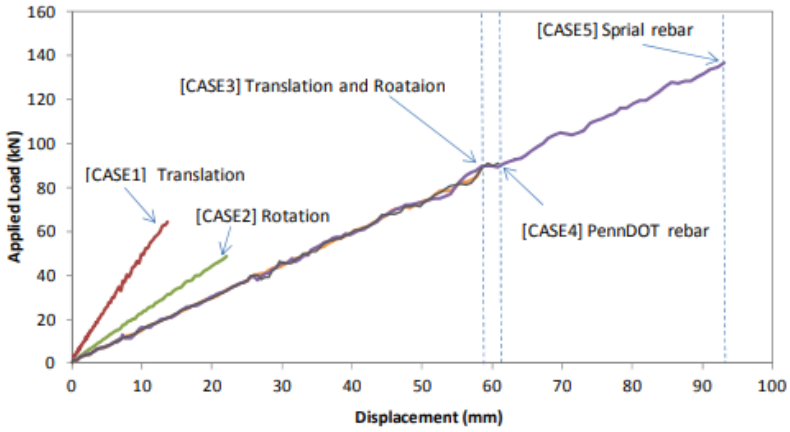

Figure 2.105 *Comparison of load-displacement curves*. (Lee, Kim, & Jeoung, 2013)

CHAPTER 3. ABC INTEGRAL ABUTMENT DESIGN

The basis of the designs listed in this section was on the concept of ABC, as well as the results from (Hosteng, Phares, & Redd, 2016).

Through discussion of the results from the testing of two connections, the grouted reinforcing bar coupler and pile coupler; the designs of these specimens were adjusted to address any design or construction issues found in (Hosteng, Phares, & Redd, 2016). In addition to the two modified connections, a new connection was developed by the Iowa DOT and finalized through meetings and discussions between the Iowa DOT and the Iowa State Bridge Engineering Center. The connections were created based on ABC methods and the desire to eliminate a closure-pour to achieve a "jointless" bridge. Contractor friendly construction methods and materials were a major driving force behind the designs, as were the strength and durability of each connection.

3.1 UHPC-Joint

The Iowa DOT developed this connection to utilize the ABC method of "slide-in construction," and UHPC. UHPC was chosen in lieu of concrete or a grouting material due to the increased flowability characteristic of UHPC, as well as its impermeability and high strength. The placement of reinforcement throughout the specimen was based on the reinforcement of the original grouted reinforcing bar coupler specimen design, except for the connection bars which are seventeen #7 reinforcing bars (Figure 3.1).

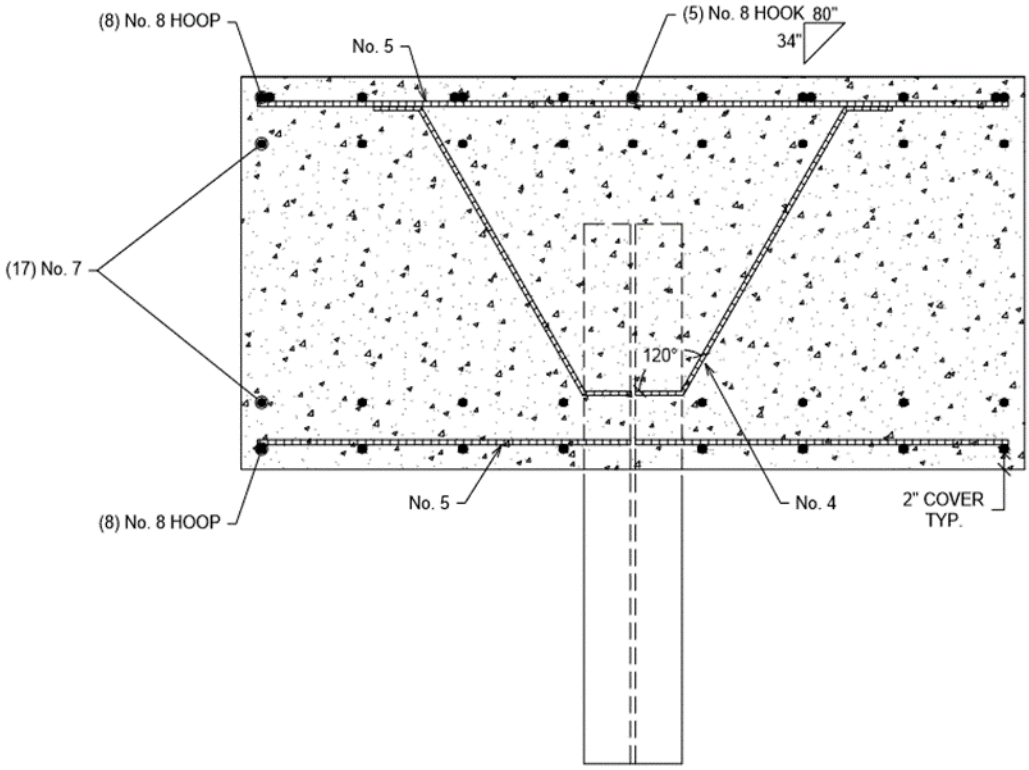

Figure 3.1 *Plan view of UHPC-Joint specimen showing locations of connection bars.*

One of the initial design notes for this specimen was the eight #7 reinforcing connection bars on the front face of the pile cap of the specimen would need to utilize a mechanical coupler as to eliminate the issue of the protruding bars from the pile cap interfering with the steel beam during the slide. These mechanical couplers were designed to be Dayton Superior D310 Taper-Lock Standard Couplers, which were chosen over other couplers due to ease for installation in the tight space while maintaining acceptable strength and durability. Another design note was to create two 7 in. wide "chimneys" along the rear face of the integral diaphragm, which was to create a pressure head to aid the flowability of the UHPC. (Figure 3.2)

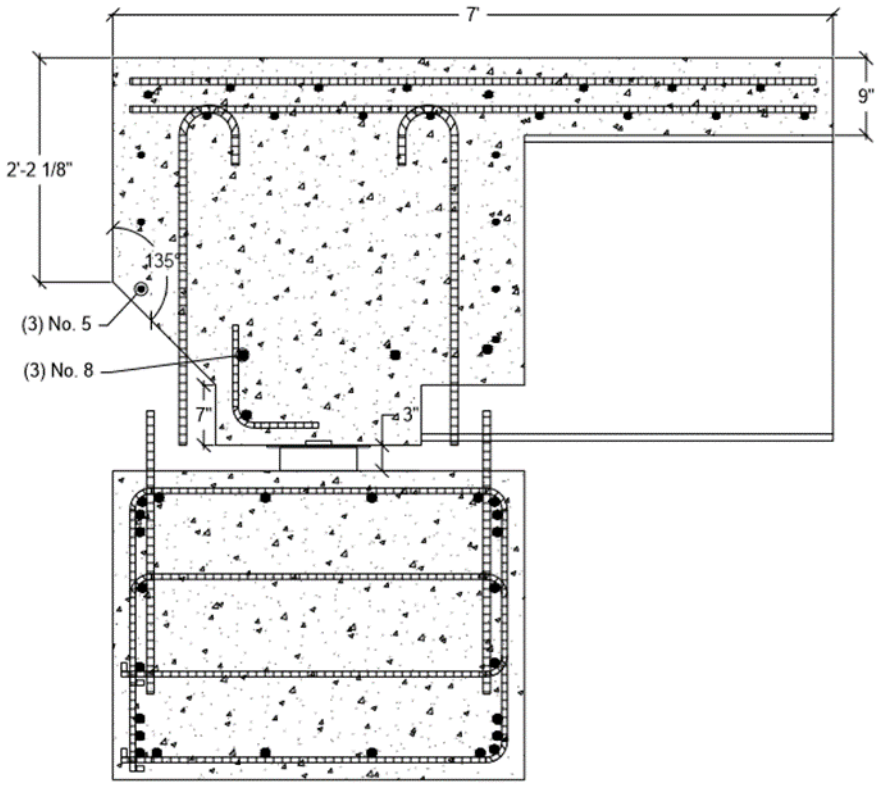

Figure 3.2 *UHPC-Joint specimen section through "chimney."*

The overall size of the specimen does not vary in size from the other two specimens, except for the height of the integral diaphragm, since the "grout-bed" for this specimen is 3 in., instead of the 3⁄4 in. grout bed seen in the other two specimens.

To maintain the overall height of the specimen, the height of the integral diaphragm is decreased (Figure 3.3 and 3.4) and is governed by the concrete cover of the steel bearing plate and beam.

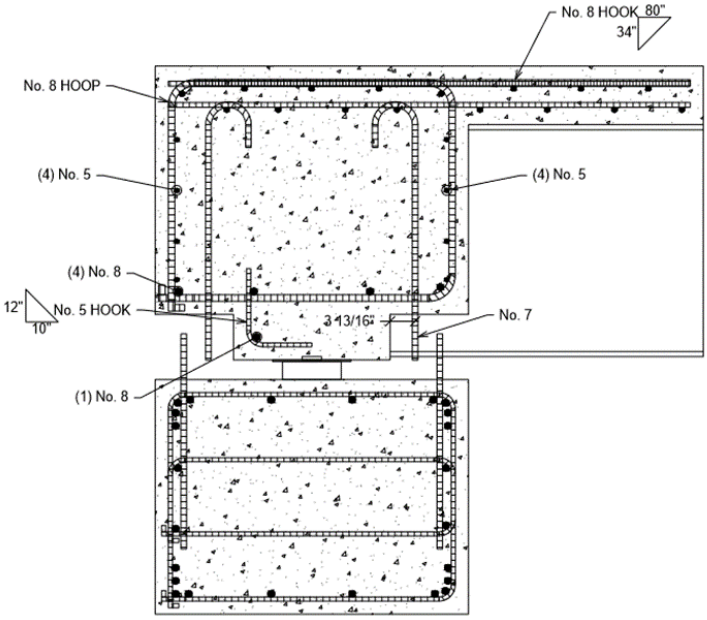

Figure 3.3 *UHPC-Joint specimen section view.*

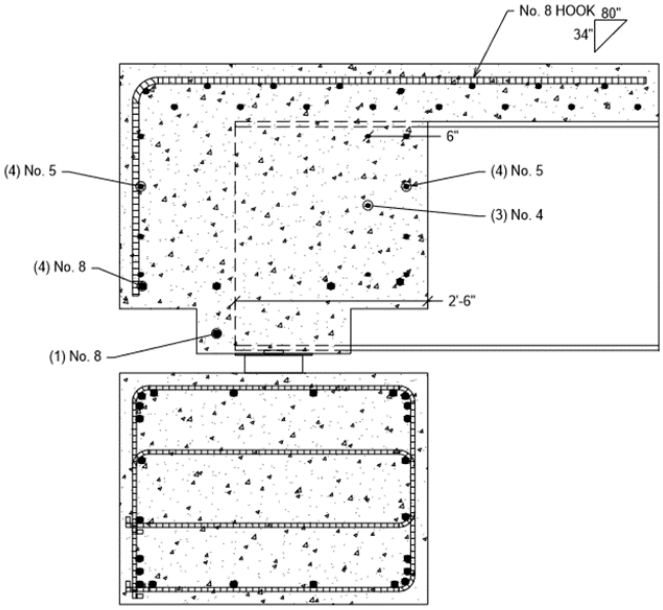

Figure 3.4 *UHPC-Joint specimen section view through beam.*

Note the steel bearing plate under the beam, the steel sliding shoe under the bearing plate, and the neoprene pads under the sliding shoe

The UHPC joint specimen would utilize the ABC application of "slide-in construction," using laminated neoprene pads with Teflon and stainless-steel sliding "shoes" (Figure 3.5).

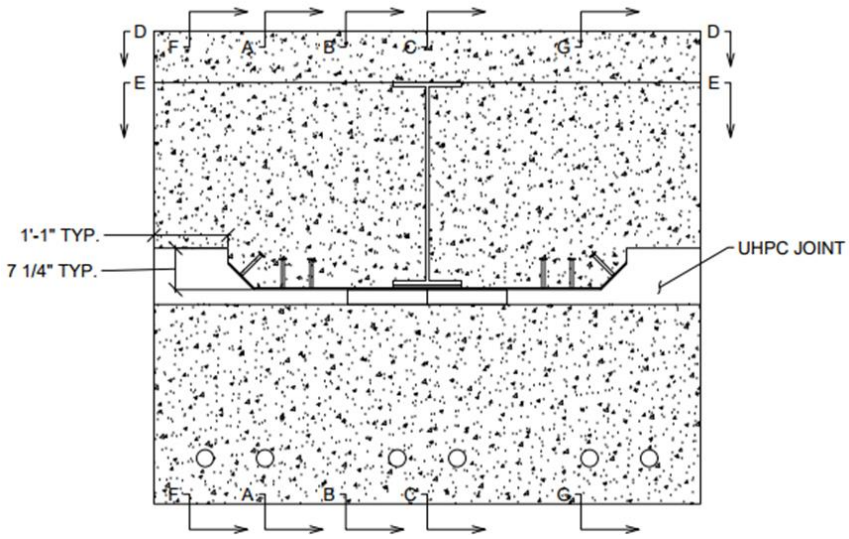

Figure 3.5 *UHPC-Joint specimen front view showing "sliding shoes" and pads.*

When the specimen is slid into its final position, the eight #7 mechanical couplers will be installed per manufacturer's instructions into the pile cap at the designed locations. Formwork will then be set for the installation of the UHPC to fill the joint and will be let to cure for the specified time per design. After the design strength of the UHPC has been met, formwork shall be removed, and this integral abutment connection is complete.

One initial concern from the design team for this connection was the ability for the UHPC to fill the entire joint without leaving voids, specifically on the front face interior corner of the joint "key." This issue was to be tested through a UHPC-flowability test, which was designed to simulate the proposed cross section (Figure 3.6), as well as a modified version (Figure 3.7), of the joint and installation procedure.

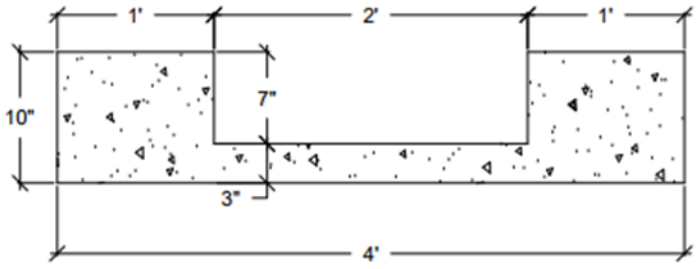

Figure 3.6 *UHPC-Flowability test design proposed cross section.*

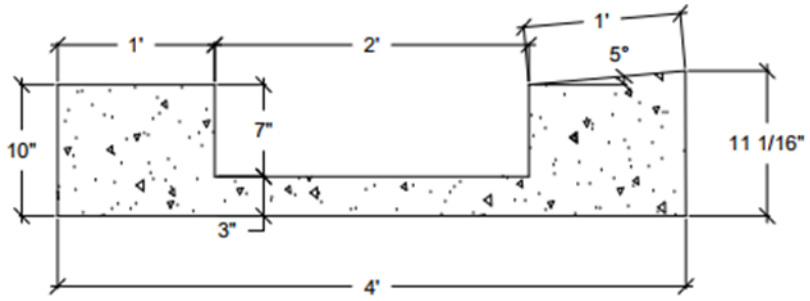

Figure 3.7 *UHPC-Flowability test design modified cross section.*

The modified cross section was to investigate the result of adding a 5° rise to aid in the removal of air. The section was designed to be 2 ft wide with the 7 in. "chimney," and be constructed out of metal and wood to provide proper formwork and support for the UHPC (Figure 3.8).

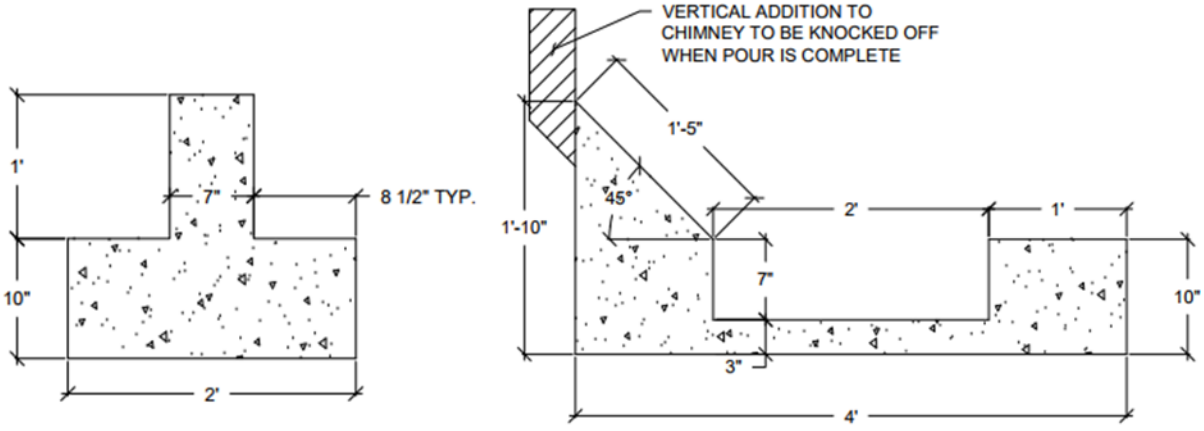

Figure 3.8 *UHPC-Flowability test setup design "chimney" cross section.*

After the UHPC had cured, the form was to be removed and observations of the final cross section were to be made as to see how well the UHPC had filled the form.

3.2 Grouted Reinforcing Bar Coupler

The design of this specimen was based on the design from the original design of the connection, with the only difference between the two phases being a reduction in the number of grouted reinforcing bar couplers. The original design had 17 couplers, while this design only has 8 (Figure 3.9).

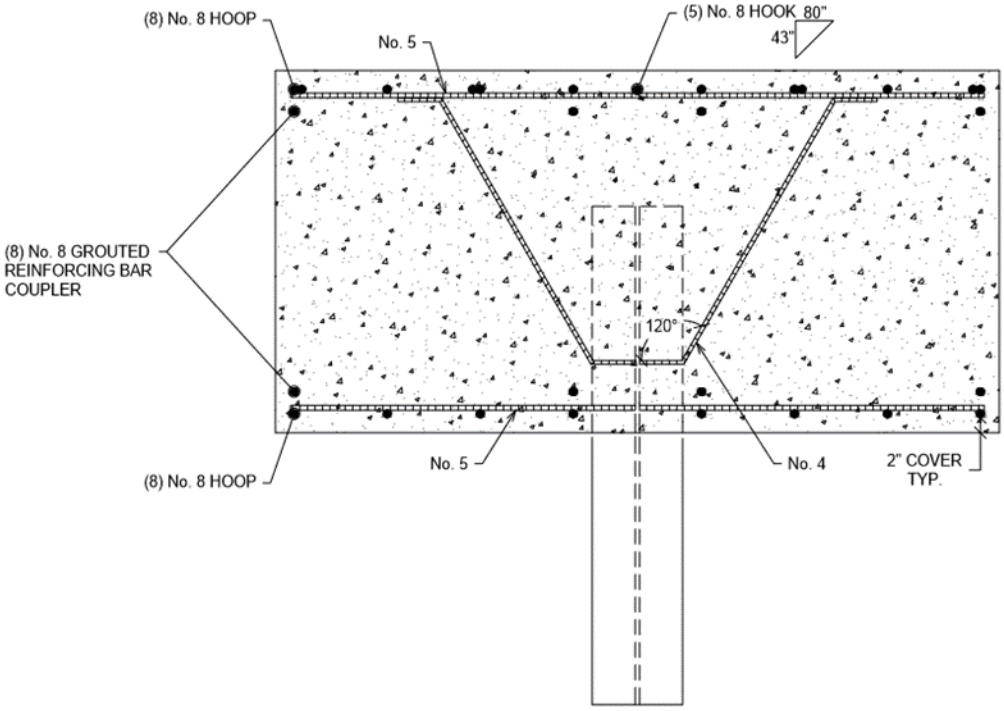

Figure 3.9 *Plan view of grouted reinforcing bar coupler showing locations of couplers.*

This reduction comes from the results of (Hosteng, Phares, & Redd, 2016) testing of the connection that is similar to the cast-in-place (control) specimen, specifically having a final crack at the back face from vertical loading of only 0.035 in. This crack was approximately 1.8 times the crack of the cast-in-place specimen, so a reduction in the number of couplers could be made to potentially simplify the construction due to a tolerance gain with the reduction of couplers.

The design of the couplers is the same as the couplers used in the original design, being the couplers were designed to be #8 epoxy-coated reinforcing bars with Dayton Superior D410 Sleeve-Lock Grout Sleeves filled with Dayton Superior D490 Grout (Figure 3.10).

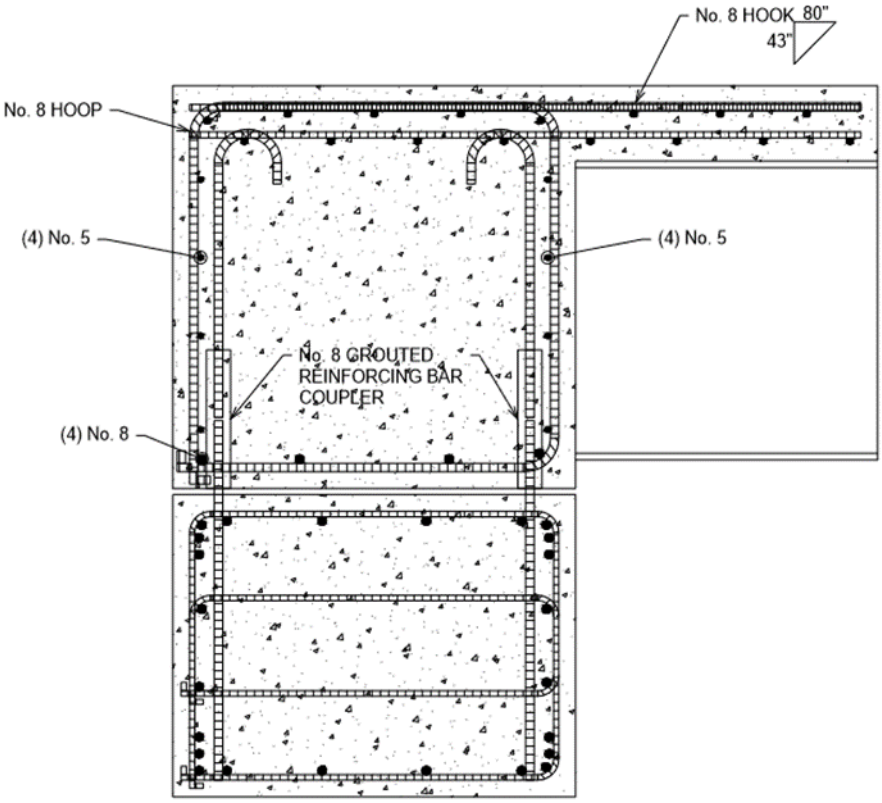

Figure 3.10 *Grouted reinforcing bar coupler section view through couplers.*

The overall size of the specimen and the distribution of the reinforcement is the same as the original design, which was done to eliminate variances in design other than the couplers (Figures 3.10 and 3.11).

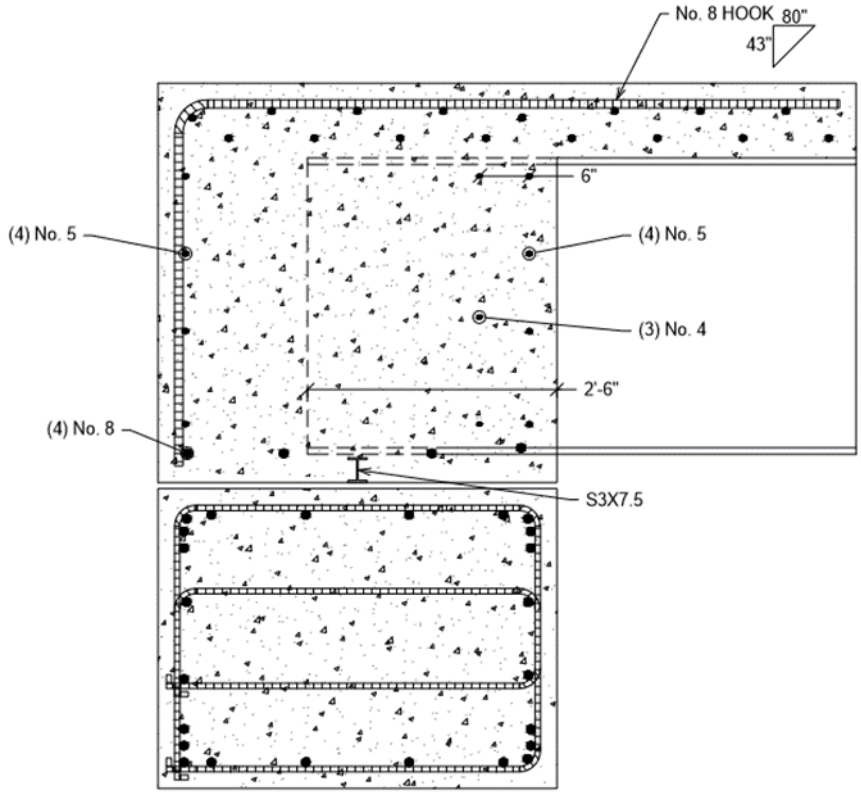

Figure 3.11 *Grouted reinforcing bar coupler section through beam.*

The grouted reinforcing bar coupler specimen would not be able to utilize slide-in ABC methods without jacking up the diaphragm due to the coupler bars protruding from the pile cap, which cannot be modified due to the design of the couplers themselves. This installation method is possible but another, and possibly preferred, installation method would be using a crane to suspend the diaphragm over the pile cap and lowering it to insert the reinforcing bars into the grout sleeves. Either way, after the protruding bars from the pile cap have been inserted into the grout sleeves of the diaphragm, the sleeves would then be filled with grout to complete the construction of this integral abutment connection.

3.3 Pile Coupler

This specimen was designed per the design and recommendations made after the results of testing by (Hosteng, Phares, & Redd, 2016). The revised pile coupler specimen uses the concept of the piles being the connection through the CMP voids being filled with a grouting material, but this design has four HP8X36 couplers acting as a force couple instead of having only two HP10X57 couplers at the center of the diaphragm/pile cap as the original design did (Figure 3.12).

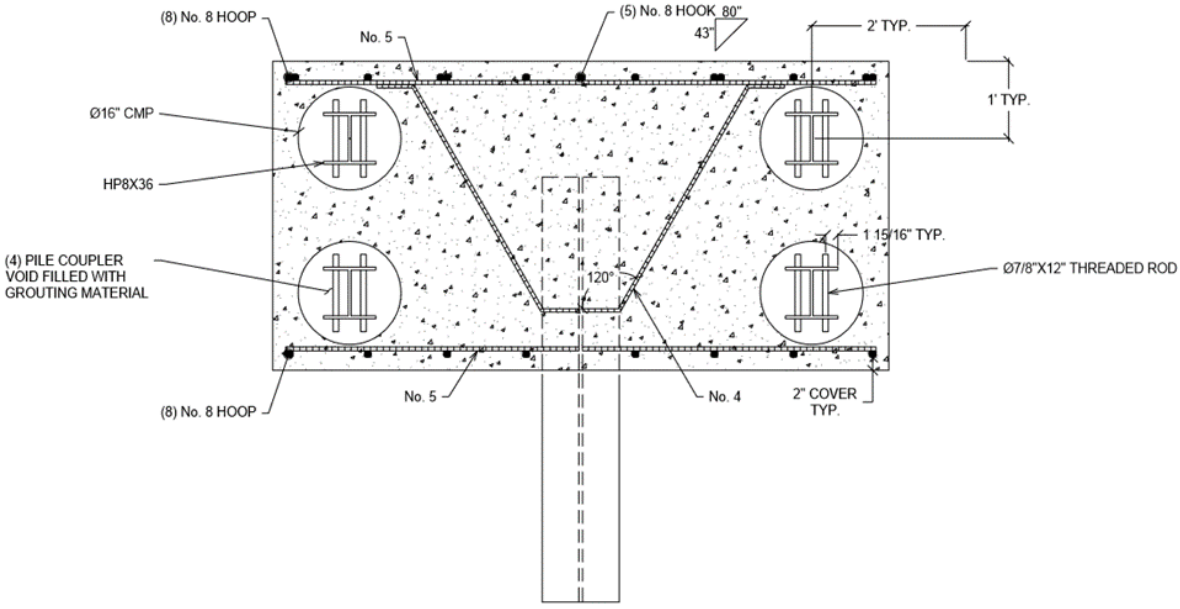

Figure 3.12 *Plan view of pile coupler showing locations of couplers.*

The couplers have the same premise as the original design couplers did, which is having the HP-sections suspended within the CMP void in the diaphragm and being lowered via a pulley system created with a U-bolt being attached to a lid on the CMP and feeding a wire holding the section through the U-bolt up through the 1 in. polyvinyl chloride (PVC) vent pipe. Then, with the HP-section lowered into place, half within the CMP void in the pile

cap and half within the CMP void in the diaphragm, a grouting material will fill the CMP voids through a 3 in. PVC grout port until the grout comes out entirely through the vent pipe and grout port, meaning that the void is filled to maximum capacity and has encased the HP-sections, and threaded rods for additional connectivity (Figure 3.13).

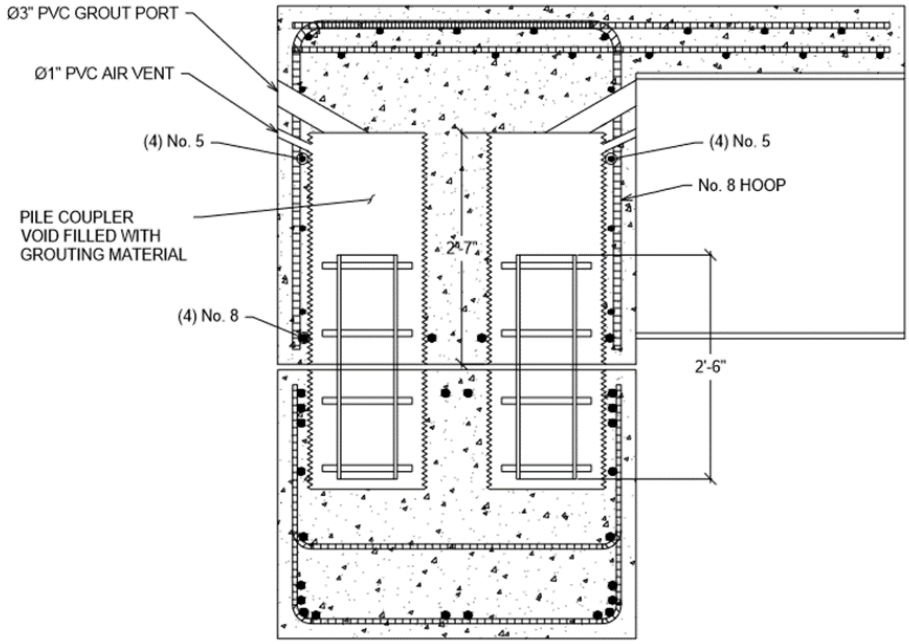

Figure 3.13 *Pile coupler section view through couplers.*

The overall size and reinforcement distribution of the pile coupler specimen are the same as the original design, which was done to eliminate any variances other than the couplers (Figure 3.14 and 3.15).

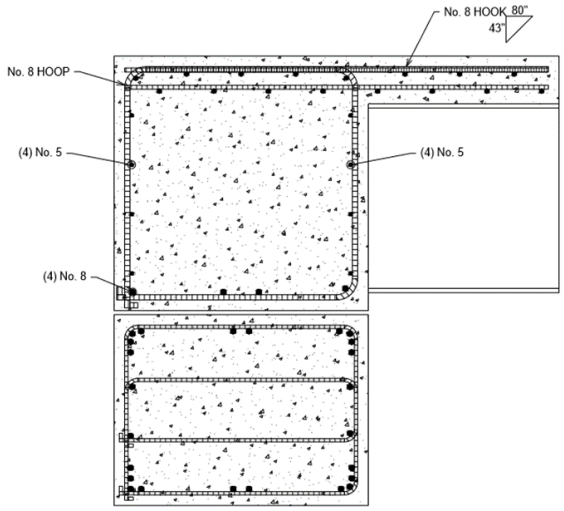

Figure 3.14 *Pile coupler section view.*

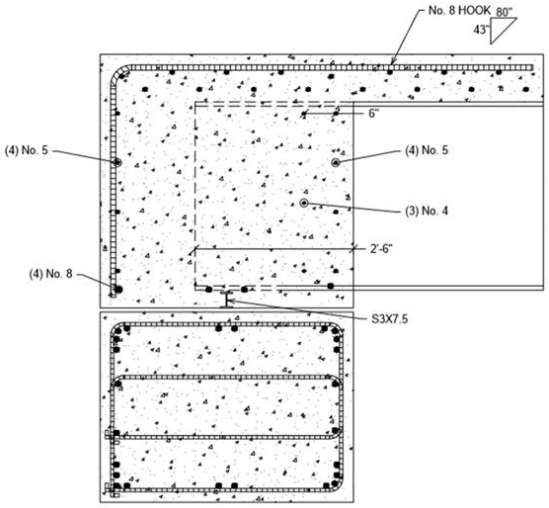

Figure 3.15 *Pile coupler section view through beam.*

The installation procedure for this specimen would be the slide-in ABC method. Since the CMPs would be near flush with the concrete surfaces and the HP-sections would be suspended within the diaphragm's CMP voids, sliding the diaphragm into place on top of the pile cap should not pose any issues. After the slide is complete, the HP-sections would be lowered, and the CMP voids would be filled with a cementitious material, which would complete this integral abutment connection.

CHAPTER 4. CONSTRUCTION

4.1 UHPC-Joint

4.1.1 Pile Cap

Construction of the specimen began with the pile cap. A reinforcing cage was erected following the design drawings (Figure 4.1).

Figure 4.1 *UHPC-Joint pile cap reinforcing cage.*

Multiple checks were done to ensure the protruding bars were at their designed locations, specifically in respect to elevation to ensure the 8 in. protrusion required for proper development in the UHPC filled joint. Also, the D310 threaded couplers had to be checked to ensure the tops would be flush with the top of the concrete when complete.

With the cage complete, formwork for the pile cap was erected and the cage was then placed inside (Figure 4.2).

Figure 4.2 *UHPC-Joint pile cap formwork.*

Since a process referred to as “match-casting” was to be done to align the PVC ducts to the reaction blocks, the blocks were utilized as formwork in addition to the EFCO steel formwork. With the cage set in the forms, checks were done to ensure the 2 in. concrete cover required per design were going to be met, all reinforcement was secure and installed as the designed locations, and the formwork was properly fastened.

Concrete from a local Ames redi-mix plant was cast in the formwork using materials in the Structural Engineering Research Laboratory at Iowa State University. Electric concrete vibrators were used to make sure the concrete was encasing the cage and filling the form to maximum capacity. The surface was given a roughened finish to ensure a 1/4 in. amplitude, which is required by the IowaDOT, by roughly brushing with a stiff-bristled broom in multiple directions (Figure 4.3 and 4.4).

Figure 4.3 *UHPC-Joint pile cap cast in concrete.*

Figure 4.4 *UHPC-Joint pile cap completed.*

Issues/Recommendations:

- Not all coupler bars resulted in the required 8 in. protrusion after casting concrete.
    - Add more “double-ties” to coupler bars to ensure no movement of coupler bars.

4.1.2 Integral Diaphragm

The initial step for constructing the integral diaphragm for the UHPC-Joint specimen was to conduct the flowability test of the UHPC in the proposed cross section. A decision

was made by the design team to negate the initial cross section, and test only the 5° rise cross section (Figure 4.5).

Figure 4.5 *UHPC flowability test formwork.*

The UHPC mix produced by Ductal from Lafarge was used as the UHPC material for this project, and the mix proportions used were that of the Special Provisions document by the IowaDOT for Ultra-High-Performance Concrete. (IowaDOT, 2014) The flowability quantity of approximately 5.11 ft^3 was designed to fill the test section, fill multiple testing cylinders, and account for material loss. The section was filled and left to cure for three days, at which point the formwork was stripped to analyze the adequacy of the flowability of the UHPC (Figure 4.6).

Figure 4.6 *UHPC flowability test completed.*

As shown in Figure 4.1.6, it is apparent that the UHPC material successfully filled the entirety of the cross section without any issues of voids caused by the volume of air. With this knowledge, the formwork for the integral diaphragm could be constructed through multiple 3/4 in. plywood diaphragms fastened together, which had the same dimensions used for the flowability test section (Figures 4.7 through 4.9).

Figure 4.7 *UHPC integral diaphragm formwork top view of diaphragms.*

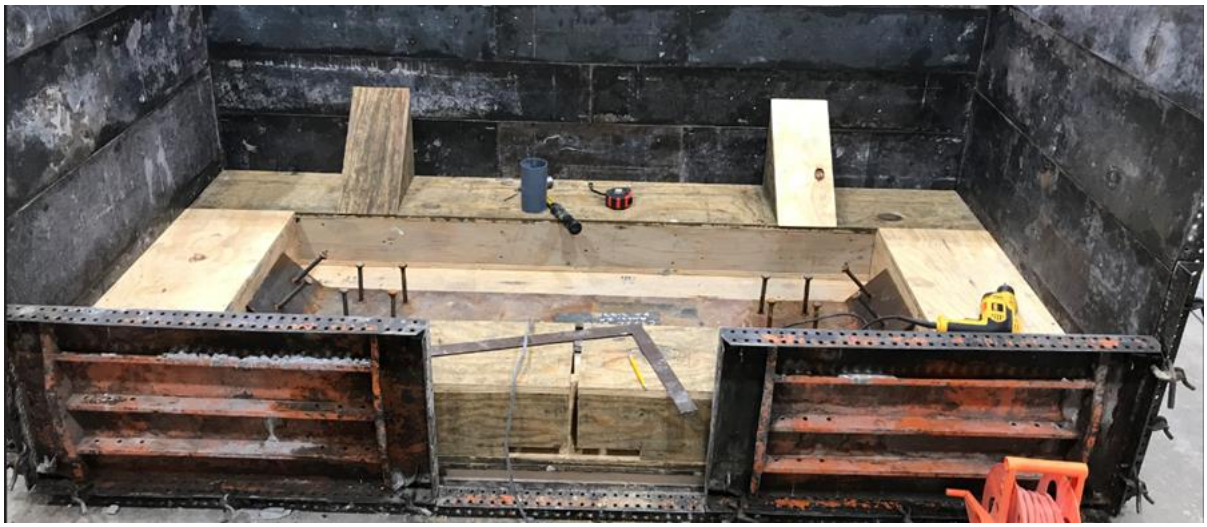

Figure 4.8 *UHPC integral diaphragm formwork completed.*

Figure 4.9 *UHPC integral diaphragm bottom formwork side view.*

With the bottom formwork completed, the reinforcement cage was erected. One important note was to ensure the 17 coupling #7 bars would protrude through the bottom plywood formwork by 1 in. to ensure the bars would protrude through the bottom of the section at the required 8 in. (Figure 4.10 and 4.11).

Figure 4.10 *UHPC integral diaphragm reinforcement cage.*

Note the coupler bars passing through the plywood formwork.

Figure 4.11 *UHPC integral diaphragm reinforcement cage completed.*

Also, the design drawings called for the sliding shoe to protrude from the bottom of the integral diaphragm, but this was not done for the specimen in the laboratory. The purpose of this protrusion is to prevent any concrete catching on the laminated neoprene pads with

Teflon during the actual slide of the bridge, but no slide would be done in the laboratory, instead, the diaphragm was to be lifted into place by crane. Therefore, to simplify formwork in the laboratory, the sliding shoe was not protruding from the bottom of the diaphragm. To create the best bond surface for the UHPC and precast concrete interface, a form retarder needed to be applied to the bottom formwork of the integral diaphragm. To apply the form retarder (Figure 4.12), it was decided to use a paint roller and brush to ensure the form retarder would be applied to the entirety of the formwork, while not being applied to any reinforcing bars (Figures 4.13 and 4.14).

Figure 4.12 *Form retarder to be applied to integral diaphragm formwork.*

Figure 4.13 *Form retarder being applied to integral diaphragm formwork.*

Figure 4.14 *Form retarder application completed.*

With the form retarder applied and final checks done to the formwork, the integral diaphragm was cast in concrete (Figure 4.15).

Figure 4.15 *UHPC integral diaphragm cast in concrete.*

The formwork was stripped, and the integral diaphragm was inspected, and it was noted that concrete did not pass underneath the beam as intended, and the coupler bars did not have consistent protruding lengths from the bottom of the section (Figure 4.16).

Figure 4.16 *UHPC integral diaphragm completed.*

To finish the required bottom-side finish for the integral diaphragm, a 3,000-psi power wash was used to spray off the form retarder and leave an exposed aggregate finish (Figure 4.17).

Figure 4.17 *UHPC integral diaphragm exposed aggregate finish.*

Issues/Recommendations:

- Variation of protruding length for coupler bars.
    - Add more "double-ties" to coupler bars to ensure no movement of coupler bars and check protruding length for each bar.
- Bottom of beam was not completely cast in concrete.
    - Ensure to do additional vibrating around beam to allow for movement of concrete.
- #5 hooks behind beam to hold #8 longitudinal bar did not stay in place.
    - Revise this area of reinforcement, specifically how to tie the #5 hooks to the rest of the cage.
- #7 coupler bars were not easily tied to reinforcing cage.
    - Revise length of coupler bars, or orientation, to ensure proper areas to tie bars to rest of reinforcing cage.

4.1.3 Connection

The integral diaphragm was craned over to the test area where the pile cap was installed and ready for the connection. Since this connection would utilize the ABC method

of “slide-in” construction, a slide had to be simulated to ensure the protruding bars on the back side of the abutment would have proper clearance during the installation process. The integral diaphragm was suspended just over the neoprene pads enough to allow for movement, the slide was simulated, and the clearance of the rear bars was proven to be adequate (Figure 4.18).

Figure 4.18 *UHPC joint rear connection bars with adequate clearance.*

After the integral diaphragm was placed in its final location, the threaded bars on the front side of the specimen were installed. One concern was the available space to insert the bar into the threaded coupler in the pile cap and be able to properly tighten the bar, but this was proven to be done without any issues (Figure 4.19).

Figure 4.19 *Front connection bars with installed threaded bars in pile cap.*

With the connection bars properly installed, the joint formwork was erected. This formwork included ports along the side and front faces to allow for air to be pushed out by the UHPC during the install, and a spout and chimney system to allow for a simplified installation of the material into the joint from the mixer (Figures 4.20 through 4.22).

Figure 4.20 *Front face joint formwork with air ports.*

Figure 4.21 *Rear face joint formwork with chimneys.*

Figure 4.22 *Spout and chimney system for installation of UHPC material.*

The UHPC material, Ductal by LaFarge, had to be installed in five batches due to the equipment available in the Structural Research Laboratory, and each batch took approximately 30 minutes to mix and then pour into the joint. This caused issues with the casting of the joint since each batch set up too quickly to allow for the batch being cast to

flow into the previous batch, which caused layers of material within the joint instead of one layer of material (Figure 4.23).

Figure 4.23 *Completed UHPC joint showing the multiple layers of material.*

Issues/Recommendations:

- UHPC layers due to installing material in multiple batches.
    - Have construction procedures and equipment available to install the UHPC joint in one large batch instead of multiple batches, which should allow the material to flow as it did in the flowability test.

4.2 Grouted Reinforcing Bar Coupler

4.2.1 Pile Cap

Construction of the specimen began with the pile cap. A reinforcing cage was erected following the design drawings (Figure 4.24).

Figure 4.24 *GRBC pile cap reinforcing cage.*

Multiple checks were done to ensure the protruding bars were at their designed locations, specifically in respect to elevation to ensure the 8 in. protrusion required for proper development in the grout sleeves.

With the cage complete, formwork for the pile cap was erected and the cage was then placed inside (Figure 4.25).

Figure 4.25 *GRBC pile cap formwork.*

Since a process referred to as “match-casting” was to be done to align the PVC ducts to the reaction blocks, the blocks were utilized as formwork in addition to the EFCO steel formwork. With the cage set in the forms, checks were done to ensure the 2 in. concrete cover required per design were going to be met, all reinforcement was secured and installed at the designed locations, and the formwork was properly fastened.

Concrete from a local plant was cast in the formwork using materials in the Structural Research Laboratory at Iowa State University. Electric concrete vibrators were used to make sure the concrete was encasing the cage and filling the form to maximum capacity. The surface was given a roughened finish by brushing with a stiff-bristled broom along the long direction (Figure 4.26).

Figure 4.26 *GRBC pile cap completed.*

Issues/Recommendations:

- No significant issues.

4.2.2 Integral Diaphragm

To properly align the protruding bars to the grout sleeves, match-casting was used to set the locations of the grout sleeves. Using a full 4 ft x 8 ft x 3/4 in. sheet of plywood, the Dayton Superior D492 Sleeve-Lock form plugs (Figure 4.27) were installed to hold the grout sleeves in place during erection of the GRBC integral diaphragm.

Figure 4.27 *Dayton Superior form plug.*

The plywood was placed on top of the pile cap and ensured that it was square with the pile cap. Then, marks were placed on the plywood where the protruding bars were located, and those marks were then drilled with two different drilling bits. A 1 in. diameter spade bit was used to cause the nuts and washers of the form plug to be recessed in the plywood so that the bottom surface would be flat, and a 7/16 in. diameter twist drill bit was used to make holes in the plywood for the form plug bolt to pass through (Figure 4.27 middle).

The form plugs were installed and tightened, with a 14-mm socket, enough to allow for the grout sleeves to be placed and turned to have the port plugs facing the designed locations, which were out the front and back faces of the integral diaphragm. When the position of the sleeves was verified, the form plugs were tightened until the sleeves would not turn, and the Dayton Superior D487 seal plugs were placed on the tops of the grout sleeves (Figure 4.28).

Figure 4.28 *Dayton Superior form plug.*

The bolts of the form plugs were cut to be flush with the plywood surface, and then the match-casted formwork was placed down to begin the formwork for casting the integral diaphragm in concrete (Figure 4.29).

Figure 4.29 *GRBC reinforcing cage with Dayton Superior grout sleeves.*

With the grout sleeves and steel beam set in their designed places, the reinforcing cage was erected, and formwork was placed. Steel forms made most of the formwork, but custom woodwork was required to adequately provide formwork for the area around the beam. Finally, the integral diaphragm was encased in concrete (Figures 4.30 through 4.32).

Figure 4.30 *GRBC reinforcing cage.*

Figure 4.31 *GRBC integral diaphragm formwork.*

When the GRBC integral diaphragm was stripped from the formwork, the grout sleeves and ports were checked to ensure there was no concrete blocking any holes. All eight sleeve bottoms were open, and all the ports for the sleeves were located (Figure 4.33).

Figure 4.32 *GRBC integral diaphragm completed.*

Figure 4.33 *GRBC grout sleeve ports located post concrete casting.*

Issues/Recommendations:

- Had to adjust reinforcing cage slightly to accommodate grout sleeve ports.
    - Shifted reinforcement and redlined design drawings.
- One port was not at the concrete surface after casting, so chipping away of concrete was required to locate it.
    - Ensure all ports are long enough to extend to slightly beyond formwork.

4.2.3 Connection

After the pile cap was set in place for testing, the integral diaphragm was lowered into position. A dry fit was done to make sure all the protruding bars and grout sleeves were in alignment, and all eight connections lined up without any issues (Figure 4.34).

Figure 4.34 *GRBC connection alignment.*

To create the 3/4 in. gap between the pile cap and integral diaphragm for the grout bed, 3/4 in. neoprene pads were installed. These pads were cut to be larger than the grout sleeve opening and have a hole in the middle for the protruding bar. To ensure a seal around the neoprene pads and grout sleeves, silicone was placed around the neoprene pads and dispersed when the integral diaphragm was installed (Figure 4.35).

Figure 4.35 *GRBC 3/4 in. neoprene pad and silicone seal.*

Next, the formwork for the grout bed was erected, and Dayton Superior D490 grout mix was pumped into various ports within the formwork with a grout pump (Figure 4.36).

Figure 4.36 *Grout pump.*

Port plugs were installed into ports when the grout would begin to seep out until the entirety of the bed was filled with grout and all ports were plugged (Figure 4.37).

Figure 4.37 *GRBC grout bed completed.*

One important note was to ensure the lower port for the grout sleeves was plugged so no grout from the grout bed would enter the port.

The formwork was removed after the grout bed had set, then the eight grout sleeves were filled with the Dayton Superior grout mix. After the sleeves were verified to be clear of debris, the pump hose was placed into the lower port and grout was pumped so that the grout was seeping out of the top port, then both ports were plugged (Figure 4.38).

Figure 4.38 *GRBC grout sleeve completed.*

This procedure is meant to ensure that the air within the sleeves is pushed out by the grout and properly encasing the coupling bars.

Issues/Recommendations:

- Dayton Superior D490 Grout-Mix was slightly plastic after mixing per specifications.
    - Added water until a flowable consistency was achieved.

4.3 Pile Coupler

4.3.1 Pile Cap

Construction of the specimen began with the pile cap. A reinforcing cage was erected following the design drawings (Figure 4.39).

Figure 4.39 *Pile coupler pile cap reinforcing cage.*

Multiple checks were done to ensure the corrugated metal pipes (CMPs) were in the proper locations, specifically that the tops of the CMPs would be flush with the top surface of the pile cap. The CMPs were installed into the reinforcing cage using salvage rebar to set the elevation (Figure 4.40), and metal wire to set the locations (Figure 4.41).

Figure 4.40 *Salvage reinforcing steel bar holding up CMPs.*

Figure 4.41 *Metal wire holding CMPs in designed locations.*

To keep the concrete from flowing to the inside of the CMP's, a plug was constructed by using a circle of plywood cut to the inside diameter of the CMP, cut in half to allow for pullout when casting is complete, and a 2x4 holding the two halves together (Figure 4.42).

Figure 4.42 *CMP plug.*

With the cage complete, formwork for the pile cap was erected and the cage was then placed inside (Figure 4.43).

Figure 4.43 *Pile coupler pile cap formwork.*

Since a process referred as “match-casting” was to be done to align the PVC ducts to the reaction blocks, the blocks were utilized as formwork in addition to the EFCO steel

formwork. With the cage set in the forms, checks were done to ensure the 2 in. concrete cover required per design were going to be met, all reinforcement was secure and installed at the designed locations, and the formwork was properly fastened.

Concrete from a local Ames redi-mix plant was cast in the formwork using materials in the Structural Research Laboratory at Iowa State University. Electric concrete vibrators were used to make sure the concrete was encasing the cage and filling the form to maximum capacity. The surface was given a roughened finish by brushing with a stiff-bristled broom along the long direction (Figure 4.44).

Figure 4.44 *Pile coupler pile cap completed.*

After the concrete had cured, the formwork was removed, and the plugs were taken out of the CMPs (Figure 4.45).

Figure 4.45 *CMP void completed.*

Issues/Recommendations:

- CMP movement during concrete pour.
    - Additional metal wire tying the bottom of the CMP to the reinforcing cage.
- One CMP plug blew out and let concrete come up in void.
    - Additional weight added to plug.
    - Avoid using vibrator near CMP bottoms causing concrete to rapidly move upwards.

4.3.2 Integral Diaphragm

Plywood circles were made to align the CMPs in the integral diaphragm to be aligned with the CMPs of the pile cap (Figure 4.46).

Figure 4.46 *Plywood alignment of integral diaphragm CMP*.

The CMP lid was fabricated using a circular steel plate that was fabricated to have the 3 in. duct to install the cementitious material into the CMP void, four reinforcing steel bars to act as guides for the steel sections to be encased within the CMPs, and a U-bolt that would act as a pulley system for the wire to raise and lower the steel section within the CMP voids.

The wire would pass through the 1 in. duct installed at the top of the CMP just below the lid, and this duct also acts as an air-port to allow all air within the voids to be forced out when the cementitious material is installed (Figures 4.47 through 4.49).

Figure 4.47 *CMP lid with accessories.*

Figure 4.48 *Bottom view of CMP void.*

Figure 4.49 *CMP ducts against formwork.*

The ducts for the specimen constructed in the laboratory were designed to surface at the sides of the specimen, opposed to the design details requiring the ducts to surface at the front and back faces, to make the installation of the cementitious material easier with the equipment available in the laboratory. Larger equipment available to contractors would allow for the ducts to be on the front and back faces, since having the surface of the duct at the sides of the real-world application would not be possible due to multiple sections being adjacent to each other, which would prevent the installation of the cementitious material.

To ensure the CMPs would not shift upwards when casting the integral diaphragm, a "locking" mechanism was installed within the reinforcement cage. This mechanism consisted of using salvage reinforcing steel bars to span across the CMP lids to be tied to other reinforcing bars, which were then tied to the reinforcement cage (Figure 4.50).

Figure 4.50 *CMP "locking" reinforcing steel bar.*

With the CMPs, and accessories, and steel beam set in their designed places, the reinforcing cage was erected, and formwork was placed. Just as the GRBC specimen, steel forms made most of the formwork, but custom woodwork was required to adequately provide formwork for the area around the beam. Finally, the integral diaphragm was encased in concrete (Figures 4.51 and 4.52).

Figure 4.51 *Pile coupler reinforcement cage.*

Figure 4.52 *Pile coupler integral diaphragm completed.*

When the formwork was stripped from the completed pile coupler integral diaphragm, a few of the 1 in. ducts had to be found through chipping away of concrete, but all the 3 in. ducts and CMP voids had successfully surfaced (Figures 4.53 and 4.54).

Figure 4.53 *Surfaced 3 in. duct and 1 in. duct found after chipping concrete.*

Figure 4.54 *Surfaced CMPs.*

Issues/Recommendations:

- Three of four 1 in. CMP ducts did not appear at the concrete surface after casting, so chipping away of concrete was required to locate it.
    - Ensure all ports are long enough to extend slightly beyond formwork.

4.3.3 Connection

The design of the steel sections was revised from having four lines of threaded rods along the length of the section, to have two rows of shear studs on each face of the web along the length of the section (Figure 4.55).

Figure 4.55 *Steel section coupler with shear studs.*

This was done based on the studs being able to cause the axial development of the sections as the threaded rods would but would also simplify the fabrication.

Steel wire was used to suspend the steel sections within the CMP voids in the integral diaphragm during the installation of the diaphragm, and then the sections were lowered into the CMPs in the pile cap after the diaphragm was in position (Figure 4.56).

Figure 4.56 *Steel sections suspended within integral diaphragm CMPs.*

The CMPs were filled with a self-consolidating concrete (SCC) mix from a local plant, which had an 18 in. spread (Figure 4.57).

Figure 4.57 *SCC 18 in. spread.*

The SCC was installed by using a barrel with a funnel, as well as dumping with buckets (Figure 4.58).

Figure 4.58 *Barrel with funnel to install SCC.*

The SCC was installed through the 3 in. ducts until filled, and the 1 in. duct was plugged when material began to flow through it (Figures 4.59 and 4.60).

Figure 4.59 *SCC installed through 3 in. duct.*

Figure 4.60 *SCC completed install with 1 in. duct plugged and 3 in. duct filled.*

The 3/4 in. grout bed was created by using 3/4 in. thick nuts to create the required gap. To ensure a seal around the CMP voids, 1 in. insulation foam rings were glued around the pile cap CMP voids, which would compress when the diaphragm was installed. Formwork similar to the GRBC grout bed formwork was erected and a non-shrink grout complying to Iowa DOT standards (Figure 4.61) was installed using the grout pump and procedure used for the GRBC grout bed (Figure 4.62).

Figure 4.61 *Non-shrink grout used for pile coupler grout bed.*

Figure 4.62 *Pile coupler grout bed completed.*

Issues/Recommendations:

- SCC aggregate consolidated to the bottom of barrel with funnel when installing, and bucketing material had to be done to finish install.
    - Avoid using equipment that would allow for settlement of SCC aggregate.
    - Add water to SCC to cause larger spread, and higher flowability.
- Reinforcing steel bar guides for steel sections were too close to edges of web and flanges, preventing the sections from being completely suspended within CMP voids.
    - Revise design of guides to avoid this “pinching” issue.

- Steel wire would not move smoothly through pulley system when attempting to shift steel sections within CMP voids.
    - Use material other than steel wire to suspend sections.
    - Use a pulley wheel in place of the U-bolt to be the pulley system to shift the steel sections in the CMP voids.

CHAPTER 5. LABORATORY TESTING

5.1 Methodology

The setup for testing the strength and durability of the three integral abutment connection details required the construction of, two reaction blocks to attach the specimens to the strong floor of the structural laboratory with post-tensioning, causing the specimens to have a fully-fixed boundary condition (Figures 5.1 through 5.3).

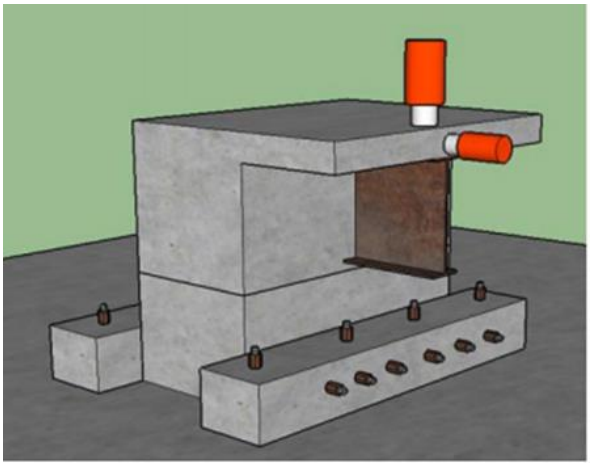

Figure 5.1 *Model of testing setup – front view.*

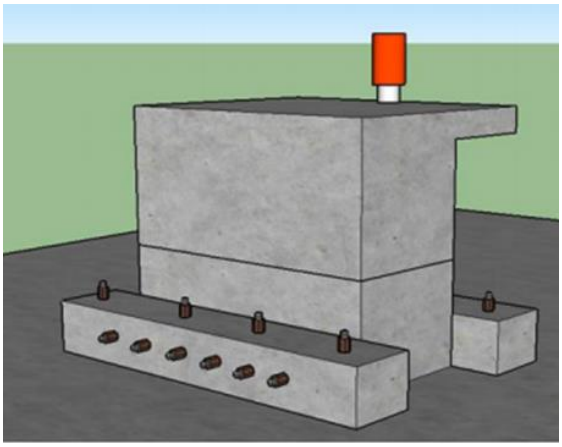

Figure 5.2 *Model of testing setup – rear view.*

Figure 5.3 *Laboratory testing setup.*

Actuators and load frames were used to apply two loads onto the specimens to simulate thermal loads and live loads, which tested the strength and durability of the three integral abutment connection details, as well as the adequacy of the design of the precast segments of the specimens. The analysis for strength and durability of the connection details would be conducted by only static loading and observing the structural responses of the specimen, specifically the magnitude of the crack widths between the precast segments and the stresses of coupling materials. The values recorded would then be presented and compared to the results of the same testing procedures presented in (Hosteng, Phares, & Redd, 2016).

The fixed boundary condition applied to the specimens through the reaction blocks and post-tensioning caused the specimens' structural response to be a worst-case scenario for the connection details. This is apparent since in the field application of the details,

translations and rotations of the integral abutment would be present due to the flexibility of the driven piles connected to the pile cap as well as the girders connected to the integral diaphragm.

Two static loads were applied to the specimens, the first was a horizontal load meant to cause tension on the front face of the abutment, and the second was a vertical load to cause tension at the rear face of the abutment. The horizontal load was to simulate thermal contraction of the integral abutment bridge, while the vertical load was to simulate thermal expansion of the bridge as well as live loading. Both load cases, and how the structure response should be, are shown in Figures 5.4 through 5.6.

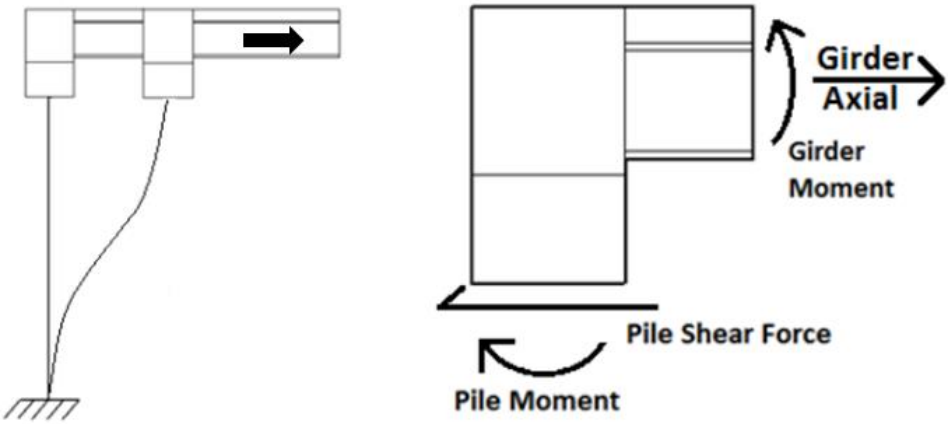

Figure 5.4 *Structural analysis for thermal contraction of bridge.*

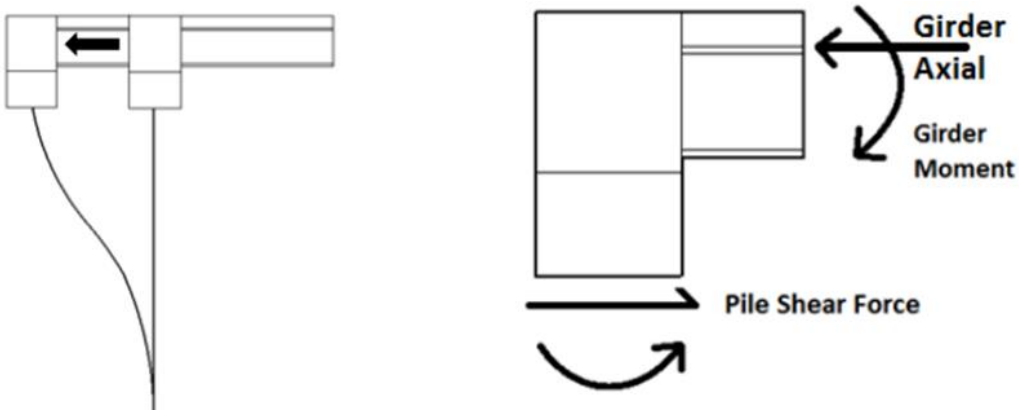

Figure 5.5 *Structural analysis for thermal expansion of bridge.*

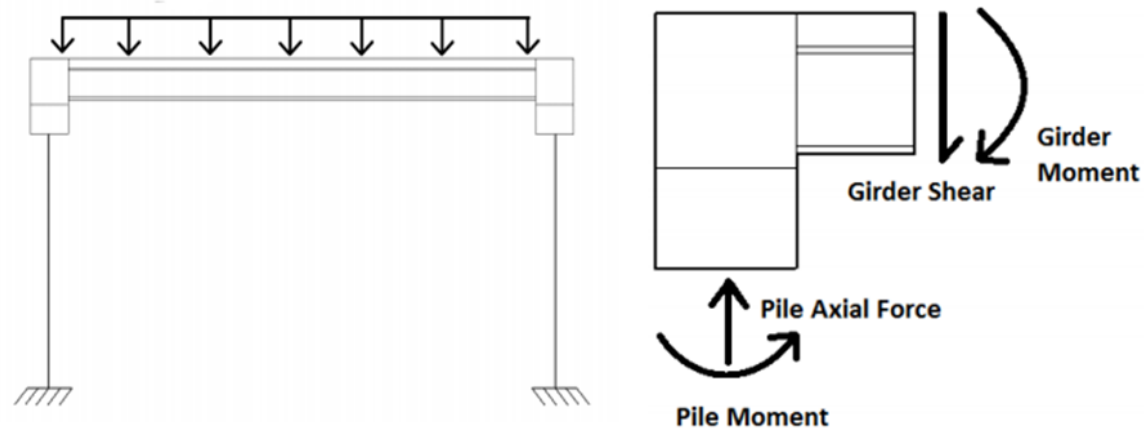

Figure 5.6 *Structural analysis for live loading of bridge.*

The magnitude of loads to be applied was the same for (Hosteng, Phares, & Redd, 2016) so comparisons could be made with the results. The horizontal loading was set to 100 kips from a study of thermal forces typically resisted by the stiffness of the foundation piles and surrounding soil. This load was not designed to fail the specimen, but to analyze the results at service loading. The vertical loading was set to 400 kips since it was the largest load that would be able to be applied in the structural laboratory. This vertical load is much greater than the service level loading conditions to the integral abutment and maximum stresses that can be present in the foundation piles but was used to establish the failure mode of the connection details. Utilizing the results of these failure modes will aid in designing an

appropriate factor of safety and help with designs using these integral abutment connection details.

5.2 Instrumentation

A variety of instruments were installed on the specimens to monitor and analyze the strength and durability of the three integral abutment connection details. First, to record the magnitude of the tension-side crack widths for each loading case, displacement transducers, called DCDTs, were installed at three positions on both the front and rear face of the specimens. These transducers would record the vertical displacements caused by cracking of the cold joint between the integral diaphragm and pile cap of the integral abutment. The result of these recordings would be compared to those of (Hosteng, Phares, & Redd, 2016) and report the severity of the possibility of infiltration of water or other chemicals that could cause structural deterioration of the connection details. Another two displacement transducers were installed at the rear face of the specimen to monitor any horizontal displacement, or slip, between the integral diaphragm and pile cap during horizontal loading.

Second, to record the development of the coupling materials, sacrificial strain gauges were installed on some of the coupling reinforcing steel bars for the UHPC joint and GRBC specimens, and on the steel sections of the pile coupler. These gauges would monitor the development of strains in the materials, which can be tabulated into stresses to determine the level of strength of the coupling materials during both loading cases.

Third, external strain gauges, called BDIs, were installed at the locations of the vertical displacement transducers to record the overall strength of the integral abutment during both load cases. The recorded values would be compared to values determined by AASHTO to declare which type of failure was present during the test.

Finally, displacement gauges, called string-pots, were installed at four corners of the pile cap to monitor any rotation of the pile cap that would be opposed to the assumed fixed boundary condition. Also, one displacement gauge was installed at the end of the cantilever beam to record the displacement of the beam during both load cases and compare it to the displacement of the joint crack.

The layout of the instrumentation for each specimen is shown in Figures 5.7 through 5.10.

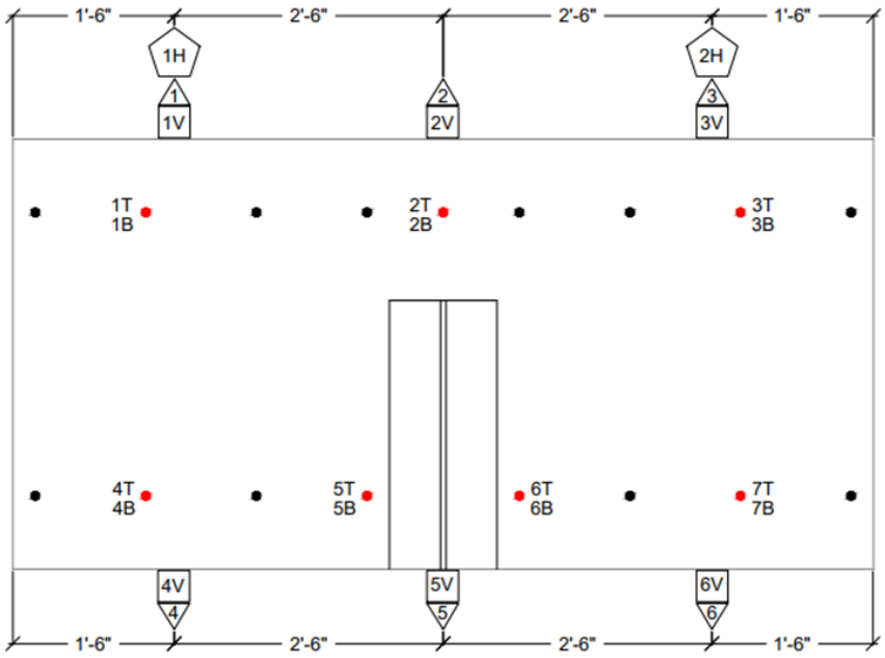

Figure 5.7 *Instrumentation plan for UHPC joint.*

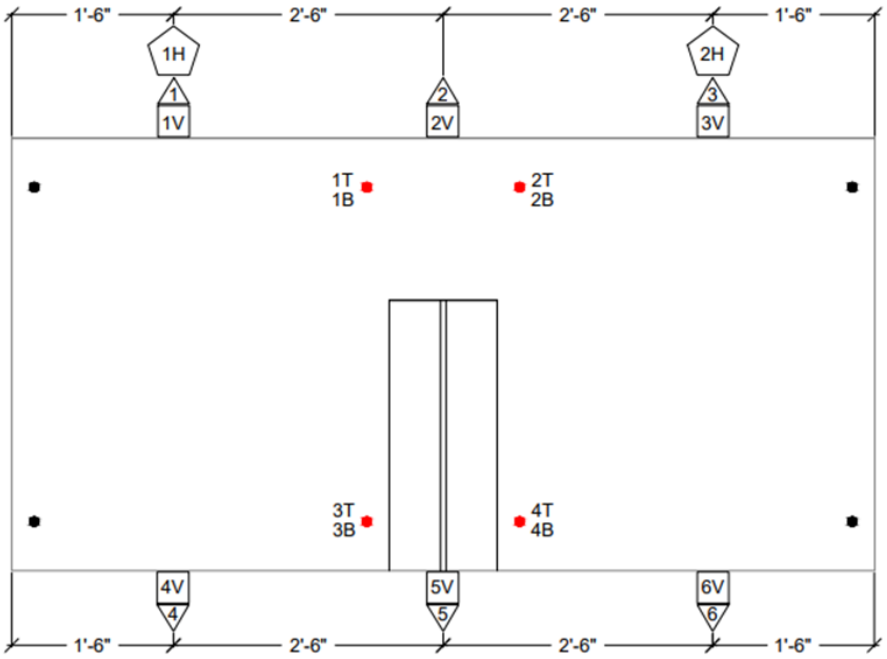

Figure 5.8 *Instrumentation plan for GRBC.*

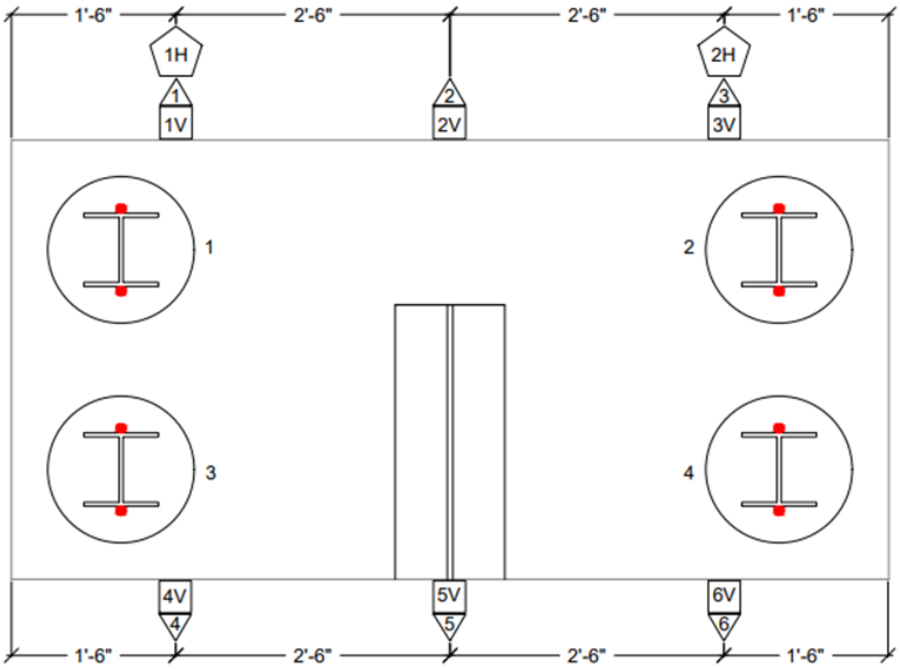

Figure 5.9 *Instrumentation plan for pile coupler.*

The squares represent the vertical displacement transducers, the pentagons represent the horizontal displacement transducers, the triangles represent the external strain gauges, and the red dots represent the locations of the sacrificial strain gauges.

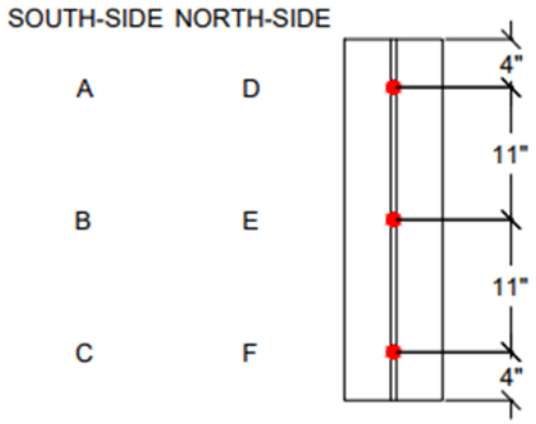

Figure 5.10 *Sacrificial strain gauge plan for pile coupler steel sections.*

Photographs of the setup of the instrumentation for each specimen are shown in Figure 5.11.

Figure 5.11 *External strain gauge (left), vertical displacement transducer, horizontal displacement transducer, and external strain gauge (center), and sacrificial strain gauge (right).*

5.3 Results

5.3.1 UHPC Joint

The horizontal loading reached the maximum value of 100 kips, which caused a crack at the front face of the abutment to be 0.018 in. (Figure 5.12).

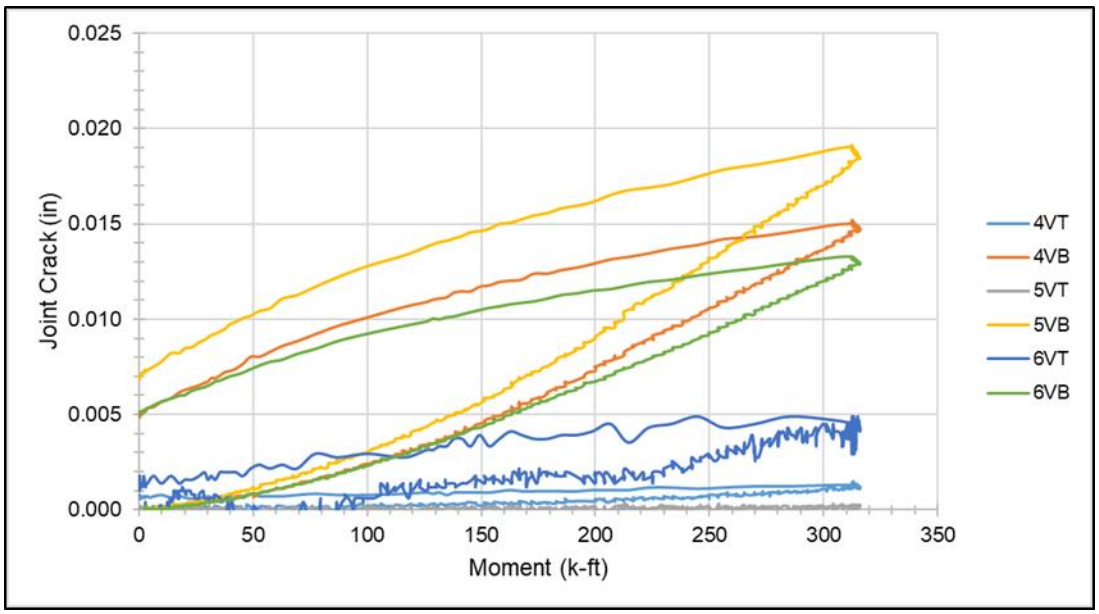

Figure 5.12 *Crack width versus moment due to horizontal load*.

The control specimen from (Hosteng, Phares, & Redd, 2016) had a crack of 0.001 in. for the same loading; therefore, the crack seen from the UHPC joint connection was approximately 1.8 times greater.

Note that for this specimen, two displacement transducers were used to capture the crack propagation of both the integral diaphragm to joint interface (4VT, 5VT, and 6VT) and the joint to pile cap interface (4VB, 5VB, and 6VB), and the larger values of the cracks came from the joint to pile cap interface. This is reasonable since the surface preparation of the pile cap was not as complex as that for the integral diaphragm.

No horizontal slip was recorded for the connection, and the maximum reinforcing bar stress for the connection bars was approximately 12 ksi in the connection bars protruding from the pile cap.

The vertical load was then applied up to a value of 397 kips, at which point the beam began to fail due to the buckling of the web (Figure 5.13).

Figure 5.13 *Beam buckling failure causing end of test*.

The maximum joint crack recorded at the rear face of the specimen at the maximum load was 0.032 in. (Figure 5.14).

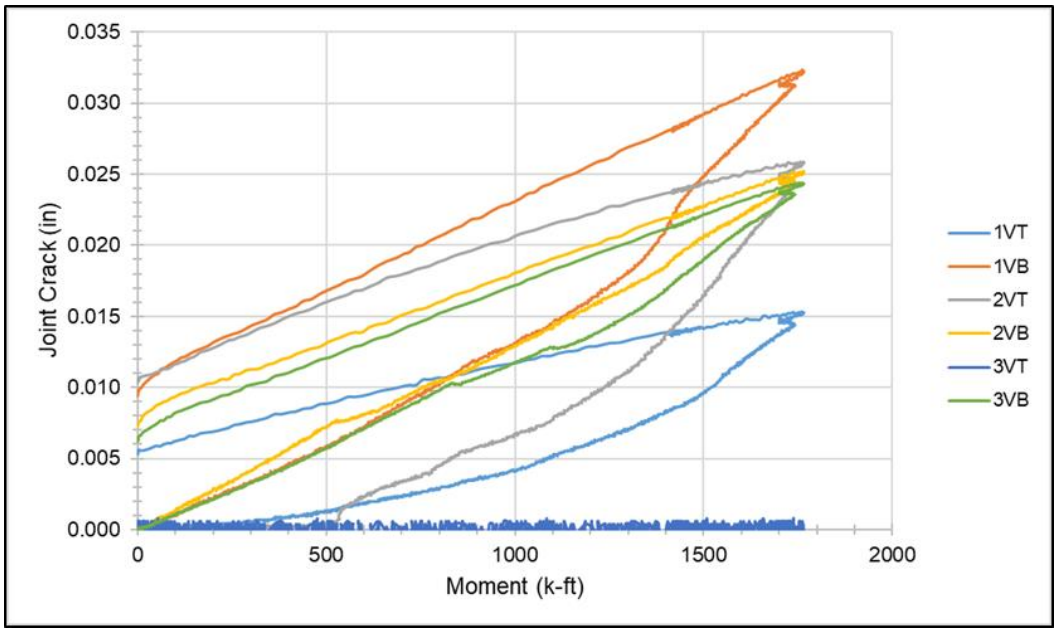

Figure 5.14 *Crack width versus moment due to vertical load.*

The control specimen reached a maximum load of 385 kips and reported a maximum joint crack of 0.025 in. The UHPC joint specimen had a crack of 0.031 in. under a 385-kip load, which is approximately 1.3 times greater than the control specimen. Again, it is shown most of the maximum joint cracks derived from the joint to pile cap interface, but after unloading the cracks closed (Figure 5.15).

Figure 5.15 *UHPC joint rear face after testing.*

The maximum reinforcing bar stress recorded during the test was 48.1 ksi at the maximum load of 397 kips, which means none of the connection bars yielded (Figure 5.16).

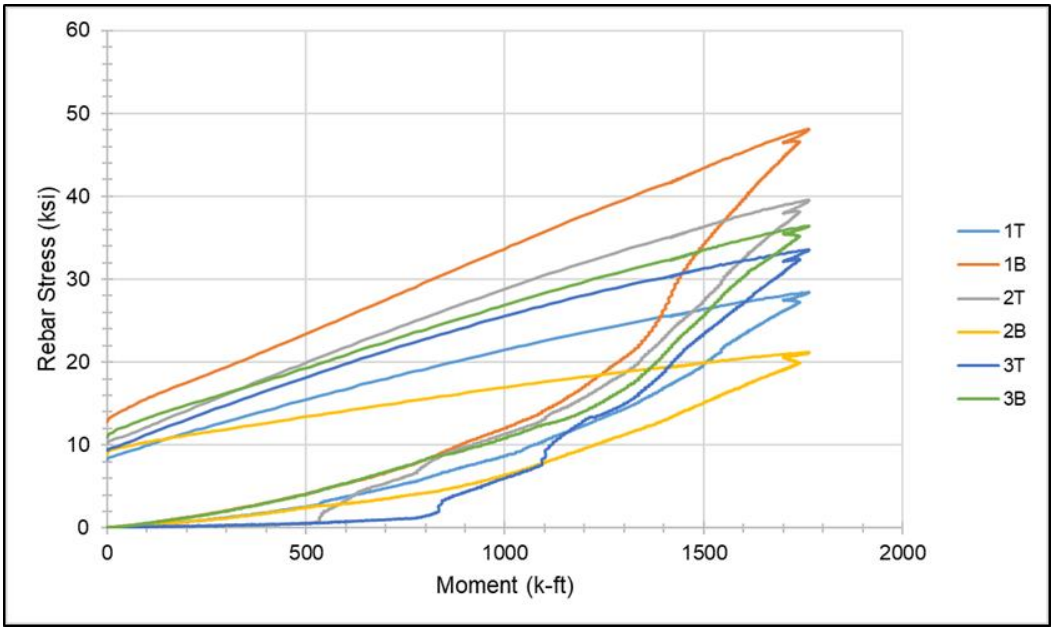

Figure 5.16 *Tension reinforcing bar stress versus moment due to vertical load*.

Figure 5.16 shows the connection bars protruding from the integral diaphragm and the pile cap both had adequate, and near even, development which proves the design allowed for a proper amount of protrusion for the connection bars within the UHPC joint.

5.3.2 Grouted Reinforcing Bar Coupler

The horizontal loading reached a maximum value of 100 kips, which caused the crack at the front face of the abutment to be 0.020 in. (Figure 5.17).

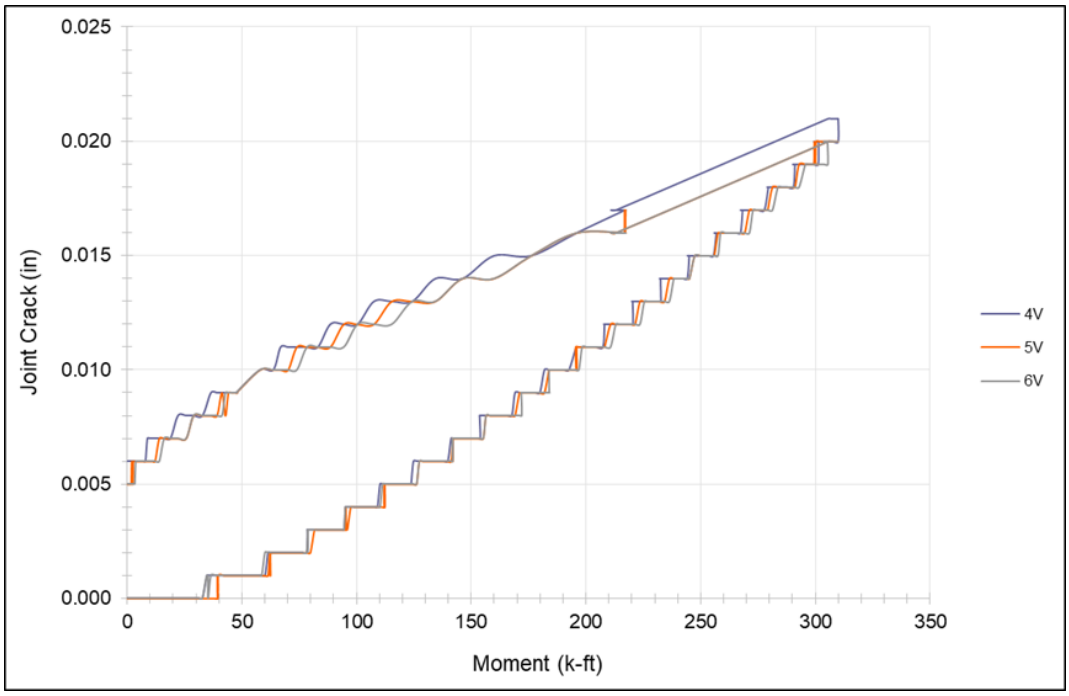

Figure 5.17 *Crack width versus moment due to horizontal load*.

This value was compared to the GRBC design from (Hosteng, Phares, & Redd, 2016) under the same loading, which was a crack of 0.001 in., and the cast-in-place specimen, which had a crack of 0.001 in.

No horizontal slip was recorded between the integral diaphragm and the pile cap. And the maximum reinforcing bar stress was tabulated to be about 20 ksi in the coupling bars protruding from the pile cap, which is only a third of the yielding stress for the reinforcing bars used.

The vertical load was then applied to a maximum of 400 kips, or a moment of 1,778-k-ft, which caused a crack at the rear face of the abutment to be 0.348 in. (Figures 5.18 and 5.19).

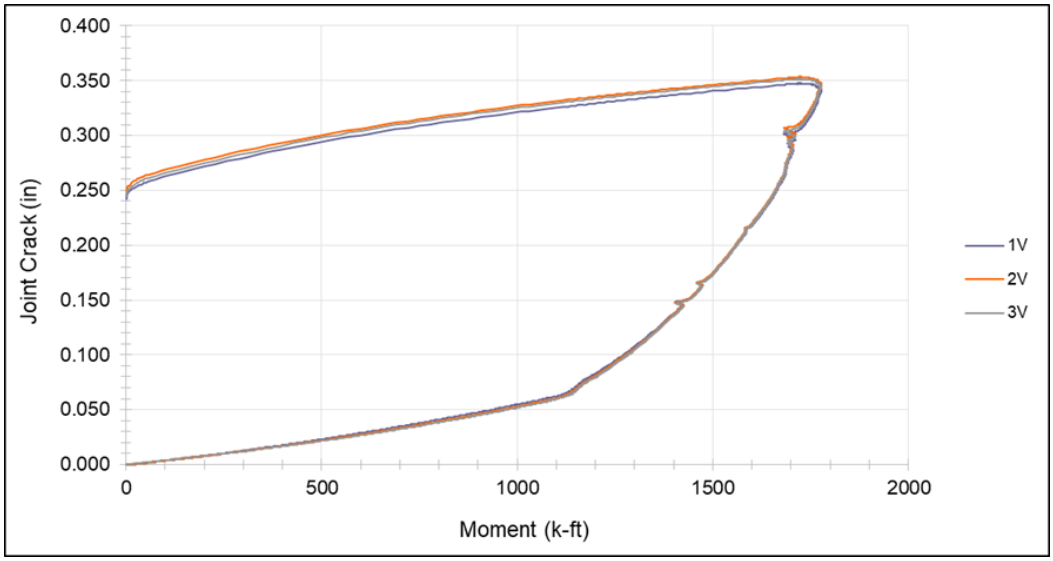

Figure 5.18 *Crack width versus moment due to vertical load.*

Figure 5.19 *GRBC rear face crack due to vertical load.*

The original GRBC design reached a maximum vertical load of 338 kips, causing a crack at the rear face of the abutment of 0.035 in., while the revised GRBC design had a crack of 0.176 in. at the same load, which is approximately 5 times greater. This is a reasonable result since the revised design had half the couplers than that of (Hosteng, Phares,

& Redd, 2016). The cast-in-place specimen had a maximum vertical load of 385 kips causing a rear face crack of 0.025 in., the revised GRBC specimen at the same load had a crack of 0.309 in., which is approximately 12 times greater than the control specimen.

Analyzing the tension stresses in the coupling bars for the GRBC design show that at the maximum load of 400-kips, the coupling bars protruding from the pile cap had tabulated stresses of 123-ksi and 90-ksi for bars 1B and 2B, respectively, which shows these bars had yielded (Figure 5.20).

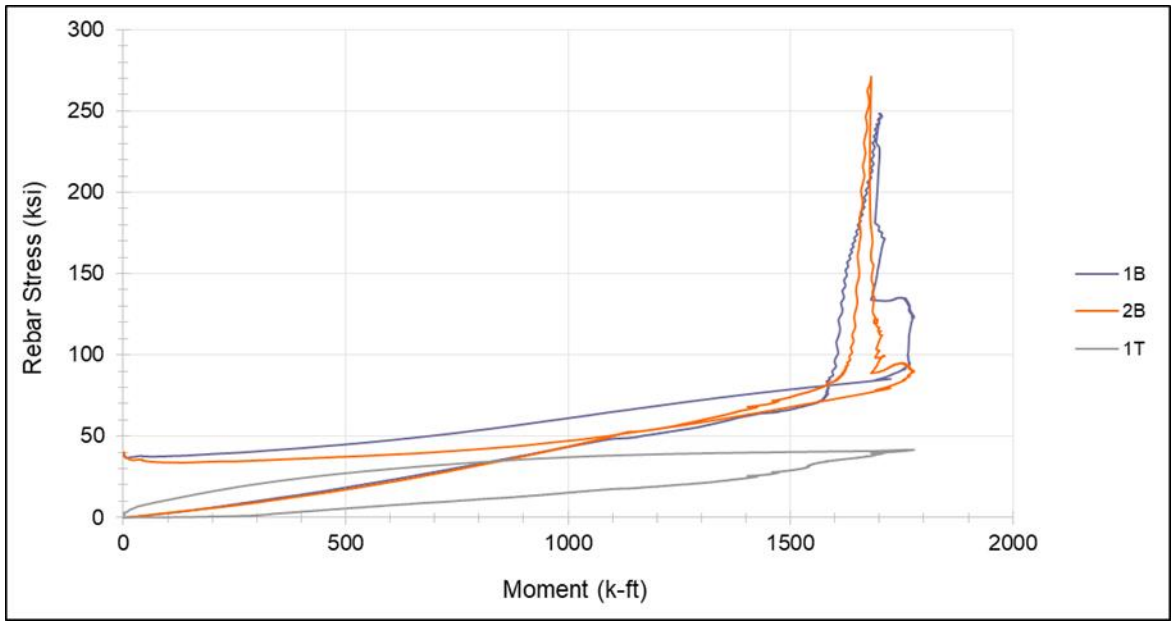

Figure 5.20 *Tension reinforcing bar stress versus moment due to vertical load.*

The yield stress for the reinforcing bars used was 60 ksi, which was achieved at a loading of approximately 295 kips. For the original GRBC design, at a load of 338 kips the maximum tensile stress in the coupling bars was 43 ksi, while the revised design coupler bars experienced a stress of 74.3 ksi at the same load, which is approximately 1.7 times greater. Again, this is a reasonable result due to revised design having half the couplers than that of (Hosteng, Phares, & Redd, 2016). The cast-in-place specimen experienced a maximum tensile reinforcing bar stress of 42 ksi at a load of 385 kips, for the revised GRBC design at

the same load the maximum reinforcing bar tensile stress was 133 ksi, which is approximately 3 times greater.

It is important to note that the coupler bars in the integral diaphragm experienced a tabulated stress of 42 ksi for bar 1T, noting that bar 2Ts sensor malfunctioned. Thus, the difference in stress between bars 1B and 1T is approximately a factor of 3 and can be the result of the grout sleeves and the coupler bars in the integral diaphragm tending to rotate with the integral diaphragm causing the development of the coupler bars protruding from the pile cap to be much greater.

Referring to Figure 5.20, it can be seen there is a large spike in the reinforcing bar stresses toward the peak of loading. This is most likely due to the already yielded bars elongating even further due to a sustained load when observations were taking place.

Comparing the figures of the revised design to those from (Hosteng, Phares, & Redd, 2016), specifically the cracking due to vertical loading, the original GRBC and the cast-in-place specimens resisted cracking for some load. This is not the case for the revised GRBC specimen, which began recording cracks at lower loads, almost half of that for the original GRBC specimen. Again, due to the lesser amount of coupler bars, this result is not surprising and is reasonable.

5.3.3 Pile Coupler

The horizontal loading reached a maximum value of 100 kips, which caused the crack at the front face of the abutment to be 0.007 in. (Figure 5.21).

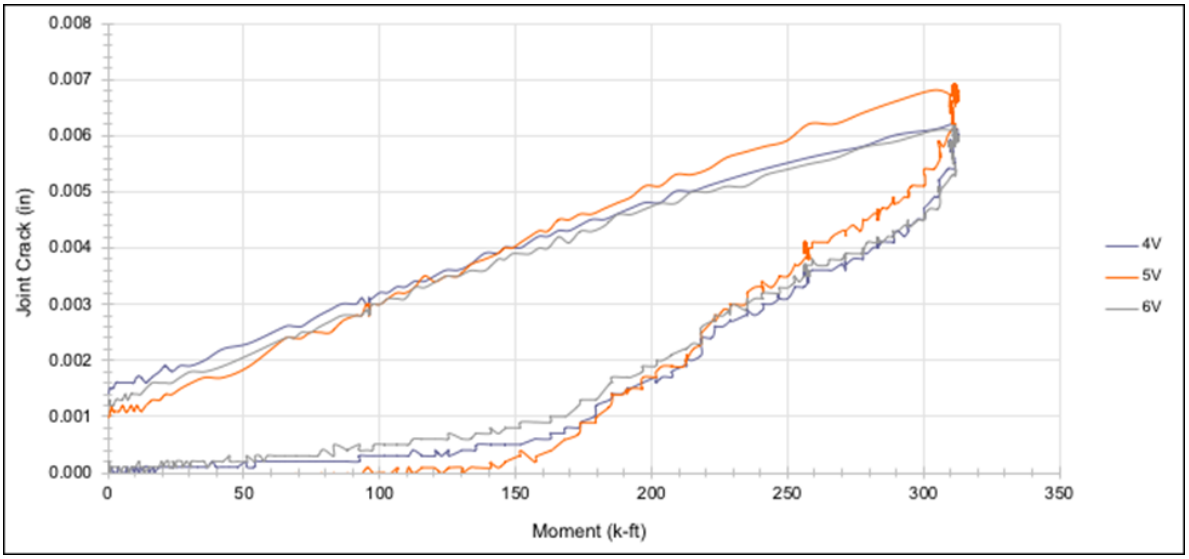

Figure 5.21 *Crack width versus moment due to horizontal load*.

This value was compared to the original pile coupler design under the same loading, which was a crack of 0.050 in., and the cast-in-place specimen, which had a crack of 0.001 in.

No horizontal slip was recorded between the integral diaphragm and the pile cap. And the maximum coupler stress was tabulated to be about 3.34 ksi in the coupling steel sections, which is essentially no stress in the coupling steel.

The vertical load was then applied to a maximum of 377 kips, or a moment of 1,677-k-ft, which caused a crack at the rear face of the abutment to be 0.306 in. (Figures 5.22 and 5.23).

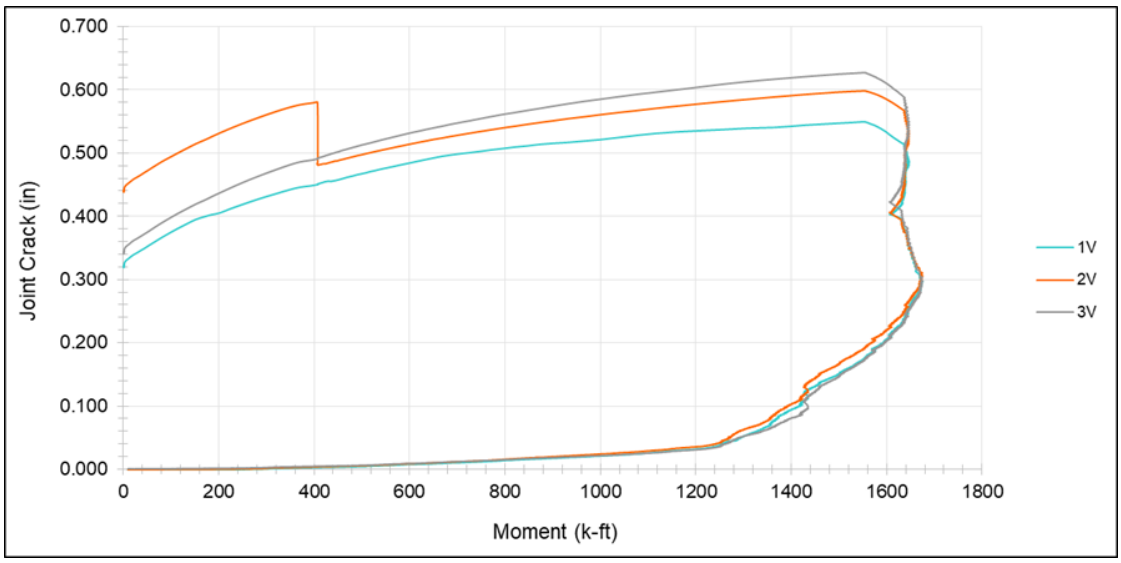

Figure 5.22 *Crack width versus moment due to vertical load.*

Figure 5.23 *Crack width versus moment due to vertical load.*

When more load was attempted to be applied, only more displacement was gained from the specimen. During the sustained load, the joint crack reached a maximum value of 0.627 in. Also, during loading cracks propagated in the pile cap of the abutment near the

bottom of the CMPs within the pile cap. These cracks led to larger cracks causing rotation of the pile cap recorded by the string pots (Figure 5.24).

Figure 5.24 *Pile coupler pile cap cracking due to vertical load.*

The maximum displacement recorded by the string pots was 0.353 in., which did occur at the same recording time at the largest joint cracking. So, it may be possible that the pile cap cracking assisted in the increase in the joint crack value. The pile coupler design in (Hosteng, Phares, & Redd, 2016) reached a maximum moment due to vertical loading of 1,124-k-ft, causing a crack at the rear face of the abutment of 1.75 in., while the revised pile coupler design had a crack of 0.031 in. near the same load, which is approximately 56 times less. This shows that the concept of a moment couple, and longer piles, greatly improved the design of this connection. The cast-in-place specimen at a vertical load of 377 kips caused a rear face crack of 0.024 in., the revised pile coupler specimen at the same load had a crack of 0.306 in., which is approximately 12 times greater than the control specimen.

Analyzing the tension stresses in the coupling sections for the pile coupler show at the maximum load of 377 kips, the sections on the tension side of the abutment had a maximum tabulated tensile stress of 22.1 ksi, which is less than the 50 ksi yield stress for the sections (Figure 5.25).

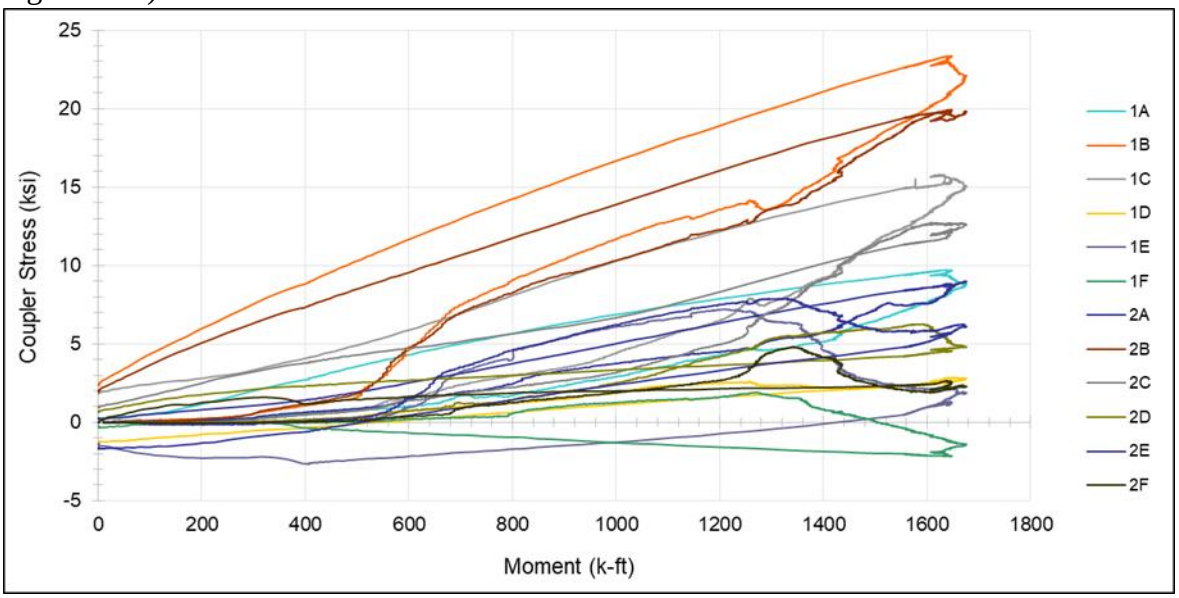

Figure 5.25 *Abutment tension-side steel section stresses versus moment due to vertical load.*

For the original pile coupler design, the maximum stress in the steel sections was reported to be 26 ksi at the maximum loading of 1,124-k-ft, while the revised design sections experienced a maximum stress of 13 ksi at the same load, which is approximately 2 times less. This is a reasonable result since there were double the amount of couplers for the revised design than that of (Hosteng, Phares, & Redd, 2016).

Figure 5.25 depicts how the steel sections on the tension-side of the abutment developed during the vertical loading. It can be seen that the south-side mid-point of each coupler section, 1B and 2B, developed the maximum stresses compared to the rest of the areas recorded. This is reasonable due to those sensors being at the location of the cold joint between the pile cap and integral diaphragm for the specimen where failure would initiate. Also, the south-side sensors for each coupler section, 1A-1C and 2A-2C, developed higher

stresses than that of the north-side sensors for the same sections, 1D-1F and 2D-2F. This shows the steel sections had slight bending within the CMPs instead of acting purely axially.

Comparing the original design to the revised design for the pile coupler, it is apparent the structural performance for the revised design was successful. This is shown through the maximum rear face crack at the maximum loading and maximum tensile stresses within the coupling sections.

CHAPTER 6. FINITE ELEMENT SIMULATION

6.1 Modeling Setup

To further investigate the abutment connections tested in the laboratory, a set of finite element (FE) simulations were conducted using ABAQUS CAE. The geometry for these models (Figure 6.1) was based on the geometry constructed in the laboratory, and the material properties were taken from material testing done during the laboratory testing. The concrete damaged plasticity was employed to model the structural components made of ordinary concrete, grout, and UHPC. The steel reinforcing bar cage and reinforcing coupler bars, however, were modeled using the elastic-perfectly plastic steel material model. Solid elements were used to create the concrete, grout, UHPC, and girder for each model, while reinforcing cages were recreated in ABAQUS using wire geometry with beam elements. The boundary conditions at the bottom surface of the models were set to fixed constraints since both rotations and displacements recorded at the base of the laboratory specimens were not significant. The design vertical load, in addition to self-weight, of 49 kips was used which was based on IowaDOT suggested service loading of steel girder integral abutment bridges that use the same girder size as used in the laboratory specimens (Figure 6.2).

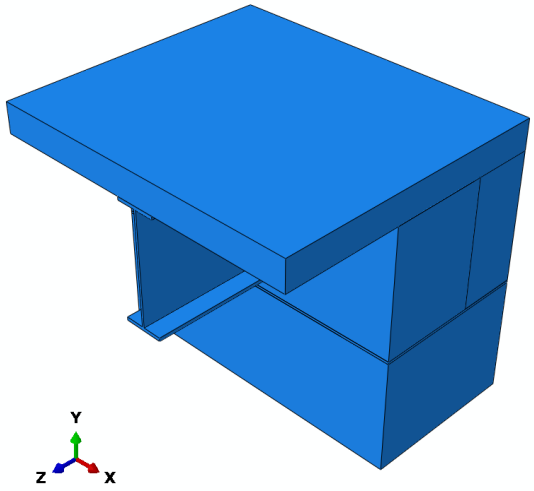

Figure 6.1 *Geometry for ABAQUS Finite Element Modeling.*

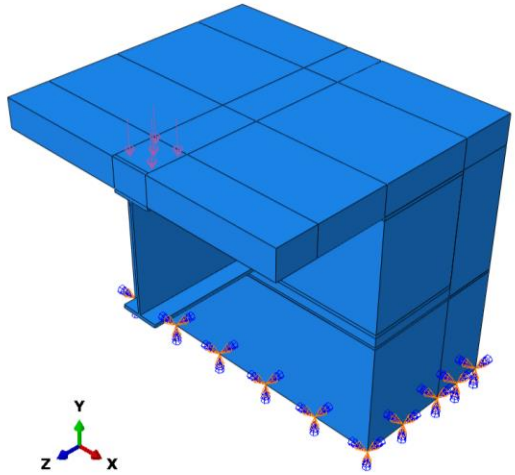

Figure 6.2 *Loading and Boundary Conditions for ABAQUS Finite Element Modeling.*

A mesh sensitivity analysis showed that a mesh size of 2 inches is not only small enough to provide results that were near the results of finer mesh but also it substantially helped reduced the computational time (Figure 6.3).

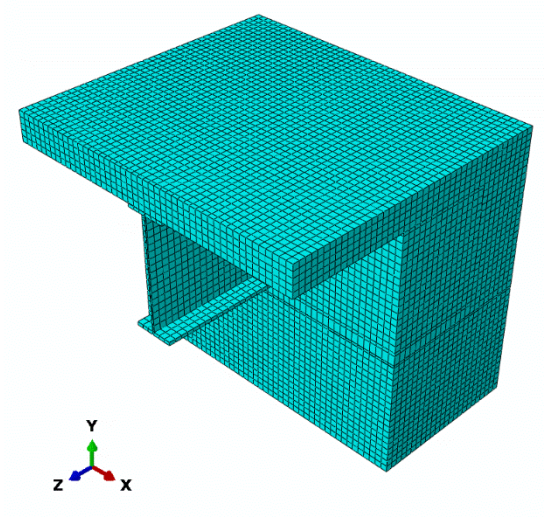

Figure 6.3 *2-inch Mesh for ABAQUS Finite Element Modeling.*

The tied constraint was used to connect the solid parts for the models, while the embedded region constraint was used to connect the reinforcing cage to the rest of the model. To ensure that no overclosure of the joint would occur, consistent with the behavior observed in the laboratory, a surface-to-surface contact interaction was defined for surfaces along the joint interface. This contact input would allow for separation after contact to let the joint open under loading but would not let the surfaces of the interface to overclose.

Validation of the models was attempted to be done through methods suggested in the literature when modeling contact separation, but those methods required very detailed information not gathered during the laboratory testing such as normal and shear stresses during separation as well as additional dimensional information for the opening during loading. So, a simpler method was attempted to create the joint opening which involved a grid system, 3 in. by 3 in., of springs with varying stiffnesses from the front face to rear face of the specimens. Many iterations of these stiffnesses were done, but the results of end beam displacement, maximum joint opening, and coupler bar stress were consistently significantly lower than the laboratory testing results. It was deemed by the research team to neglect

validation of the model since the contact analysis is a very complex problem that needs its own research efforts. Nonetheless, a systematic investigation was performed to analyze the modeled specimens under two extreme cases, instead. The extreme cases were a “tied” condition where perfect construction practices would result in nearly no joint opening during loading, while a “hinged” condition where there are no contact properties between the elements of the integral abutment connection and the connection area would rotate freely under loading about the front face edge of the diaphragm hinged to that of the pile cap.

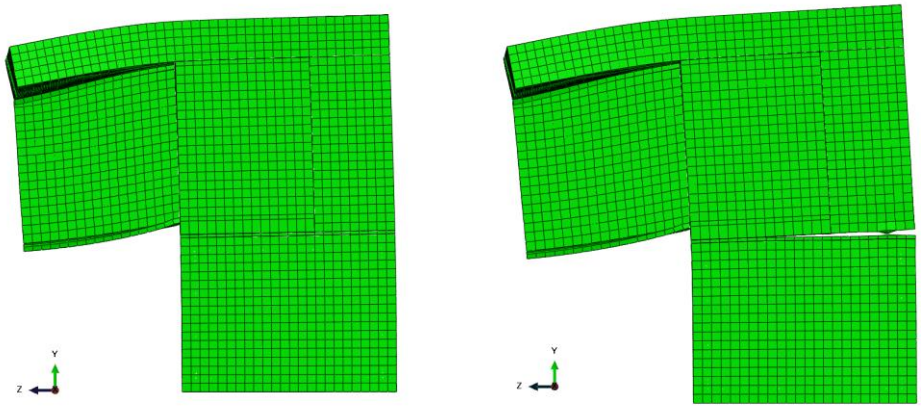

Figure 6.4 *“Tied” (Left) and “Hinged” (Right) conditions for simulations.*

6.2 Parametric Study

A systematic parametric study was conducted on the abutment connections to investigate the effects of adjusting the number of couplers on the performance of the modeled specimens compared to the responses observed in the laboratory under the design load of 49 kips. This study was carried out for the Grouted Reinforcing Bar Coupler and the UHPC-Joint connection details and investigated the results of having four, eight, twelve, thirteen, and seventeen reinforcing bar couplers for the joint connection using both the tied and hinged conditions. These coupler orientations were chosen to accommodate real-world applications

that would provide the structural connections required for the integral abutment joint as well as be able to be constructed.

Results for the maximum beam displacement, joint opening for the hinged condition, maximum reinforcing bar coupler stress, and maximum deck strain were extracted to make comparisons for each coupler orientation using both connections under each joint connectivity condition. It is worth noting that the hinged condition for the Grouted Reinforcing Bar Coupler with four couplers did not successfully run in ABAQUS, this is assumed to be due to there not being enough couplers to keep the connection intact.

Figure 6.5 and Figure 6.6 show the results of the parametric study for the results of maximum beam displacement which occurred at the end of the 3 ft cantilevered beam in the specimen.

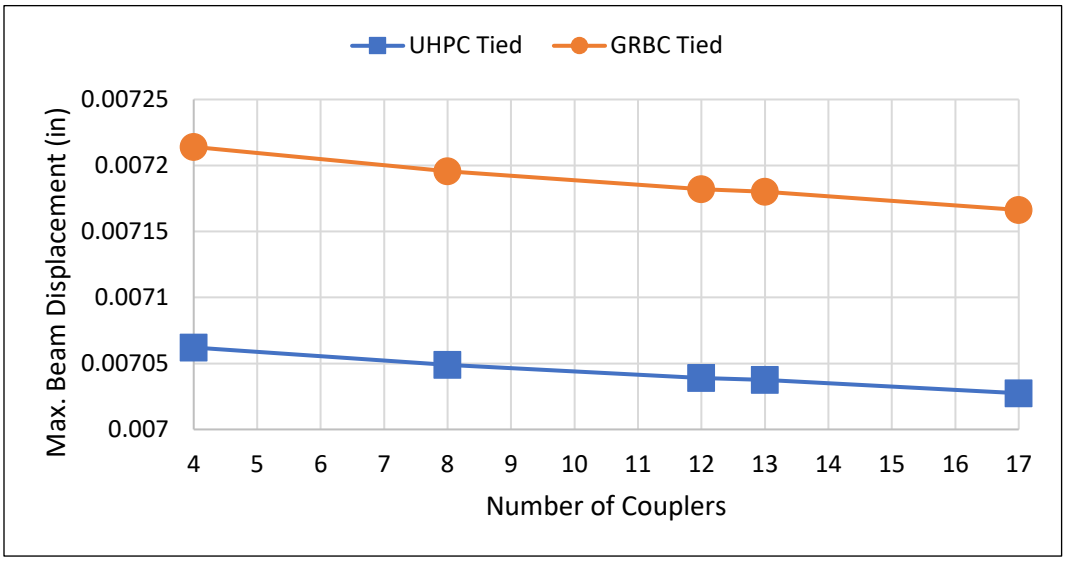

Figure 6.5 *Parametric Study – Maximum Beam Displacement for Tied Condition.*

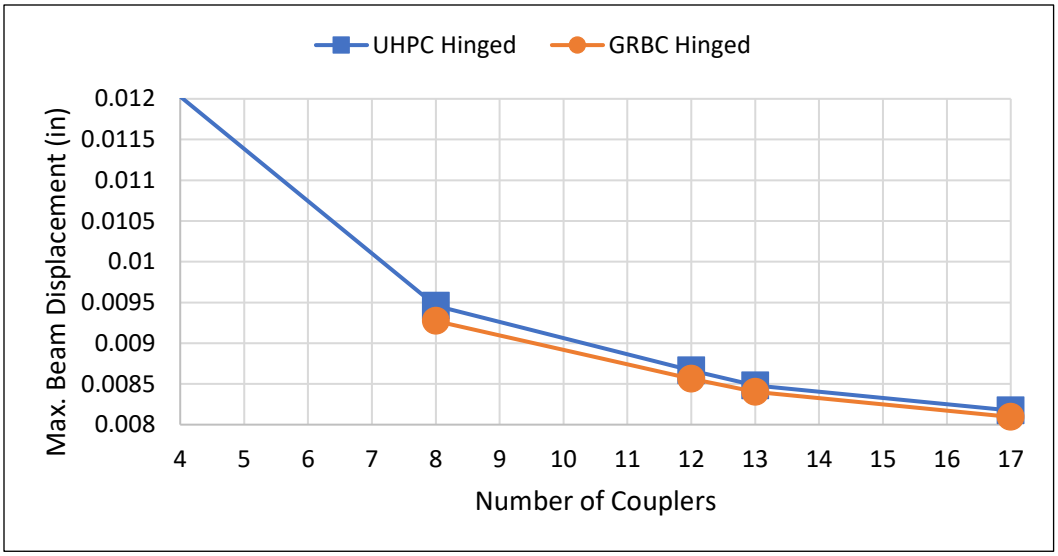

Figure 6.6 *Parametric Study – Maximum Beam Displacement for Hinged Condition.*

It is apparent through the results of the parametric study for maximum beam displacement that as the number of couplers increases, the maximum beam displacement decreases. This is due to the additional stiffness from the additional reinforcing coupler bars within the joint connection. The values of maximum beam displacement are higher for the Grouted Reinforcing Bar Coupler than the UHPC-Joint for the tied condition, approximately 2% higher, due to the UHPC-Joint having a stiffer connection with the utilization of the UHPC within the joint interface. This difference is mitigated for the hinged condition.

The increase in the range of the vertical axis of the graph is due to the significantly higher beam deflection induced on the four coupler orientation for the UHPC-Joint specimen and it can be assumed that if the Grouted Reinforcing Bar Coupler model with the four coupler orientation using the hinged condition had ran it would have a similar high level beam deflection. However, the beam deflection of the hinged condition was greater than that of the tied condition due to the allowance of additional movement of the diaphragm about the hinged connection to the pile cap. The difference of the beam displacement between the

hinged condition to the tied condition ranged from approximately 52% for the four-coupler orientation to approximately 15% for the seventeen-coupler orientation.

Figure 6.7 shows the results of maximum joint opening for the parametric study which occurred at the rear face of the specimen at the joint interface. It should be noted that the joint opening was only available to be monitored for the hinged condition due to the tied condition being under the assumption that high quality construction methods would result in nearly no joint deformations under loading.

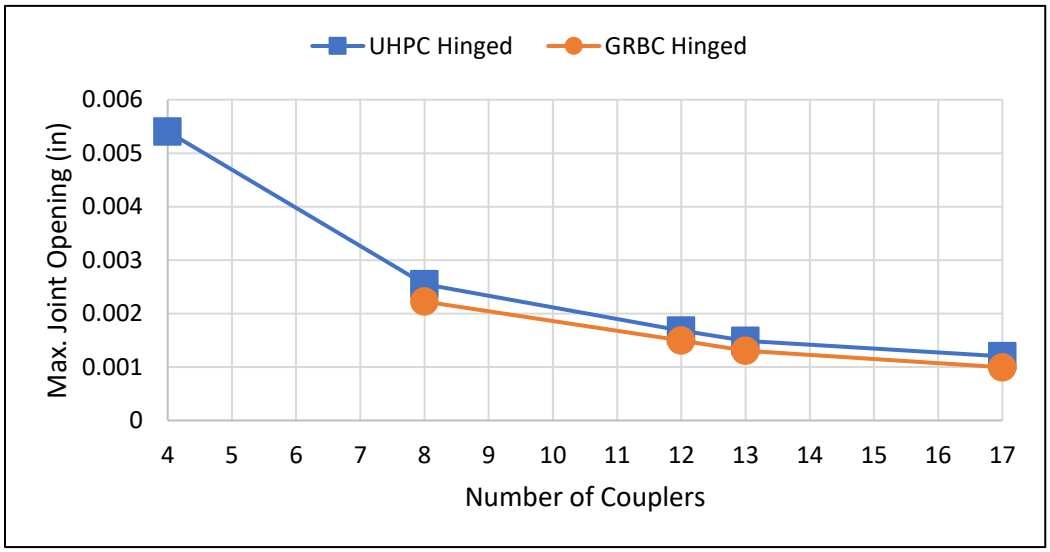

Figure 6.7 *Parametric Study – Maximum Joint Opening for Hinged Condition.*

Consistent with the maximum beam displacements, the maximum joint opening decreased as the number of reinforcing coupler bars increased. This, again, is due to the increased stiffness of the joint connection from the increase of reinforcing bars. The difference between the joint opening between the four-coupler orientation and the seventeen-coupler orientation is approximately 125%, which shows the significance of the presence of the reinforcing coupler bars. Comparing the maximum joint opening of the UHPC-joint to the Grouted Reinforcing Bar Coupler it can be seen the Grouted Reinforcing Bar Coupler had a smaller opening than the UHPC-Joint, approximately 18% smaller, but recall that it also

had a near equivalent beam deflection. Further investigating this result, it can be seen that the distribution of these maximum joint opening is different for each connection. The Grouted Reinforcing Bar Coupler may have a smaller magnitude for joint opening (Figure 6.8), but it is distributed over a greater area than that of the UHPC-Joint (6.9).

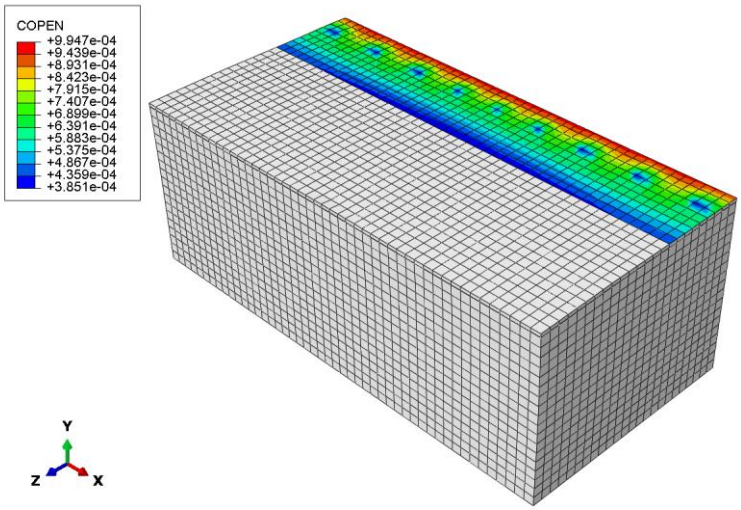

Figure 6.8 *Parametric Study – Maximum Joint Opening for Grouted Reinforcing Bar Coupler for Hinged Condition.*

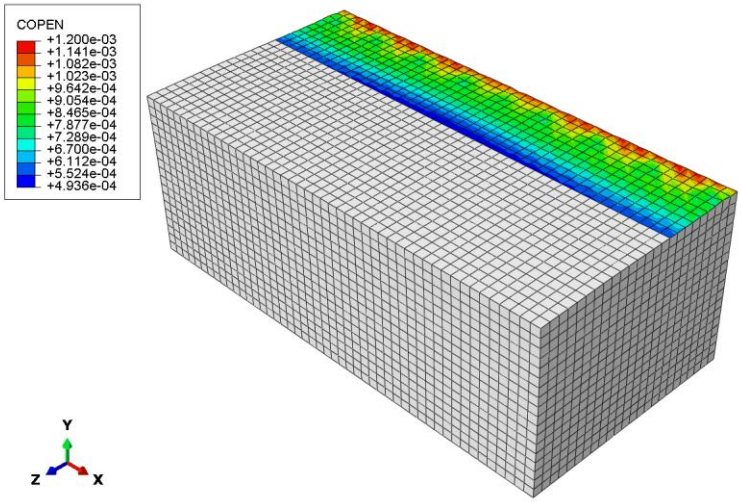

Figure 6.9 *Parametric Study – Maximum Joint Opening for UHPC-Joint for Hinged Condition.*

Figure 6.10 and Figure 6.11 show the results of maximum reinforcing coupler bar stress for the parametric study. These values were taken as the maximum tensile stress of the

reinforcing bars near the rear face of the specimen since the tensile stresses were significantly higher than the compressive stresses for the reinforcing coupler bars and would be critical for the strength and durability of the joint connection detail.

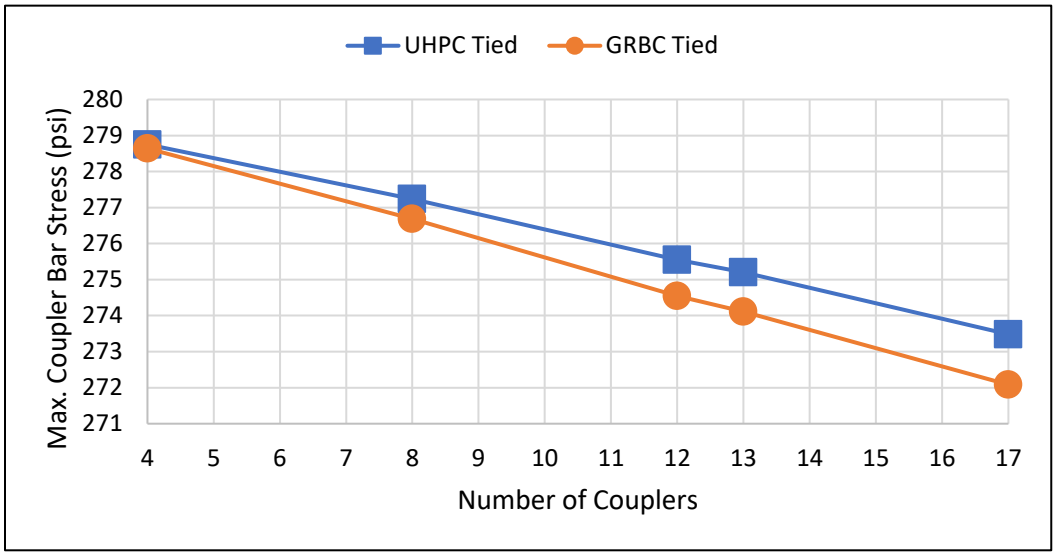

Figure 6.10 *Parametric Study – Maximum Reinforcing Coupler Bar Stress for Tied Condition.*

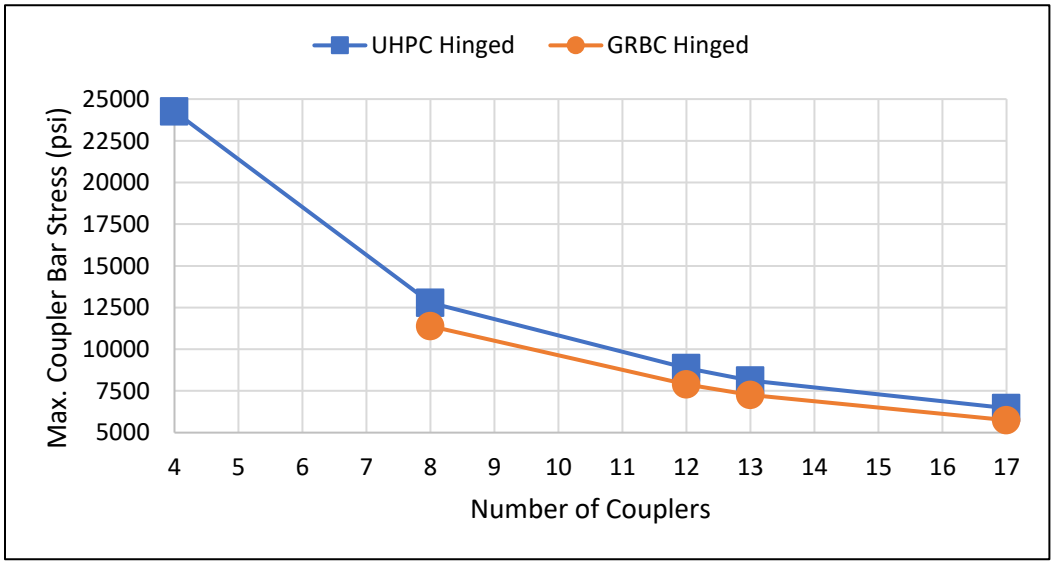

Figure 6.11 *Parametric Study – Maximum Reinforcing Coupler Bar Stress for Hinged Condition.*

As the number of reinforcing coupler bars increases, the maximum tensile stress decreases for reinforcing bars along the joint connection. This is expected as a larger number

of bars is available to undergo the same overall state of stress due to the applied load. Another observation from the parametric study results for reinforcing coupler bar stress is the difference in tensile stresses between the Grouted Reinforcing Bar Coupler and UHPC-Joint connection details. The maximum values of tensile stress in the reinforcing coupler bar is higher for the UHPC-Joint connection compared to the Grouted Reinforcing Bar Coupler. This is mainly attributed to the location of the reinforcing coupler bars for each joint connection detail along the section of the specimen. The UHPC-Joint connection detail has the reinforcing coupler bars closer to the rear face of the specimen which would result in a longer moment arm for the same induced moment about the abutment compared to the Grouted Reinforcing Bar Coupler, therefore causing the force within the reinforcing bars, and consequently the tensile stress, for the Grouted Reinforcing Bar Coupler to be less than the UHPC-Joint connection detail.

In addition to the value of maximum reinforcing coupler bar stress, it can be observed in the results screenshots of the model that the location and distribution of these maximum values change along with the change in the number of couplers present in the joint connection. The location of maximum tensile stress changes for each orientation of the UHPC-Joint (Figure 6.12 through Figure 6.16) and Grouted Reinforcing Bar Coupler (Figure 6.17 through Figure 6.21) using both the hinged and tied condition.

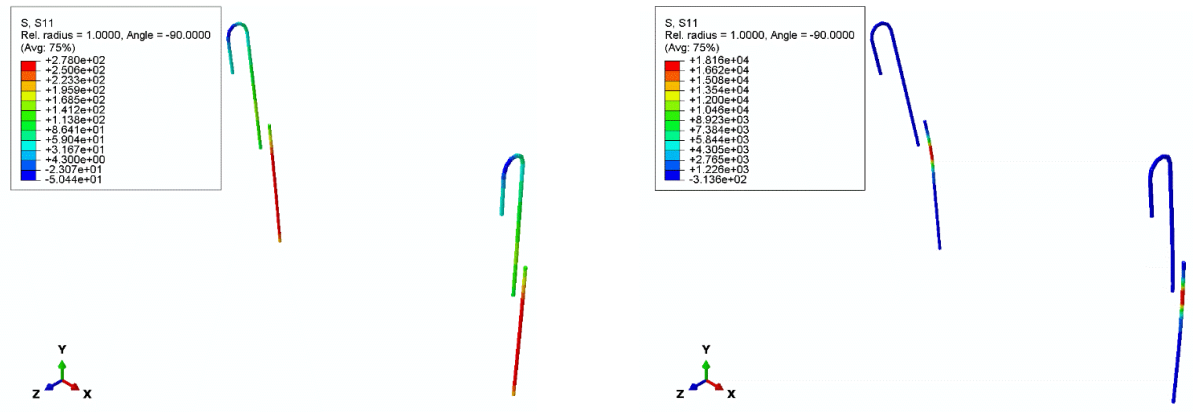

Figure 6.12 *Maximum Tensile Stress in Reinforcing Coupler Bars for UHPC-Joint Four Couplers under Tied (Left) and Hinged (Right) conditions.*

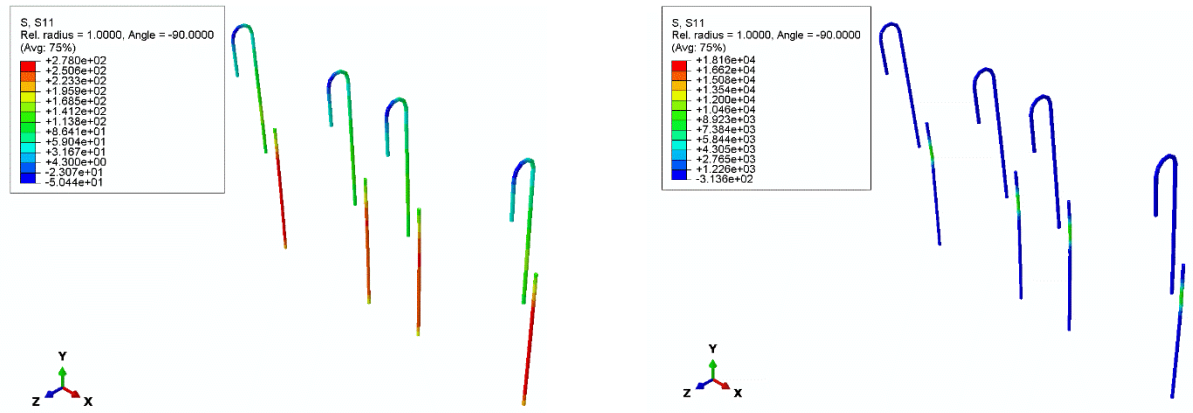

Figure 6.13 *Maximum Tensile Stress in Reinforcing Coupler Bars for UHPC-Joint Eight Couplers under Tied (Left) and Hinged (Right) conditions.*

The main difference between the location and distribution of the stress contours is the tied condition has a maximum stress contour that encases nearly the entire reinforcing coupler bar within the pile cap, and the maximum contour for the hinged condition is focused around the same elevation of the hinged joint.

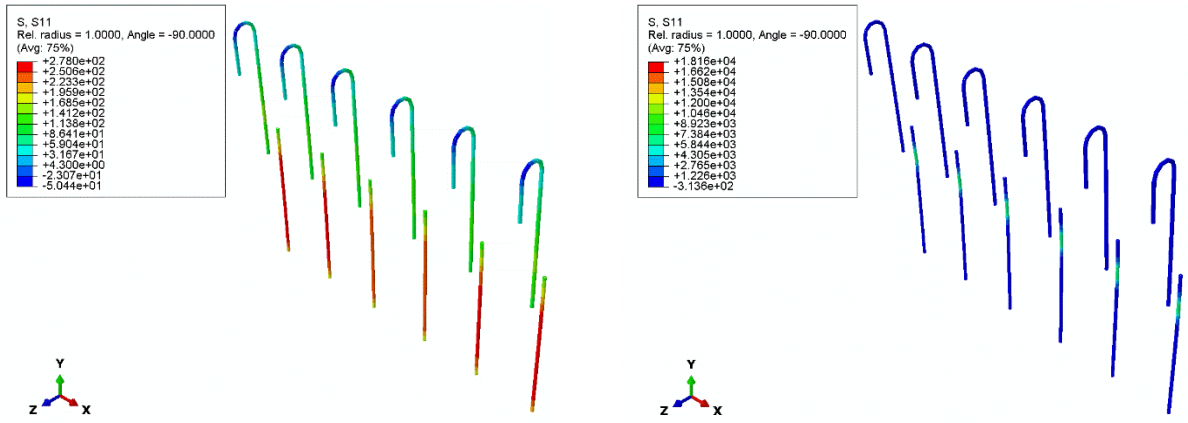

Figure 6.14 *Maximum Tensile Stress in Reinforcing Coupler Bars for UHPC-Joint Twelve Couplers under Tied (Left) and Hinged (Right) conditions.*

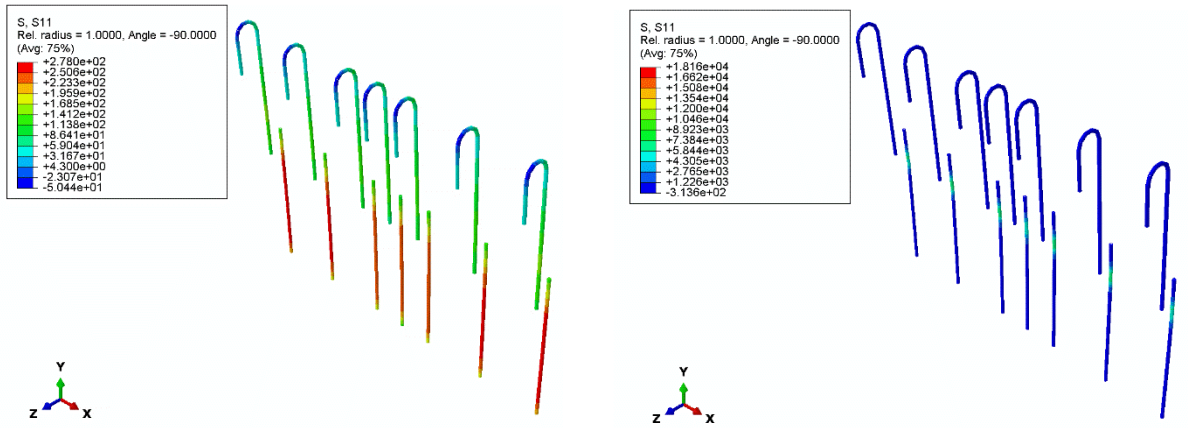

Figure 6.15 *Maximum Tensile Stress in Reinforcing Coupler Bars for UHPC-Joint Thirteen Couplers under Tied (Left) and Hinged (Right) conditions.*

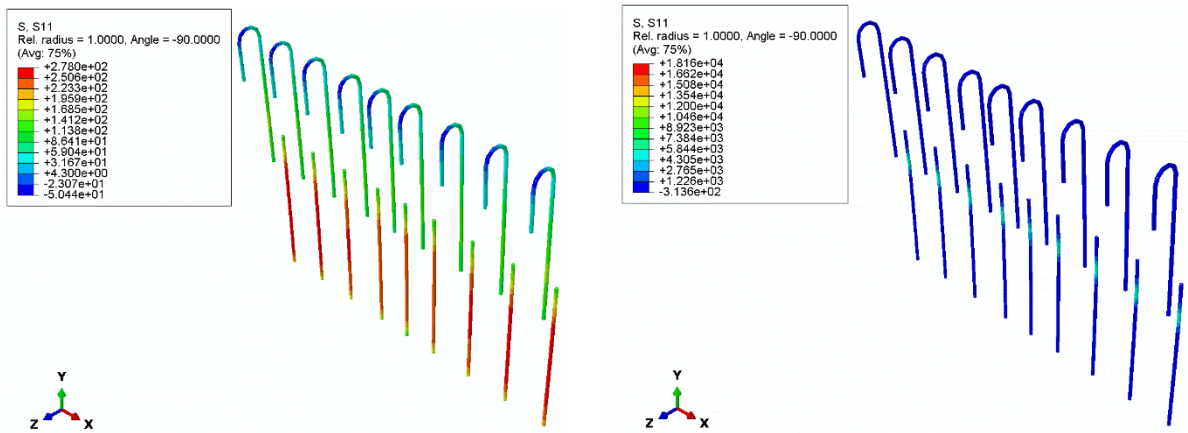

Figure 6.16 *Maximum Tensile Stress in Reinforcing Coupler Bars for UHPC-Joint Seventeen Couplers under Tied (Left) and Hinged (Right) conditions.*

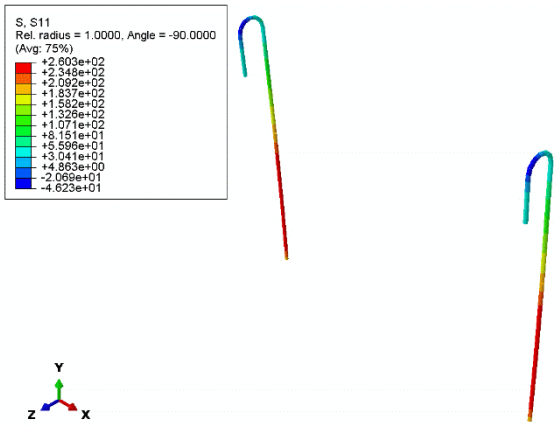

Figure 6.17 *Maximum Tensile Stress in Reinforcing Coupler Bars for Grouted Reinforcing Bar Coupler Four Couplers under Tied Condition.*

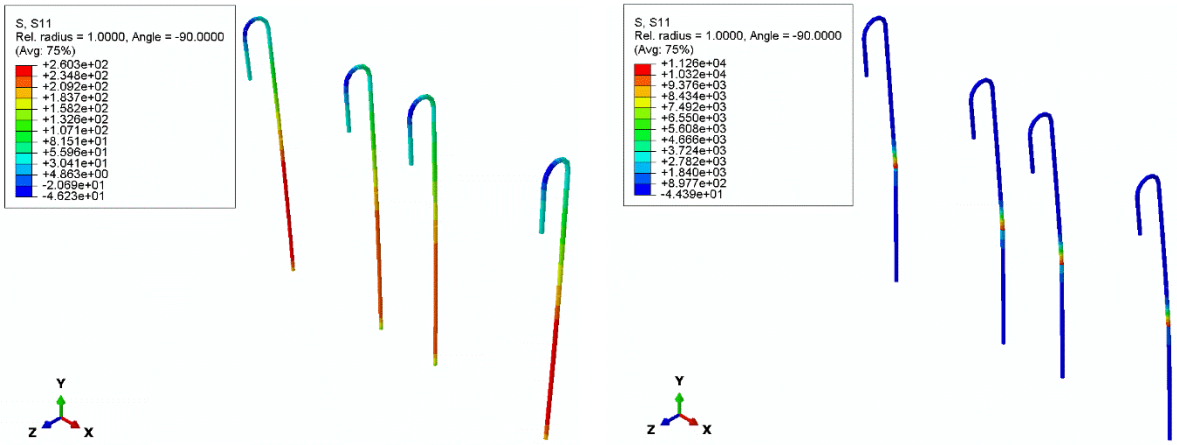

Figure 6.18 *Maximum Tensile Stress in Reinforcing Coupler Bars for Grouted Reinforcing Bar Coupler Eight Couplers under Tied (Left) and Hinged (Right) Condition.*

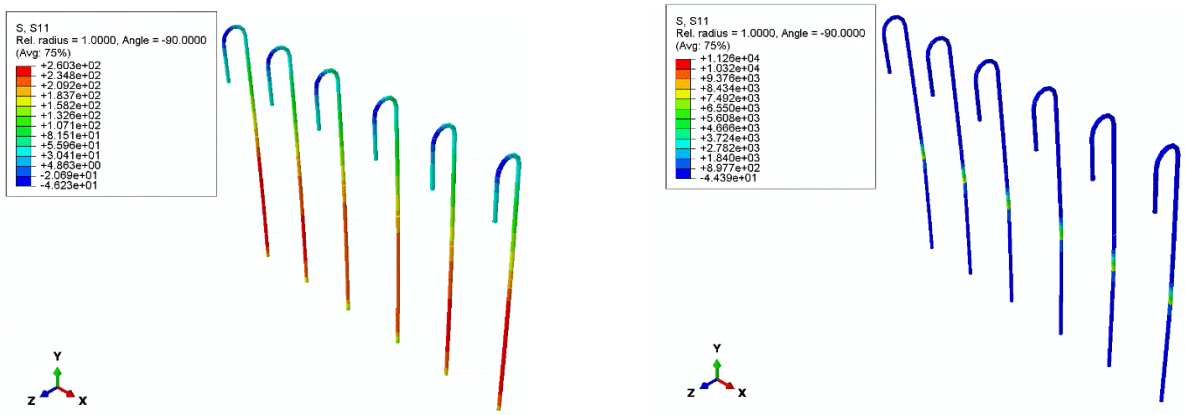

Figure 6.19 *Maximum Tensile Stress in Reinforcing Coupler Bars for Grouted Reinforcing Bar Coupler Twelve Couplers under Tied (Left) and Hinged (Right) Condition.*

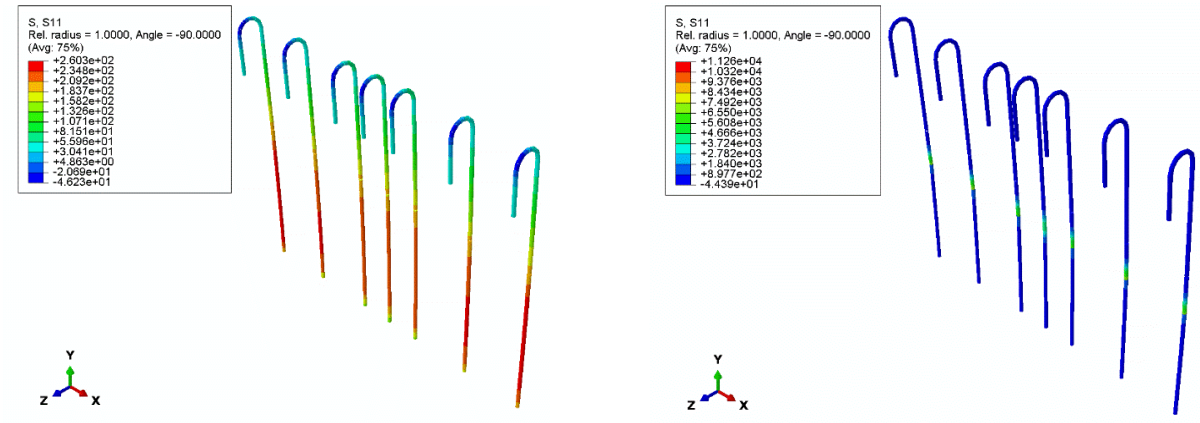

Figure 6.20 *Maximum Tensile Stress in Reinforcing Coupler Bars for Grouted Reinforcing Bar Coupler Thirteen Couplers under Tied (Left) and Hinged (Right) Condition.*

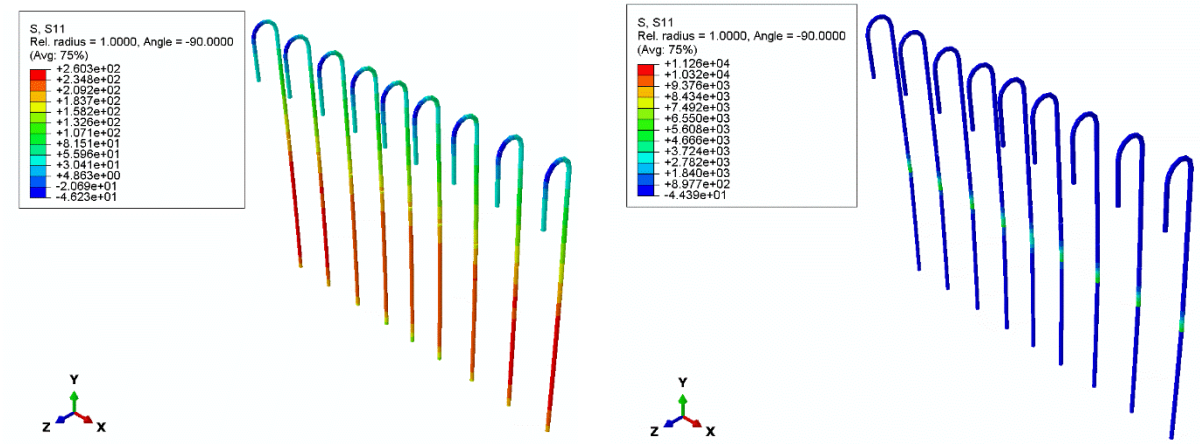

Figure 6.21 *Maximum Tensile Stress in Reinforcing Coupler Bars for Grouted Reinforcing Bar Coupler Seventeen Couplers under Tied (Left) and Hinged (Right) Condition.*

Figure 6.22 and Figure 6.23 show the results for maximum deck strain obtained from the parametric study. These values were taken as the maximum tensile strain at the location where the cantilever of the beam transitioned to the embedment of the beam, resulting in a negative moment causing maximum tensile strains at the top surface of the deck. This location would be subject to becoming the source of infiltration of water and deicing chemicals, hence why it is important to investigate the results of varying coupler orientations.

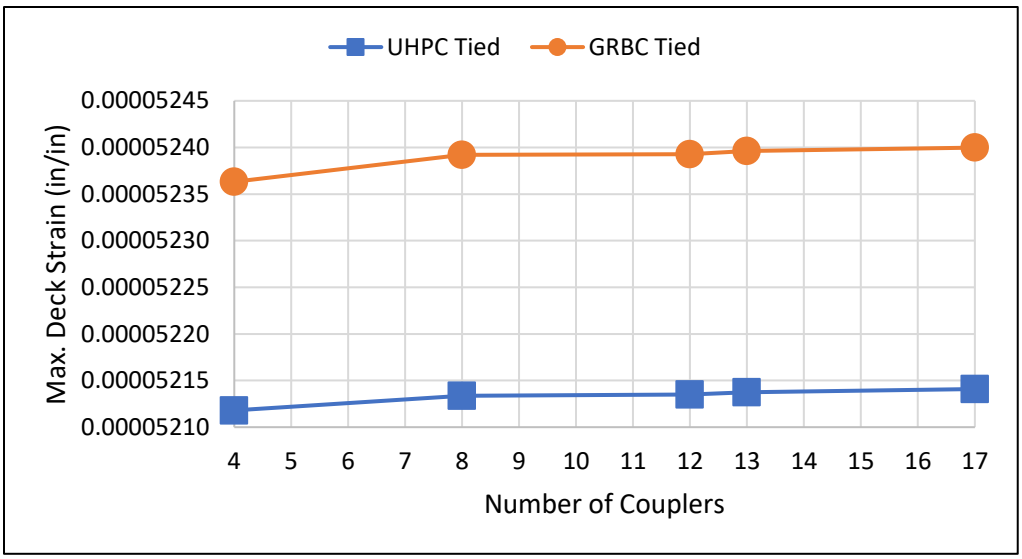

Figure 6.22 *Parametric Study – Maximum Deck Strain for Tied Condition.*

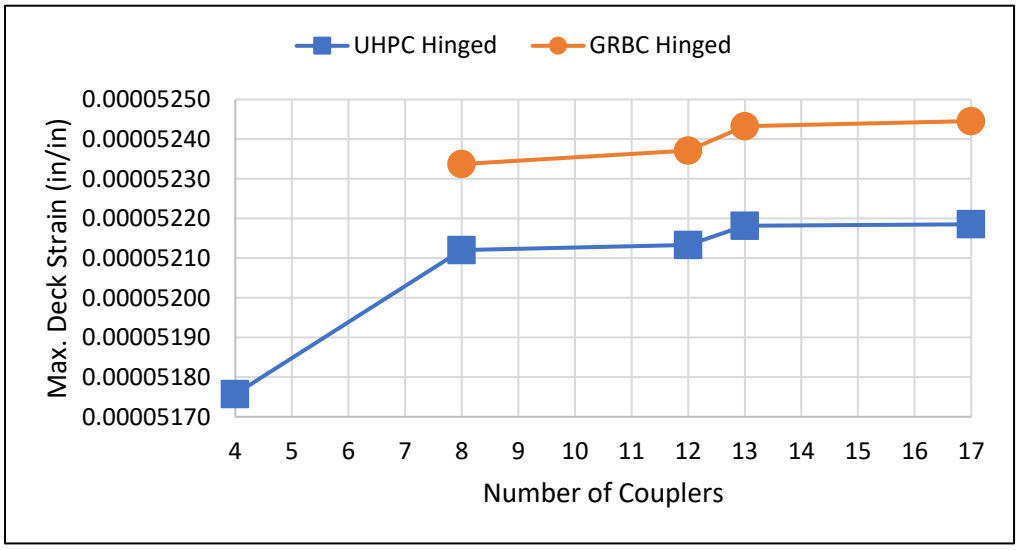

Figure 6.23 *Parametric Study – Maximum Deck Strain for Hinged Condition.*

The values of deck strain at the beam-abutment interface can be seen to increase as the number of reinforcing coupler bars increases, which is due to the increased stiffness of the joint connection causing the negative moment about the beam-abutment interface to maintain a higher magnitude rather than being relieved with joint opening and increase in reinforcing coupler bar stress. Another important observation is that the strain in the Grouted Reinforcing Bar Coupler specimen's deck is consistently higher than that of the UHPC-Joint

specimen. This leads to the conclusion that the ability of force transfer for the UHPC-Joint is better than that of the Grouted Reinforcing Bar Coupler due to the results observed not only for the deck strain, but also the maximum reinforcing bar stress and beam displacement. The Grouted Reinforcing Bar Coupler had greater movement, note the beam displacement, yet did not have higher reinforcing bar stress, but did have greater deck strain compared to those of the UHPC-Joint.

While the magnitudes of these deck strains are different between the two joint connections, the location and distribution of these strains is consistent for each specimen during the parametric study and is shown in Figures 6.24 through 6.29.

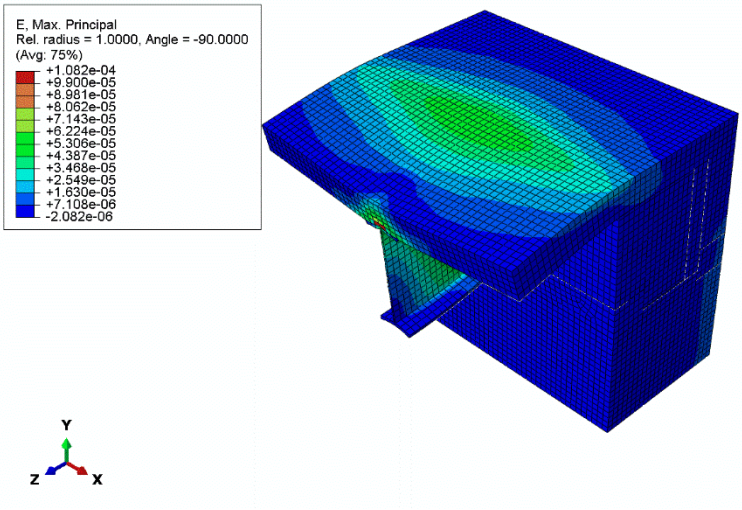

Figure 6.24 *Maximum Deck Strain for all Reinforcing Coupler Bar orientations for Tied Condition (UHPC-Joint shown).*

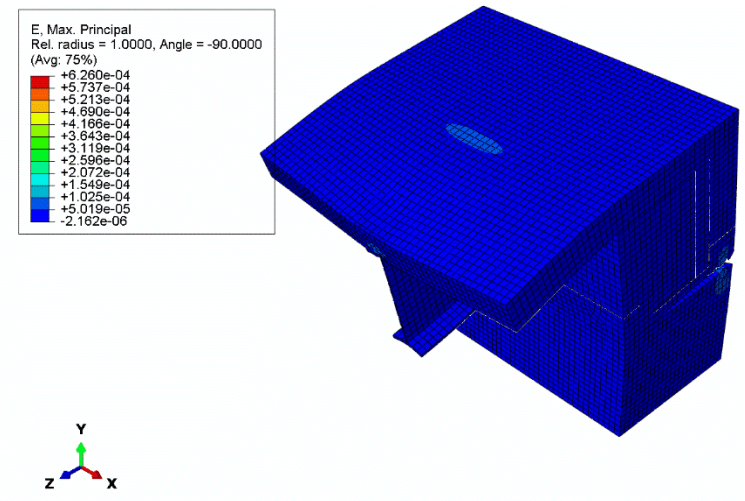

Figure 6.25 *Maximum Deck Strain for Four Couplers for Hinged Condition (UHPC-Joint shown).*

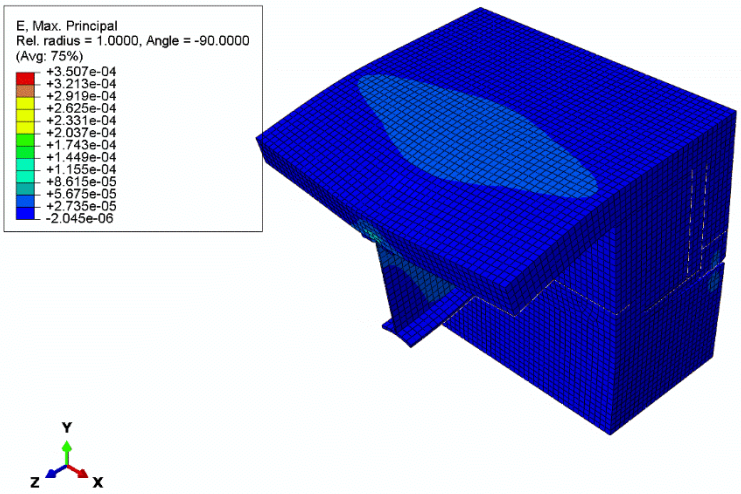

Figure 6.26 *Maximum Deck Strain for Eight Couplers for Hinged Condition (UHPC-Joint shown).*

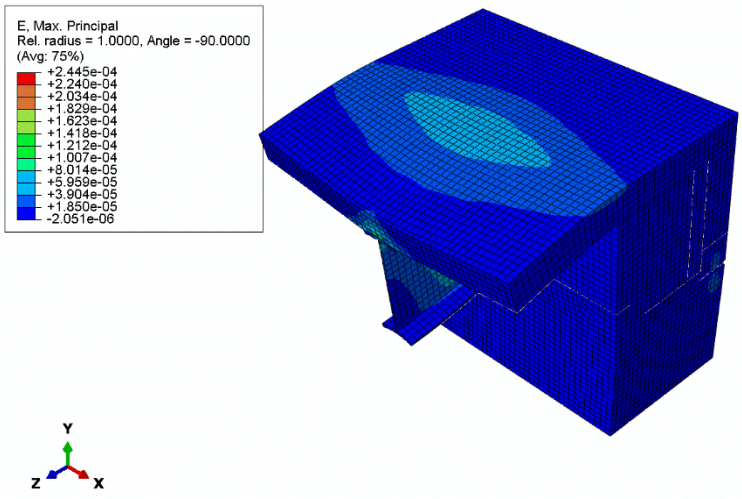

Figure 6.27 *Maximum Deck Strain for Twelve Couplers for Hinged Condition (UHPC-Joint shown).*

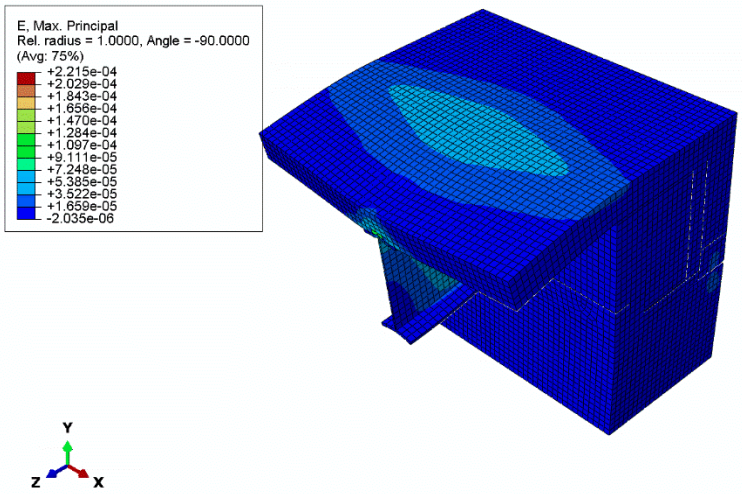

Figure 6.28 *Maximum Deck Strain for Thirteen Couplers for Hinged Condition (UHPC-Joint shown).*

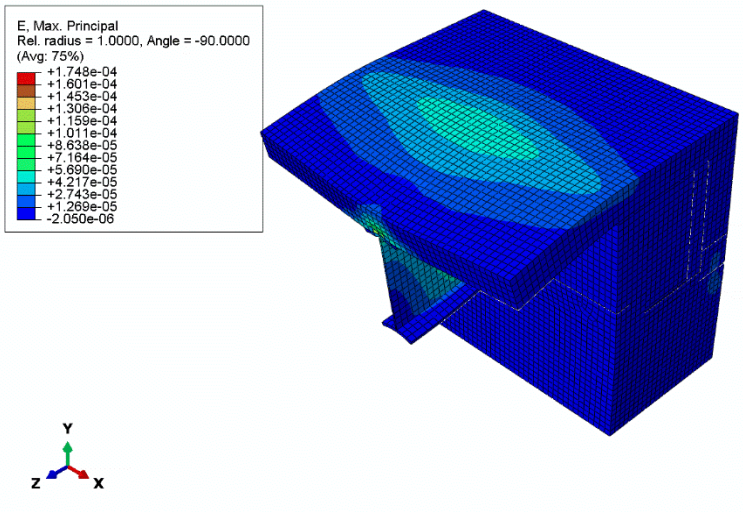

Figure 6.29 *Maximum Deck Strain for Seventeen Couplers for Hinged Condition (UHPC-Joint shown).*

The deck strains shown can be validated by the cracking seen at the beam-abutment interface for each connection during testing (Figure 6.30). It was found out that the pattern and distribution of the cracks recorded during the laboratory experiments are in excellent agreement with the strain contours observed from the FE simulations.

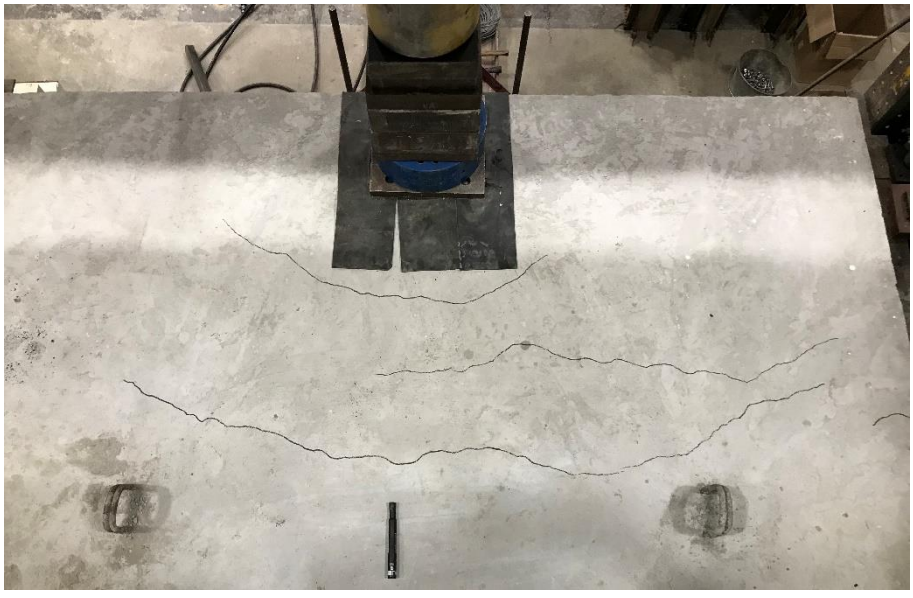

Figure 6.30 *Cracking pattern of deck after laboratory testing.*

A parametric study was also done for the Pile Coupler connection design. Unlike that of the UHPC-Joint and Grouted Reinforcing Bar Coupler, which used couplers consisting of reinforcing bars, the Pile Coupler parametric study had a few different aspects investigated that consisted of providing the simulations with different numbers of CMPs, varying diameters for the CMPs, different steel section sizes, various reinforcing cage longitudinal bar sizes, and changes in the reinforcing cage layout to maintain an area of steel equivalent to that of the steel sections used for the testing, (A_s = 10.3 in^2). It is important to note that only the tied condition was able to be ran for the Pile Coupler connection simulations.

First, the effect of changing the number of CMPs on the results of the analysis was studied. The number of CMPs went from two to four (Figure 6.31), since no additional CMPs would be viable to be constructed. The results of this aspect of the study are shown in Figures 6.32 through 6.34.

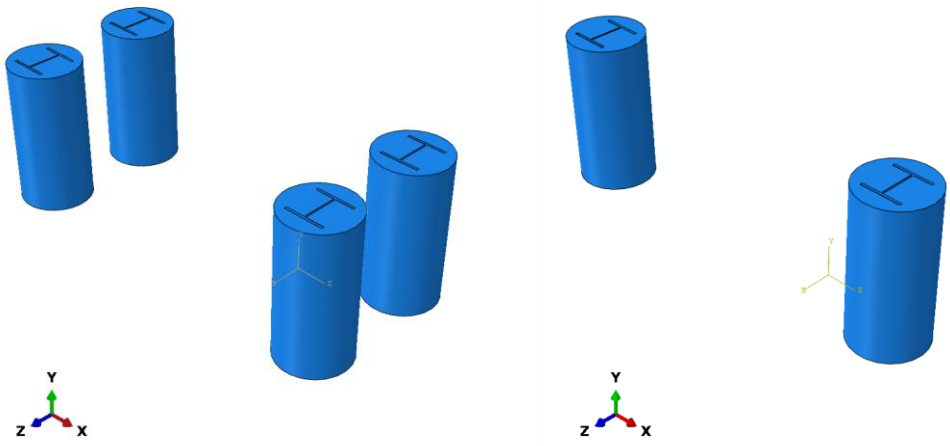

Figure 6.31 *CMP layouts of four (Left) and two (Right) for parametric study.*

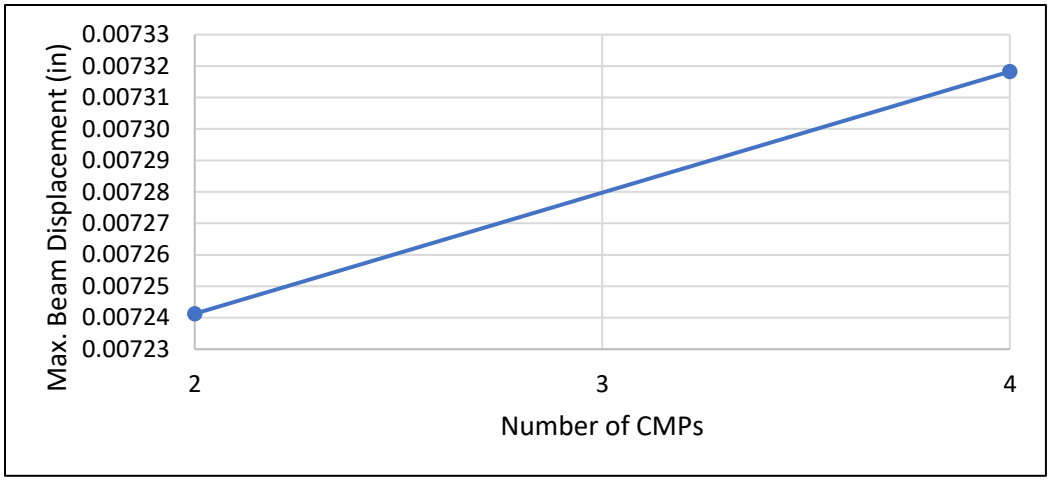

Figure 6.32 *Maximum beam displacement for varying number of CMPs.*

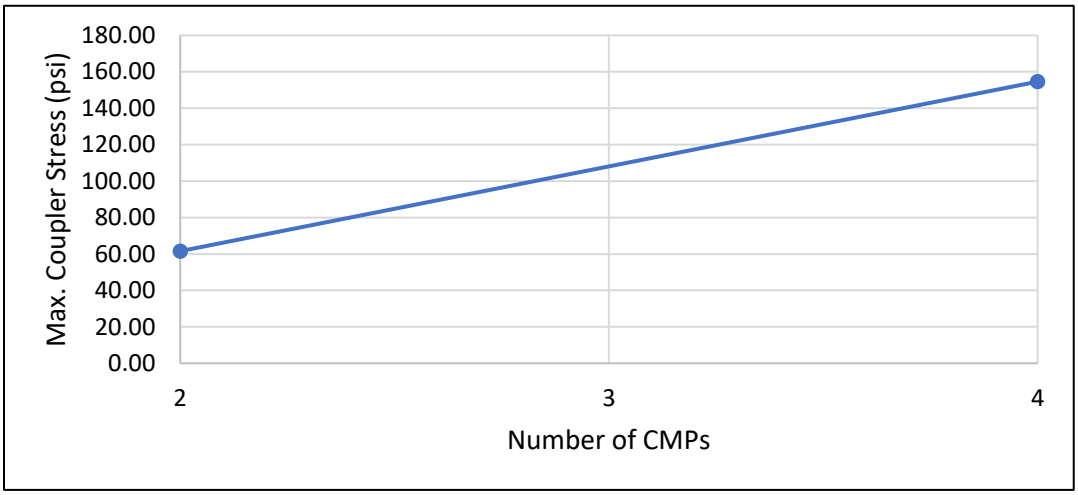

Figure 6.33 *Maximum coupler stress for varying number of CMPs.*

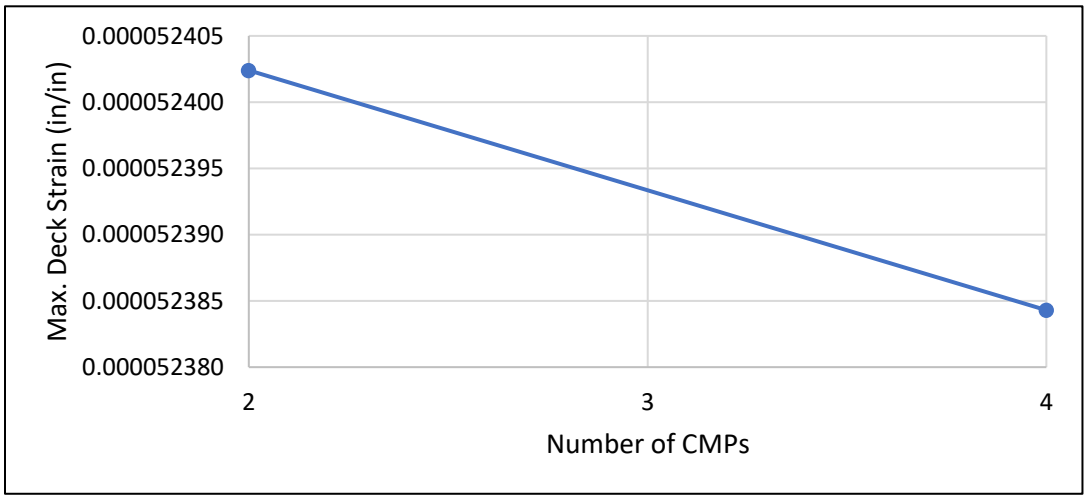

Figure 6.34 *Maximum deck strain for varying number of CMPs.*

The results of this study show that number of CMPs changing from four to two (i.e. change in designs for the laboratory aspect of this research), there is a 1.1 percent decrease in the maximum beam displacement, an 86.1 percent decrease in maximum coupler stress, and a 0.03 percent increase in the maximum deck strain. This is likely due to the tied condition causing the joint to increase in stiffness from the four to two CMPs since there would be more area for the constraint to be applied, but it was proven through the experimental testing that the four CMP coupler design performed better than that of the two CMP coupler design through the results discussed previously.

Next, the effect on the response due to changing the diameter of the CMPs was investigated, using the four CMP design from the laboratory investigations. The diameters input for the study were 15 inches, 16 inches, and 17 inches, noting that 15-inch diameter was used for the experimental testing and going to a diameter greater than 17 inches would cause congestion issues within the reinforcing cages of the abutment elements. The steel section used for each CMP diameter setup was the same used for the laboratory experiments (W8x35). The results for this study are shown in Figures 6.35 through 6.37.

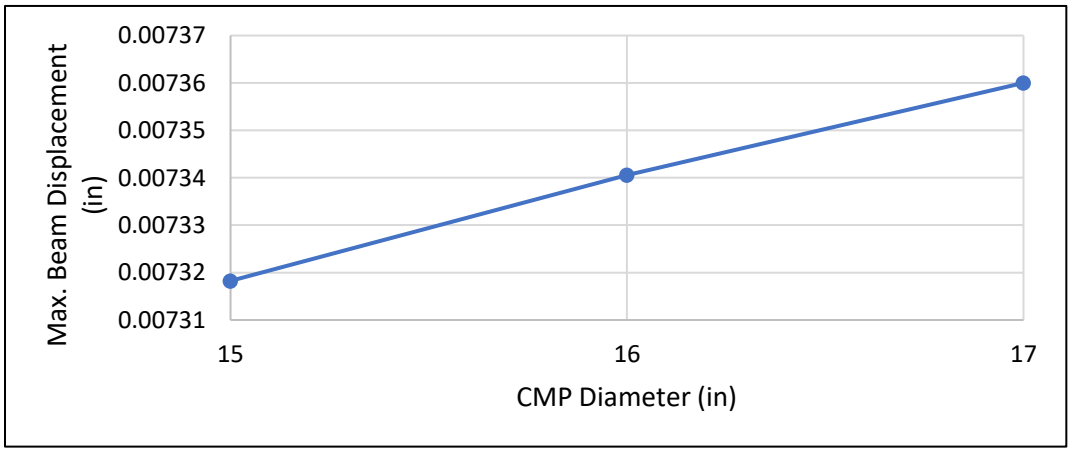

Figure 6.35 *Maximum beam displacement for varying CMP diameters.*

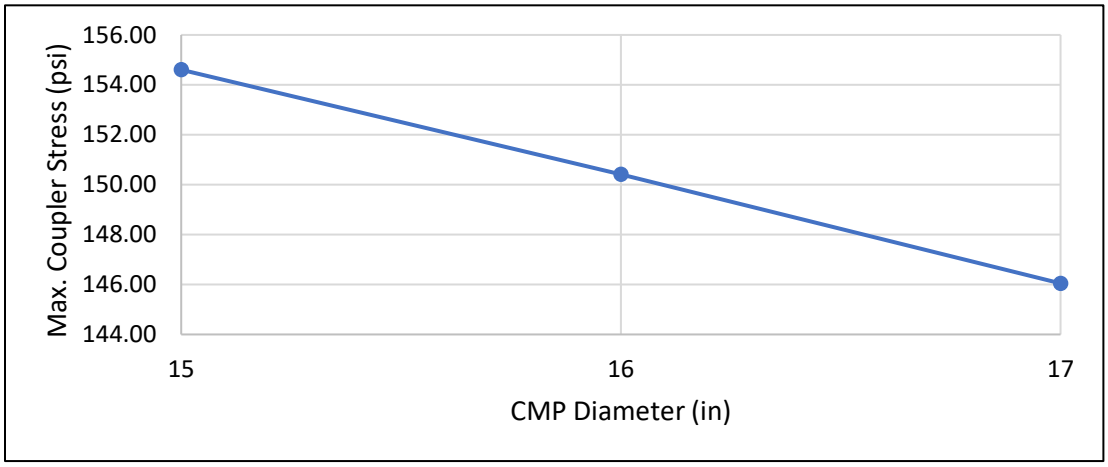

Figure 6.36 *Maximum coupler stress for varying CMP diameters.*

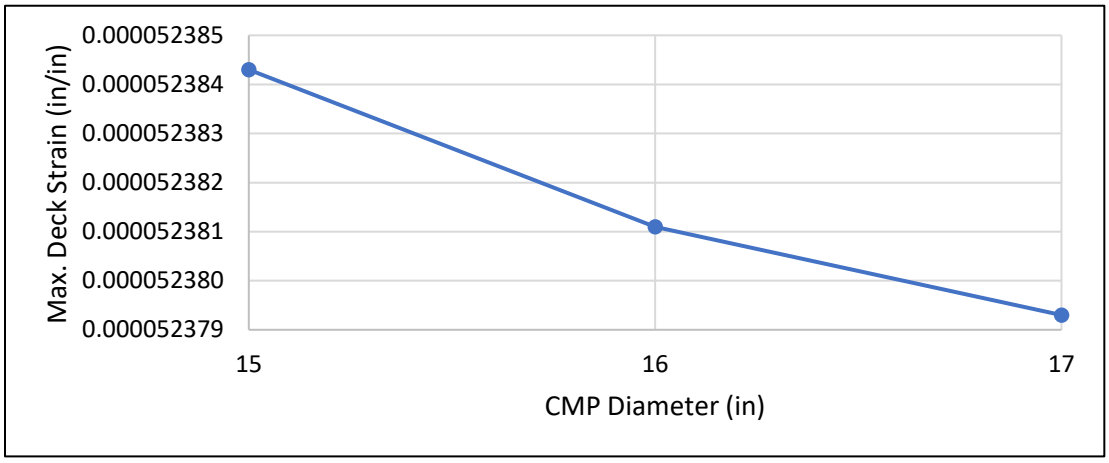

Figure 6.37 *Maximum deck strain for varying CMP diameters.*

It can be seen that as the diameter of the CMP increases, the stiffness of the connection decreases. This is shown by the 0.6 percent increase in the maximum beam displacement, the 5.7 percent decrease in maximum coupler stress, and the 0.01 percent decrease in maximum deck strain. Since this study was only done for the tied condition, it could be that as the CMP diameter increases, the area for the tied constraint to be applied will decrease, hence increasing the CMP diameter will not provide any gain in coupler effectiveness and the size of the CMP should only be based on providing proper encasement of the coupling materials.

Next, the effect of varying steel section sizes on the response of the system was looked at. The steel sections investigated were W5x19, W6x25, W8x35, and W10x33 (Figure 6.38), noting that the W8x35 section was used for the experimental testing done, and that a section larger than the W10x33 would not allow for proper encasement of the section within the 15-inch diameter CMPs, which was the set diameter for this aspect of the study using the four CMP design. The results of the study are shown in Figures 6.39 through 6.41, note that the variation of coupler section designation (1 through 5) is respective to the order of sections previously listed.

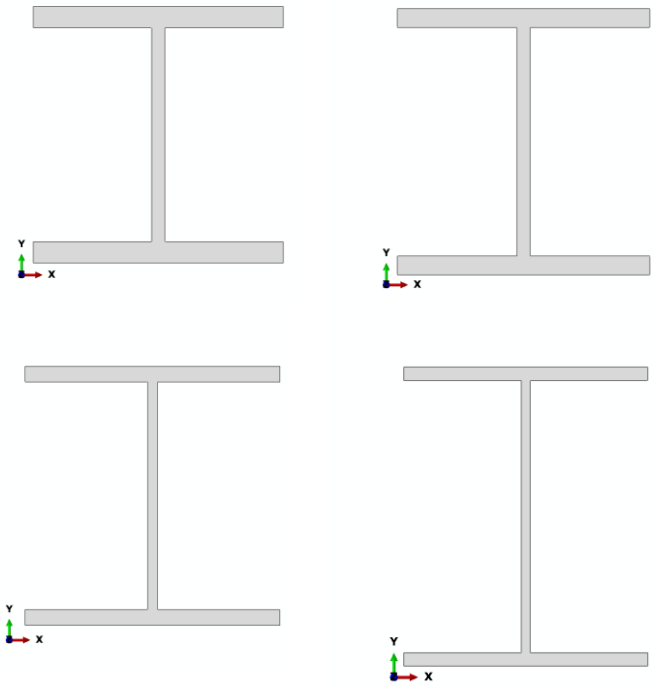

Figure 6.38 *Coupler sections for parametric study. From top left moving clockwise: W5x19, W6x25, W8x35, W10x33.*

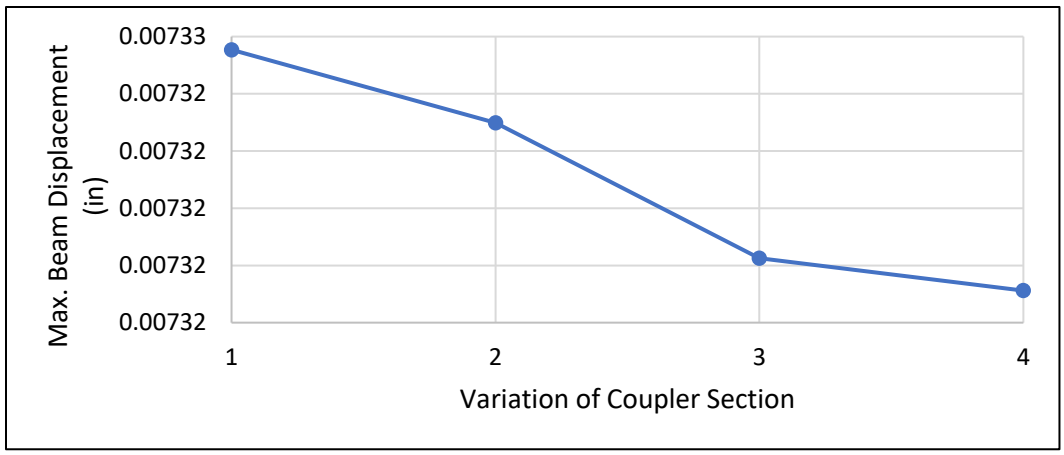

Figure 6.39 *Maximum beam displacement for varying coupler steel sections.*

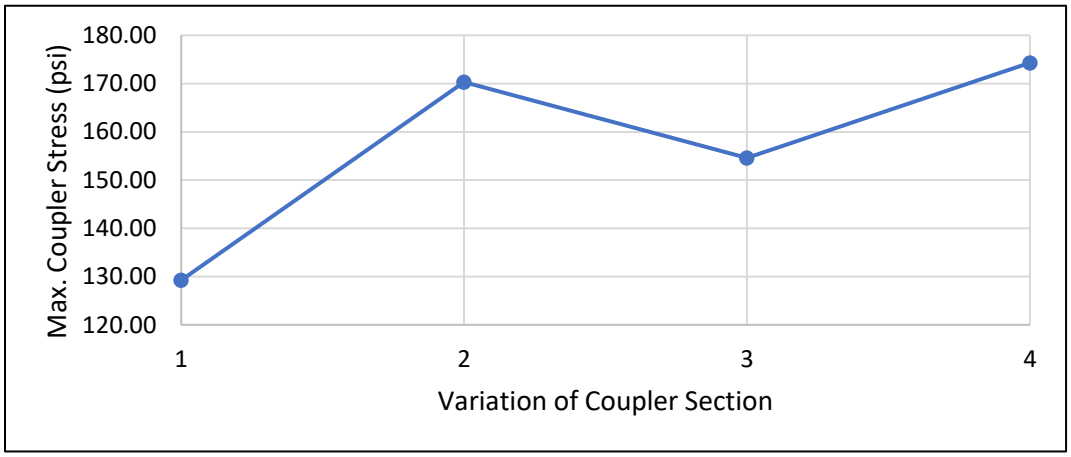

Figure 6.40 *Maximum coupler stress for varying coupler steel sections.*

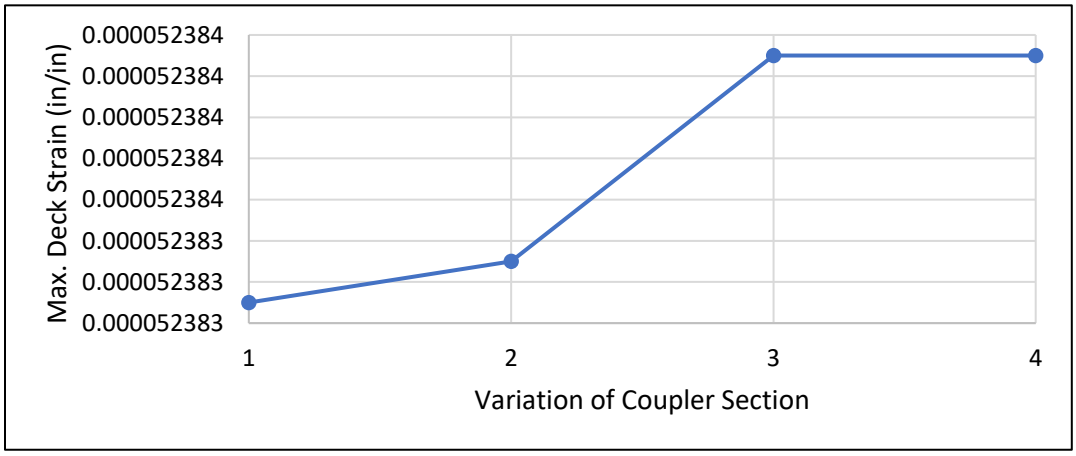

Figure 6.41 *Maximum deck strain for varying coupler steel sections.*

With the increase in the size of the sections, the stiffness of the connection increases. This is shown through the maximum beam displacement decreasing 0.12 percent, while the maximum coupler stress increased 29.7 percent and maximum deck strain increased 0.002 percent.

Next, a proposed design revision of changing the coupler steel to a reinforcing cage from the steel sections had its own investigation. Longitudinal reinforcing bars for the cages ranged in size, #6, #8, and #10, while maintaining use of eight of those bars for the reinforcing coupler bar cage within the four 15-inch CMPs. Figures 6.42 through 6.44 show the results of this study.

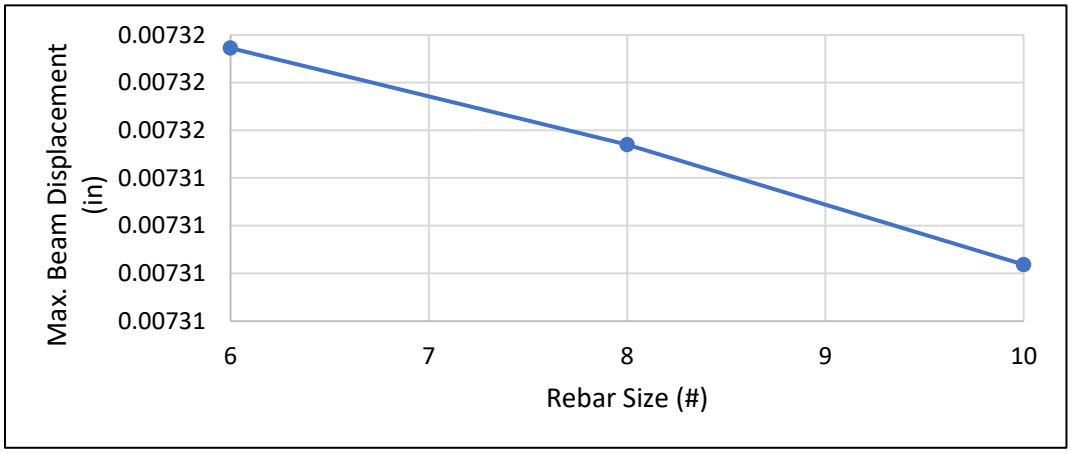

Figure 6.42 *Maximum beam displacement for varying longitudinal reinforcing bar sizes.*

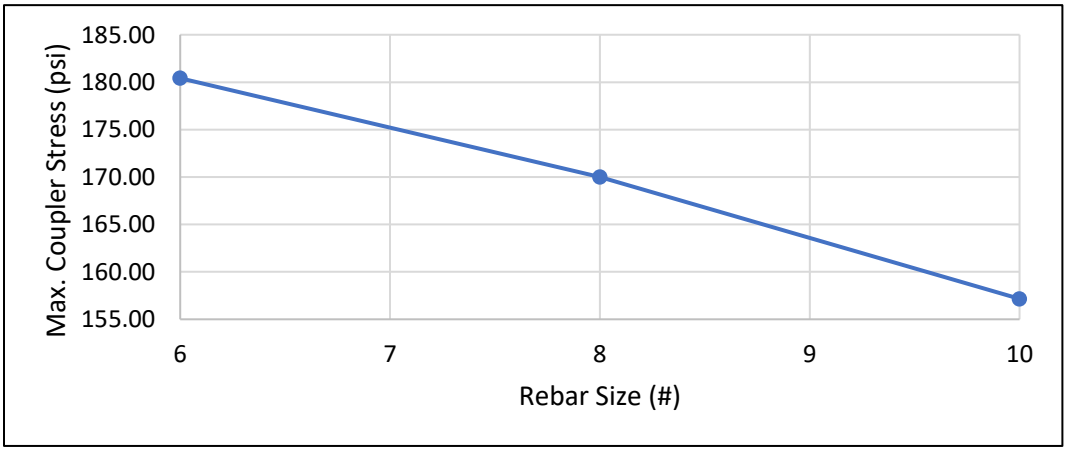

Figure 6.43 *Maximum coupler stress for varying longitudinal reinforcing bar sizes.*

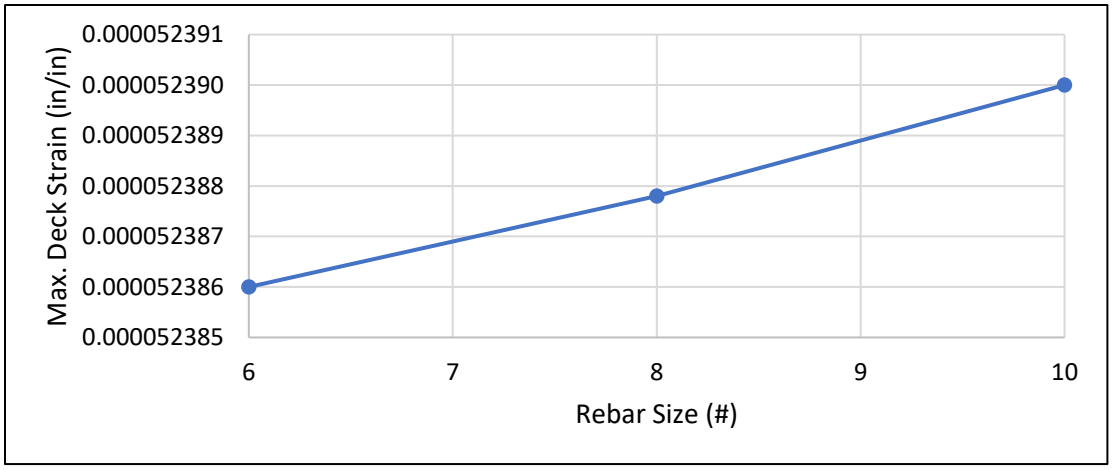

Figure 6.44 *Maximum deck strain for varying longitudinal reinforcing bar sizes.*

With the increase in the size of the longitudinal reinforcing bars for the coupler cages, there is an increase of the stiffness of the connection. This is apparent through the 0.12 percent decrease in the maximum beam displacement and the 0.008 percent increase of the maximum deck strain with an increase in reinforcing bar size. However, is it also seen that as the size of the reinforcing bars increases, the maximum coupler stress seen by the connection decreases by 13.8 percent since the same force is being applied over the same number of reinforcing bars, but the increase in bar size allows for less stress to be induced.

Finally, variations of the longitudinal reinforcing bar layouts were investigated on how it affected the structural response. The layouts were to keep the area of steel similar to that of the steel sections used for the experimental testing, which were W8x35 sections with an area of 10.3in^2. The layouts used were (8) #10, (6) #11, and (4) #14 longitudinal reinforcing bars (Figure 6.45) for the coupler cages. The results of this study are shown in Figures 6.46 through 6.48, note that the variation (1 through 3) is respective to the order of the layouts previously stated.

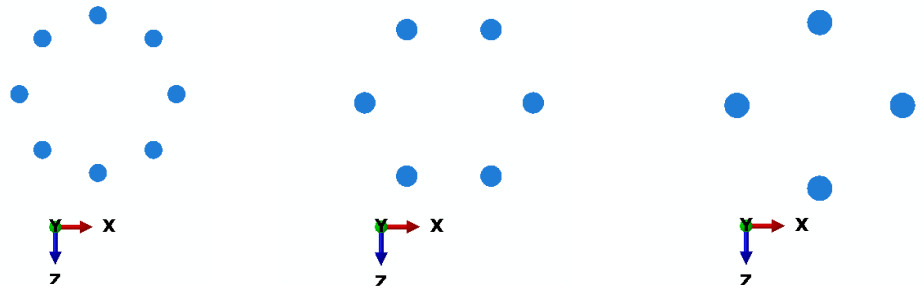

Figure 6.45 *Various reinforcing cage layouts of (Left to Right) (8) #10, (6) #11, and (4) #14 reinforcing bars.*

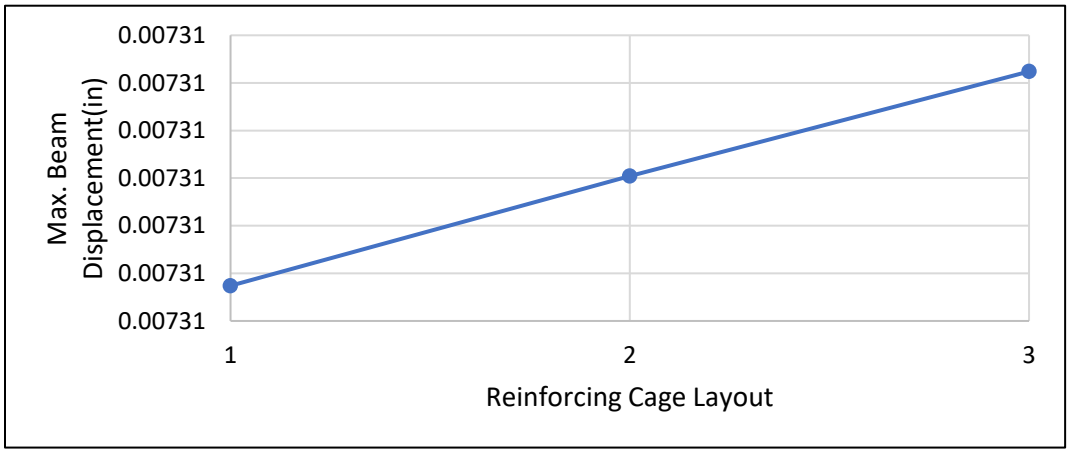

Figure 6.46 *Maximum beam displacement for varying longitudinal reinforcing bar layouts.*

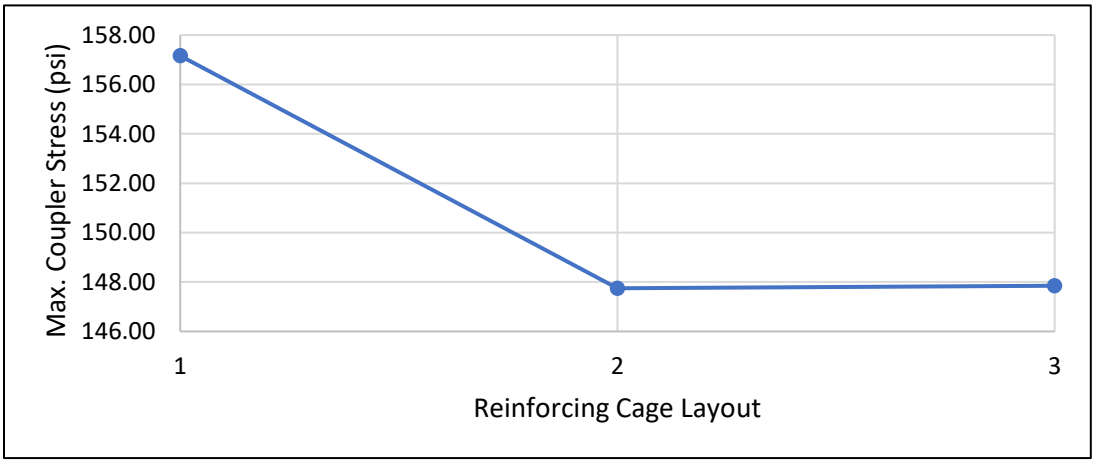

Figure 6.47 *Maximum coupler stress for varying longitudinal reinforcing bar layouts.*

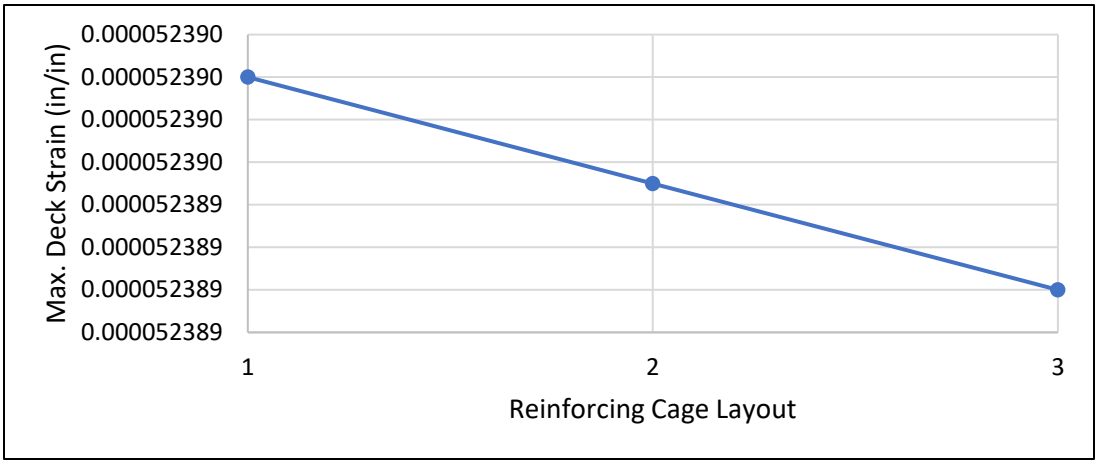

Figure 6.48 *Maximum deck strain for varying longitudinal reinforcing bar layouts*.

As the longitudinal reinforcing bar layout changes, (8) #10, (6) #11, and (4) #14, the stiffness of the connection decreases. This is shown by the maximum beam displacement increasing by 0.03 percent, while the maximum coupler stress and maximum deck strain decrease by 6.1 percent and 0.002, respectively, along with the change in layouts. This could be due to a smaller number of bars being present for the connection.

6.3 Conclusions

Several important conclusions can be drawn from the finite element modeling and the paramedic study conducted. One is that an all tied condition can be assumed for modeling purposes when high-quality construction is performed to ensure nearly no joint deformation occurs under loading. On the other hand, a hinged condition represents another extreme case scenario in which there would be no contact properties between the integral diaphragm and the pile cap of the integral abutment connection, which would lead to force transfer being focused to the connecting reinforcing coupler bars.

Also, the parametric study validated assumptions made during the design process of the connections such as with an increase in reinforcing coupler bars, there was a decrease in maximum beam displacement, joint opening, and reinforcing coupler bar stress. It was

important to see the difference in not only the magnitude of the maximum reinforcing coupler bar stress but also how the location and distribution of these stresses varied between different coupler orientations and between the tied and hinged condition.

Some concluding observations made from the Pile Coupler parametric study was by increasing the diameter of the CMPs, the performance of the design will actually begin to decrease, hence the only design parameter for the CMP diameter should be for proper encasement of the steel section couplers. Also, increasing the size of the steel section couplers will increase the stiffness of the connection if the sections will be properly encased within the CMPs.

Finally, it is necessary to note the maximum tensile strain in the deck of the integral abutment bridge connections at the beam-abutment interface since this location has the potential for infiltration of water and deicing chemicals. It was recorded that with an increase in the number of reinforcing coupler bars, there was an increase in maximum tensile strain in the deck due to the increased stiffness of the abutment connection for the UHPC-Joint and Grouted Reinforcing Bar Coupler specimens, as well as for the Pile Coupler reinforcing coupler cages.

CHAPTER 7. SUMMARY AND CONCLUSIONS

To advance the use of integral abutments with ABC, rather than relying on a closure pour, three connection details were designed to be constructed full-scale and tested in the structures laboratory to monitor overall strength and durability of each connection detail. The design philosophy of each connection detail was to be able to complete adequate structural connections in a matter of a few days while maintaining the structural integrity and response present with the closure pour connection. Two of the connection details were revisions of those investigated by (Hosteng, Phares, & Redd, 2016), called the grouted reinforcing bar coupler and pile coupler, and the third connection detail was a design created through the Iowa DOT to be used on an upcoming real-life project.

The grouted reinforcing bar coupler utilized grouted reinforcing splice couplers, which spliced protruding reinforcing bars from the pile cap into sleeves within the integral diaphragm. The pile coupler used four 2.5-foot steel sections, which spliced the integral diaphragm and pile cap, encased in a cementitious material similar to the method used for foundation piles to pile cap connections used in ABC. The UHPC joint connection utilized a "notched" cross section with protruding reinforcing bar from the integral diaphragm and pile cap that was filled with UHPC. All three connection details were successfully constructed and documented in detail, specifically concerning any issues that arose during the construction process and were evaluated based on, not only the constructability of each detail, but also the strength and durability of the connection.

The grouted reinforcing bar coupler design was revised to use only 8 splices rather than the 17 used in (Hosteng, Phares, & Redd, 2016). This revision helped to alleviate the tight construction tolerances present with the design presented in (Hosteng, Phares, & Redd,

2016) but was designed to maintain allowable structural behavior throughout the cold joint connection. A plywood template was used to "match cast" the grouting sleeves of the integral diaphragm to the protruding bars from the pile cap and was proven successful through a "dry fit" done prior to the installation of the connection. This construction method should be applicable to the field for fabricators and result in successful alignments of the connections, but the presence of two ends of these connections could cause some issues during alignment due to any skew present within the span of the bridge and would require high quality control and great attention to detail during design, fabrication of the precast elements, and installation of the connection.

The laboratory testing of the grouted reinforcing bar coupler resulted in values that were reasonable due to the revision of the design. The maximum developed crack width under loading was 0.348 in., but the crack width to be compared to the loading from (Hosteng, Phares, & Redd, 2016), 0.035 in., was 0.176 in. or about 5 times greater. Also, with the decrease of splices within the specimen, the comparison of connection reinforcing steel bar stresses was of interest. The maximum reinforcing bar stress reported in (Hosteng, Phares, & Redd, 2016) of the grouted reinforcing bar coupler was 43 ksi, while the revised design recorded a maximum stress of 74.3 ksi or about 1.7 times greater. This was a reasonable result due to the design having about half of the connections that the design in (Hosteng, Phares, & Redd, 2016) did.

The pile coupler design was revised to have four 2.5-foot steel sections splicing the integral diaphragm and the pile cap that were encased in a cementitious material. The CMP voids' alignment was not as complex compared to the alignment for the grouted reinforcing bar coupler, which was a benefit for the connection. The overall construction of the specimen

was not difficult, but tedious due to more accessories required for the connection elements, specifically within the integral diaphragm. Fabricators and designers need to have exceptional coordination and quality assurance to ensure all materials are present for adequate and efficient construction of the precast elements, but the connection installation should be simpler than that of the grouted reinforcing bar coupler due to the larger splices.

The laboratory testing of the pile coupler was promising for the connection detail and showed great improvement with the revisions done to the design. While the design in (Hosteng, Phares, & Redd, 2016) resulted in a failed detail that had a maximum crack of 1.75 in., the revised design recorded a maximum cold joint crack of 0.031 in. under the same load. Comparing this design of the pile coupler to the control specimen, the maximum cold joint crack seen by both connection details under the same load was 0.306 in. and 0.024 in., respectively.

The UHPC joint design utilized a “notched” cross section formed into the integral diaphragm, protruding reinforcing bars from the integral diaphragm and pile cap, and filling the void between the two precast elements with UHPC. The construction of the precast elements was not difficult and should be achievable for experienced fabricators. It is important that the fabricators ensure the required protrusions for the reinforcing bars to provide adequate development length within the UHPC joint, which can be accomplished through proper quality control procedures. The connection install needs to have exceptional construction techniques and coordination to be able to cast the UHPC joint as one large batch for each abutment to prevent any layering of material within the joint which would cause additional cold joints within the connection.

The laboratory testing of the UHPC joint proved the connection would be able to prevent a high magnitude cold joint crack and consequently prevent infiltration of deteriorating chemicals and water. Since the failure mechanism seen in the specimen was the web buckling of the beam, it can be assumed the connection detail is most comparable to the closure pour connection detail for integral abutments, since under the same load the UHPC joint specimen had a maximum joint opening of 0.031 in. and the closure pour specimen had a maximum joint opening of 0.025 in.

Analyzing the connection details, it is important to note not only the maximum rear face crack, but also the propagation of the rear face crack due to vertical loading. The pile coupler did not record any cracking until a loading of approximately 400-k-ft, the grouted reinforcing bar coupler design resulted in rear face cracking almost instantaneously upon loading, and the UHPC joint had nearly no cracking throughout loading. The propagation of cracking is important to know since any cracking of the cold joint will allow for infiltration of water or other chemicals into the structure, which can lead to deterioration of the coupling materials. These propagations are the result of only one static load and would presumably increase in magnitude over cyclic loading and presence of deterioration of the connection materials.

Finite element simulations were conducted in ABAQUS CAE to investigate how differing coupler orientations for the Grouted Reinforcing Bar Coupler and UHPC-Joint would affect the structural response of the integral abutment specimens. The setup for these models was based on the geometry and material properties used during the laboratory testing. To make conclusions for the parametric study of the number of couplers, the results compared were the maximum beam displacement for the end of the cantilever beam, the

maximum joint opening between the integral diaphragm and pile cap, the maximum reinforcing coupler bar stress, and the maximum top surface deck strain at the beam-abutment interface.

The orientations of couplers chosen for the parametric study were four, eight, twelve, thirteen, and seventeen couplers which were chosen to accommodate real-world applications that would provide the structural connections required for the integral abutment joint as well as be able to be constructed. The results of the study concluded that the increase in number of reinforcing coupler bars results in a decrease in maximum beam displacement, a decrease in maximum joint opening, a decrease in maximum reinforcing coupler bar stress, but an increase in maximum top surface deck strain at the beam-abutment interface. The reasoning behind these relationships derives from the increase in abutment stiffness from the increase in reinforcing coupler bars within the integral abutment connection, and that the optimal amount of coupler bars would be up to the discretion of the bridge engineer and their respective entity's criteria for allowable reinforcing coupler bar stress and maximum joint opening.

The same parameters were used to conduct a parametric study for the Pile Coupler specimen as well but had more individual studies done. Various orientations of the CMPs, steel section couplers, and reinforcing cage couplers were investigated by analyzing their influence on the maximum beam displacement, maximum coupler stress, and maximum deck strain at the beam-abutment interface. Increasing the diameter of the CMPs resulted in decreasing the performance of the design, hence causing the only design parameter of the CMPs to allow for proper encasement of the steel coupling materials. Increasing the size of

the steel section couplers led to a stiffer connection, as did increasing the size of reinforcing bars used for the reinforcing coupler cages.

The outcome of this study can lead to the initiation of other investigations focusing on the following topics:

- Revision of the UHPC joint connection detail with the "notch" of the front face of the integral diaphragm being transferred to the front face of the pile cap. This would allow the protruding coupling bar from the pile cap to be lowered enough to not cause an issue with the beam during slide-in construction yet have enough length for proper development within the UHPC. By making this revision, formwork for the bottom of the integral diaphragm could be simplified but would require another round of research to verify.
- Presence of confinement reinforcing around the CMPs within the pile coupler since these are where cracks propagated within the precast elements.
- Introducing a spiral reinforcing cage instead of H-pile sections for the pile coupler splicing materials which may make the connection easier to standardize, while preserving the concept of the connection.
- Grouted reinforcing bar coupler construction and testing utilizing grout sleeves two sizes larger than the splicing rebar used, #10 sleeve for #8 bar for example, which is allowed by Dayton Superior and could further alleviate construction tolerances.
- Cyclic loading of the connection details with the aim of identifying its effect on the connection details, specifically the coupling materials such as the reinforcing coupler bars and contact properties.

- Analysis of real-world applications of the tested connection details through field monitoring to compare how extreme the loading of the laboratory specimens is to the actual loading that would be seen in the field. Field monitoring may also lead to more accurate and entirely different requirements for laboratory experimentation.
- Finite element simulations should be improved for the integral abutment connection details. Field monitoring data can aid in creating accurate simulations for real-world applications of the connection details. Also, with further investigations into the contact properties through experimental testing, precise simulations can be created for the specimens tested for the research in this thesis and for other implementations of the connection details.

REFERENCES

Abdel-Fattah, M. T., Abdel-Fattah, T. T., & Hemada, A. A. (2017). *Nonlinear Finite-Element Analysis of Integral Abutment Bridges due to Cyclic Thermal Changes.* Reston, VA: American Society of Civil Engineers.

Ahn, J.-H., Yoon, J.-H., Kim, J.-H., & Kim, S.-H. (2011). *Evaluation on the behavior of abutment-pile connection in integral abutment bridge.* Amsterdam, Netherlands: Journal of Constructional Steel Research.

Briseghella, B., & Zordan, T. (2015). *An innovative steel-concrete joint for integral abutment bridges.* Xi'an, China: Journal of Traffic and Transportation Engineering.

Culmo, M. P. (2011). *Accelerated Bridge Construction - Experience in Design, Fabrication and Erection of Prefabricated Bridge Elements and Systems.* McLean, VA: FHWA.

Culmo, M., Boyle, H., Nettleton, S., Chandra, V., Tadros, M., & Mallela, J. (2013). *Engineering Design, Fabrication and Erection of Prefabricated Bridge Elements and Systems.* Washington, D.C.: FHWA.

Hewes, J. T. (2013). *Analysis of the State of the Art of Precast Concrete Bridge Substructure Systems.* Phoenix, AZ: Arizona Department of Transportation.

Hosteng, T., Phares, B., & Redd, S. (2016). *Strength, Durability, and Application of Grouted Couplers for Integral Abutments in Accelerated Bridge Construction.* Ames, IA: Iowa State University.

Hosteng, T., Phares, B., Abu-Hawash, A., Bierwagen, D., & Nelson, J. (2015). *Laboratory Investigation of Grouted Coupler Connection Details for ABC Bridge Projects.* Ames, IA: Iowa State University.

Huffaker, C. D. (2013). *Behavior and Analysis of an Integral Abutment Bridge.* Logan, UT: Utah State University.

IowaDOT. (2014). *Special Provisions for Ultra High Performance Concrete.* Ames, IA: IowaDOT.

Jansson, P. O. (2008). *Evaluation of Grout-Filled Mechanical Splices for Precast Concrete Construction.* Lansing, MI: Michigan Department of Transportation.

Kapur, J., Keever, M., Yen, W. P., Sletten, J., Dekelbab, W., Tobias, D., . . . Saiidi, M. S. (2012). *Best Practices Regarding Performance of ABC Connections in Bridges Subjected to Multihazard and Extreme.* Washington, D.C.: NCHRP.

Khodair, Y. A., & Hassiotis, S. (2013). *Rigidity of abutments in integral abutment bridges.* London, England, UK: Structure and Infrastructure Engineering.

Kim, S.-H., Yoon, J.-H., Kim, J.-H., Choi, W.-J., & Ahn, J.-H. (2011). *Structural details of steel girder-abutment joints in integral bridges: An experimental study.* Amsterdam, Netherlands: Journal of Constructional Steel Research.

Kim, W., & Laman, J. A. (2012). *Seven-Year Field Monitoring of Four Integral Abutment Bridges.* Reston, VA: American Society of Civil Engineers.

Kim, W., Lee, J., & Jeoung, C. (2013). *Concrete Crack Control of Pile-to-pilecap Connection in Integral Abutment Bridges under Cyclic Bridge Movement.* Zurich, Switzerland: Trans Tech Publications.

LaFave, J. M., Fahnestock, L. A., Brambila, G., Riddle, J. K., Jarrett, M. W., Svatora, J. S., . . . An, H. (2017). *Integral Abutment Bridges under Thermal Loading: Field Monitoring and Analysis.* Urbana, IL: University of Illinois at Urbana - Champaign.

LaFave, J. M., Fahnestock, L. A., Wright, B. A., Riddle, J. K., Jarrett, M. W., Svatora, J. S., . . . Brambila, G. (2016). *Integral Abutment Bridges Under Thermal Loading: Numerical Simulations and Parametric Study.* Urbana, IL: University of Illinois at Urbana - Champaign.

Lee, J., Kim, W., & Jeoung, C. (2013). *Concrete Crack Control of Pile-to-pilecap Connection in Integral Abutment Bridges under Cyclic Bridge Movement.* Zurich, Switzerland: Trans Tech Publications.

Paraschos, A., & Amde, A. M. (2011). *A survey on the status of use, problems, and costs associated with Integral Abutment Bridges.* College Park, MD: The University of Maryland.

Tabatabai, H., Magbool, H. B., & Fu, C. (2017). *Criteria and Practices of Various States for the Design of Jointless and Integral Abutment Bridges.* Milwaukee, WI: University of Wisconsin - Milwaukee.

Unlu, D. (2010). *Rapid Bridge Construction Technology: Precast Elements for Substructures.* Madison, WI: University of Wisconsin - Madison.

Wipf, T. J., Klaiber, W., & Hockerman, S. (2009). *Precast Concrete Elements for Accelerated Bridge Construction: Laboratory Testing of Precast Substructure Components, Boone County Bridge.* Ames, IA: Iowa State University.